A High Efficiency Photovoltaic Inverter System Configuration with Maximum Power Point Tracking

By
Mohammed Ali Alqarni

Submitted in partial fulfilment of the requirements for the degree of
Doctor of Philosophy

Department of Electronic and Computer Engineering
College of Engineering, Design and Physical Science
Brunel University London
UK

March 2016

Abstract

The increase in demand for renewable energy sources has been exponential in recent years and is mainly driven by factors that include the growth of greenhouse emissions and the decline in fossil fuel reservoirs. Photovoltaic (PV) energy, one of the more prominent renewable energy sources, produces electricity directly from sunlight, noiselessly and harmlessly to the environment. Additionally, PV energy systems are easy to install and financially supported by many governments, which has helped disseminate PV technology worldwide. The total generated power from PV installations (and the number of installations) has increased more than two-fold during the past 3 years, so that now more than 177 GW of PV-generated power is delivered per year. Researchers have been led to work on the obstacles facing PV systems from different perspectives, including: installation cost, inconsistency, and conversion and interface efficiency.

The aim of this thesis is to design a high-efficiency PV inverter system configuration. The contribution to the knowledge in this thesis can be divided into two parts. The first part contains a critical analysis of different maximum power point tracking (MPPT) techniques. The second part provides a detailed design of the inverter system, which consists of a boost converter and a low-frequency H-bridge. Together, the three parts in this contribution present a complete high efficiency PV inverter system.

The proposed system maintains high-efficiency energy delivery by reducing the number of high-frequency switches, which waste a significant amount of energy and reduce system efficiency. In order to show the superiority of the proposed configuration, a power loss analysis comparison with the other existing configurations is presented. In addition, different scenarios have been simulated with Matlab/Simulink. The results of these simulations confirm the distinction of the proposed configuration as well as its low-loss, high-efficiency characteristics which is rated at 98.8%.

To my parents, Fatimah and Ali

My brother, Awad, Saeed and Khaled

& my sweet little sisters, Hanan and Yasmeen

Acknowledgments

وَفَوْقَ كُلِّ ذِي عِلْمٍ عَلِيمٌ

"Over all those endowed with knowledge is the All-Knowing (ALLAH)".

In the name of Allah, the Most Gracious and the Most Merciful. Thanks to ALLAH who is the source of all the knowledge in this world, for the strengths and guidance in completing this thesis. It is a pleasure to attribute credit to the many people who have contributed directly or indirectly to this work.

I would like to express my thanks to my supervisor Dr Mohamed Darwish for his continuous guidance from the first day of my PhD journey. He was always beside me encouraging and supporting my learning desire. One could not wish for more kind, accessible and friendlier supervisor. Additionally, I would like to thank Dr Basim Alsayid for kindly sharing his wide knowledge with me and his support. Also I am thankful to my examiners Professor Talib Alukaidey, Dr Maysam Abbod and the viva chair Dr Ahmed Zobaa.

I am hugely grateful to my parents for their support, prayers, love and care throughout my life; they have played a vital role in helping me to reach this milestone. I also would like to thanks my brothers Awad, Saeed and Khalid, my sisters Hanan and Yasmeen, relatives and friends for their continuous support and prayers. I thank those who rendered their direct or indirect support during the period of my PhD project. My friends who have helped me by any means to achieve what I have achieved: Basem, Abdulaziz Alzahrani, Edrees, Mohammed Alsubaey, Saleh, Mohamed Radi, Khaled Sehil, Mansour, Manoi, Sanar, Abdulhafeed, Mohammed Althaqafi, and Fawaz. I am also grateful to many individuals at Brunel University who provided me with academic and technical support during my research.

Lastly, I am grateful to the King Abdullah (RIP) and the government of Saudi Arabia who gave me this scholarship to pursue my PhD studies.

Author's Declaration

I hereby declare that this thesis is my own work and effort and that it has not been submitted anywhere for any award. Where other sources of information have been used, they have been acknowledged.

Mohammed Ali Alqarni

March 2016

Table of Contents

List of Figures Page No.

List of Tables Page No.

List of Abbreviations

Adj R-sq	The Degrees of Freedom Adjusted R-square
BJT	Bipolar Junction Transistor
CHB-MLI	Cascaded H-bridge Multilevel Inverter
Coeff	Number of Coefficients in the Mathematical Model
DSP	Digital Signal Processor
ESL	Equivalent Inductance
ESR	Equivalent Series Resistance
FFT	Fast Fourier Transform
HF	High Frequency
IEEE	The Institute of Electrical and Electronics Engineers
IGBT	Insulated Gate Bipolar Transistor
I-V	PV Current Vs Voltage
LC filter	Inductance Capacitance Filter
LF	Low Frequency
MOSFET	Metal Oxide Semiconductor Field Effect Transistor
MPP	Maximum Power Point
MPPT	Maximum Power Point Tracking
P&O	Perturb and Observe method
PSPICE	Simulation Program with Integrated Circuit Emphasis
PV	Photovoltaic
P-V	PV Power Vs Voltage
PWM	Pulse Width Modulation
RCC	Constant for Ripple Correlation Control
RMSE	Root Mean Squared Error or Standard Error
RSPWM	Rectified Sinusoidal Pulse Width Modulation
R-square	Square of the Correlation between the Response Values and the Predicted Response Values
S	Switch
SPWM	Sinusoidal Pulse Width Modulation
SSE	Sum of Squares due to Error
STC	Standard Testing Conditions
THD	Total Harmonic Distortion

Chapter 1

Introduction

Chapter 1. Introduction

1.1 Background

The demand for efficiency renewable energy sources has grown exponentially in recent years, driven by many factors (including the growth of greenhouse gas emissions and environmental concerns). Climate change movements worldwide have urged world leaders to take action to tackle these concerns. In response, the United Nation proclaimed 2012 as the International Year of Sustainable Energy for All. The three goals set to be achieved by 2030 as part of this initiative included: (I) to improve energy efficiency, (II) to significantly increase the implementation of renewable energy sources, and (III) to provide worldwide access to modern energy services (Sawin, 2012; Alqarni and Darwish, 2012). The other factors encouraging the greater utilisation of renewable energy include the increase in fossil fuel prices and the decline in fossil fuel reservoirs. In 2013, renewable energy sources delivered about 22.1 % of the total electricity supply worldwide (Sundareswaran *et al.*, 2016; Sawin *et al.*, 2014)   .

Photovoltaic (PV) energy is a renewable energy sources that provides clean energy by directly transforming sunlight to electricity. In addition, PV cells and panels are noiseless and harmless compared to the wind turbine. Another merit of PV energy is the easy installation of this technology on rooftops, in parking areas, and on the vertical sides of skyscrapers, allowing light to pass through and generating power as well. Moreover, government subsidies of residential PV cell installations (as well as the introduction of the feed-in tariff) have encouraged PV panel installation in residences as well as investment in PV technologies (Kouro *et al.*, 2015; Reisi, Moradi and Jamasb, 2013).

The merits of PV energy (as described above) combined with various types of incentives have positively impacted the growth of PV usage during the last 5 to 10 years. Figure 1.1 shows the growth of the PV installations for the period from 2008 to 2014 and clarifies the significant amount of interest in PV systems (Nowak, 2015; Alqarni and Darwish, 2014). The total amount of PV-generated power increased more

than two-fold within the 4 years from 2011 to 2014 (at which time PV installations delivered 177 GW of energy). The applications of PV systems, which are in grid-connected or stand-alone configurations, include water pumping, street lighting, information street signs, bus shelters, electric vehicles and military and aerospace applications (Faranda, Leva and Maugeri, 2008).
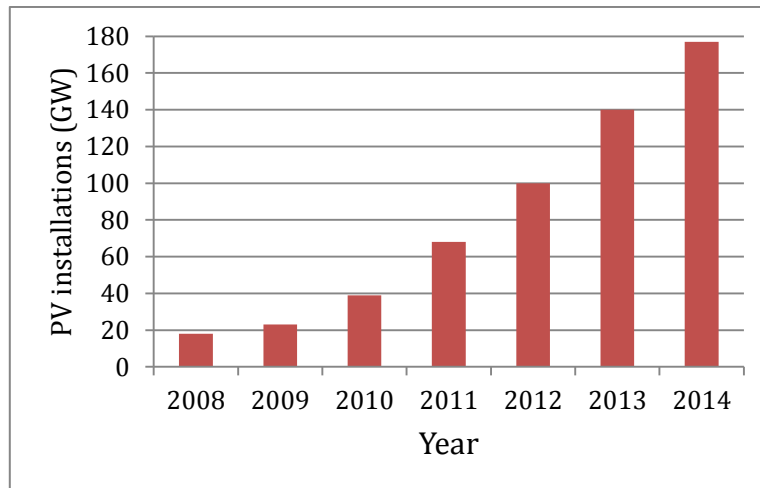
Figure 1.1: PV installation annual growth

China is the leading country in utilising new PV energy systems in 2014, powering 10.6 GW; the Chinese government's intention to make greater use of greener sources of energy is confirmed by this utilisation and other in the past 3 years. Rounding out the top 5 countries in new PV installation for this year were Japan (adding 9.7 GW), the USA (6.2 GW), the UK (2.4 GW), and Germany (1.9 GW). Currently, Germany still has the largest PV capacity in the world at 38 GW, which represents 22% of the existing PV energy capacity worldwide. The other countries with a large contribution to the total 177 GW worldwide usage are China, Japan, Italy and the USA. These countries share a total of 50% of the world PV capacity. Interestingly, more countries have lately joined the race and called for new PV installations, including Jordan, the UAE and Brazil. However, some challenges need to be finalised before entering these markets, such as compatibility with low electricity prices and regulatory restrictions that necessitate competitive solutions (Nowak, 2015).

1.2 Motivations

Although the number of PV installations worldwide (and the amount of energy they generate) has grown rapidly, drawbacks remain, including the high cost of PV energy compared to conventional electricity sources. The price of PV panel installation has dropped dramatically in the past few years, but this is still an area of active investigation for researchers. Inconsistency is the other disadvantage of PV systems, as they depend on the presence of light to produce power. To address this inconsistency, research has been conducted to improve energy storage so that the stored energy can be used when needed. The low efficiency of many PV systems is another issue needing improved solutions, including the PV efficiency of converting sunlight to electricity. To date, the best recorded energy conversion rate for a PV application is 24% (Nowak, 2015). The interface between the PV and the load (either in a grid-connected or stand-alone system) presents another efficiency issue, as the interface consists of power electronics components that can either step the voltage up or down, or convert DC to AC. Finally, the last item related to PV system efficiency is the MPPT of the system, which is responsible for improving PV efficiency by extracting its maximum power at all times. The MPPT controls the converter by receiving the PV measurements and setting the PV operating voltage at which it delivers its maximum power. Many algorithms can be used to implement MPPT, and each of them functions with a higher or lower level of efficiency.

Several areas of the PV set-up have the potential to provide efficiency improvements. Forcing the PV to deliver its maximum potential power is essential in any system to reduce the large amount of wasted energy. In addition to these factors (which can be controlled by system adjustments), uncontrollable factors such as weather conditions (irradiance and temperature) affect PV output power by shifting the location of the MPP (see Figure 1.2). High irradiance generates higher power than does lower irradiance, while high temperatures reduce PV productivity (Sundareswaran *et al.*, 2016). The MPPT should maintain maximum power delivery under different atmospheric conditions. Furthermore, the wide range of MPPT algorithms provides a rich area for evaluation and comparable studies (Reisi, Moradi and Jamasb, 2013).
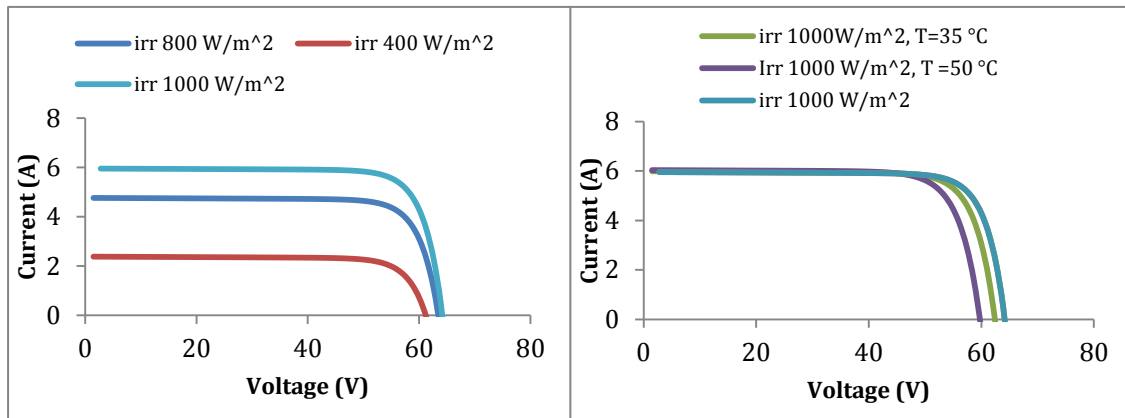
Figure 1.2: PV I-V characteristics for different weather conditions (See the datasheet of Sunpower PV panel in Appendix B)

A solution to improve the overall PV system efficiency is by increasing the efficiency of the PV inverter system configuration, which includes the converter and inverter devices (Kjær, 2005). There are four existing configurations: centralised, string, multi-string and AC module. Each of these configurations have unique advantages and drawbacks (Kouro *et al.*, 2015). Interest remains in designing a new PV inverter system configuration that maintains high efficiency; this is the primary goal of this thesis.

1.3   Aim and Objectives

The aim of this research is to improve the overall efficiency of PV systems by proposing a more efficient configuration. This goal can be achieved by designing a new PV inverter system configuration that is able to deliver power with high efficiency. The proposed inverter configuration consists of a PV array, an MPPT unit, a reshaping converter and an H-bridge inverter. A deep understanding of how a PV array performs under varying weather conditions was required for the design of this new topology. Additionally, a comprehensive evaluation of the MPPT algorithms was performed in order to optimise the system by selecting and implementing the proper MPPT technique. PV converter technologies are also subjected to a critical review in order to select the appropriate converter for the proposed configuration. The proposed system focusses on maintaining high-efficiency delivery by reducing the number of high frequency switches, which waste a significant amount of energy and reduce the

efficiency of the system. Accordingly, the objectives of this thesis can be summarised as follows:

1. To model the PV system, then perform simulations to validate the accuracy of the model and compare it to actual manufactured models under varying weather conditions.

2. To examine the functionality of the MPPT and prove its importance by simulating the PV array with and without the MPPT for the purpose of comparing the outputs.

3. To design all of the components of the proposed PV inverter configuration, simulate them in Matlab/Simulink and examine the outcomes for different scenarios. These components include the PV array, the MPPT algorithm and its converter, the reshaping converter and its control source, the H-bridge inverter, the filter and the load.

4. To examine the overall system efficiency for delivering power to the load and determine the total power losses within the configuration.

1.4 Methodology

In this thesis the methodology used is a modelling and simulation approach. Each of the circuit-block in the proposed work is modelled and simulated on Matlab/Simulink. This is followed by a testing for each block and the results are recorded and the efficiency of the whole system is evaluated.

1.5 Chapter Summary

This thesis is divided into six chapters as follow:

Chapter 1 provides a brief background about renewable energy, especially PV systems, followed by a description of the research motivation, aim, objectives and of the layout of the thesis.

Chapter 2 starts with a short review of how PV systems have evolved, followed by the mathematical model of the PV cell. The currently existing PV inverter configurations are presented, followed by a definition of the MPPT principle and a list of MPPT methods, which are then critically compared.

Chapter 3 covers the main PV converter topologies, including their functionalities, with the individual mathematical models displayed via block diagrams. Comparisons among the converters are carried out at the end of the chapter.

Chapter 4 covers the proposed PV inverter configuration, including the design criteria of each component in the configuration. Additionally, the decision matrix table that has been used in selecting the appropriate MPPT and DC-DC converter is presented.

Chapter 5 illustrates the proposed configuration simulation in Matlab/Simulink and the simulation outcomes. The different scenarios presented supported by the appropriate graphs and results. Additionally, this chapter includes the calculation of system losses and efficiency.

Chapter 6 presents the conclusions and future work.

1.6   List of Publications

[1] Alqarni, M. and Darwish, M.K., 2014, September. A maximum power point tracking for a photovoltaic system based on optimum sinusoidal modulated control pulses. In: *Power Engineering Conference (UPEC 2014), 49th International Universities,* Cluj-Napoca, (pp. 1-4).

[2] Alqarni, M; Darwish, M. K., Maximum power point tracking for photovoltaic with high efficiency converter connected to the grid. In: *Smart Grid Conference (SASG), 2014 Saudi Arabia*, 2014.

[3] Alqarni, M; Darwish, M. K., Maximum power point tracking using improved logic control method. In *Student Research Conference-Brunel University (ReSCon), 2013 United Kingdom*, 2014.

[4] Alqarni, M. and Darwish, M.K., 2012, September. Maximum power point tracking for photovoltaic system: modified perturb and observe algorithm. In: *Universities Power Engineering Conference (UPEC 2012), 47th International,* London, (pp. 1-4).

Chapter 2

Review of Photovoltaic Cells, Configurations and MPPT Methods

Chapter 2. Review of Photovoltaic Cells, Configurations and MPPT Methods

2.1 Overview

The rapid growth of interest in solar energy during the last two decades has led to considerable development in this area. Photovoltaic (PV) cells are among the leading solar energy technologies and produce more than 177 GW worldwide. This chapter briefly reviews the historical timeline of PV technologies. An illustration of a PV model is mathematically explained, and difference PV configurations are compared and discussed. Last, the maximum power point tracking (MPPT) principle is defined, with critical discussion of a set of MPPT methods included. To conclude the chapter, a critical comparison of the different MPPT methods is presented prior to a chapter summary.

2.2 History of PV

In 1839 Alexandre-Edmond noticed the impact of the photovoltaic effect while conducting an experiment with wet-cell batteries, leading him to generate electricity by using light. Several decades later, in 1873 Willoughby Smith identified the photoconductive ability of selenium (Green, 1990). Soon after, in 1876 William Adams and Richard Day conducted an experiment on the photoconductivity of selenium that successfully demonstrated the possibility of generating current with the effect of light in solid selenium (Adams and Day, 1876). This experiment was the starting point for the current PV cell.

In 1883 Charles Frittes invented what was considered the first basis of the PV cell by compressing a thin film of selenium between two layers of different materials. The top layer is made of gold, which is able to collect the free electrons released because of the impact of the light on the selenium. The gold is then able to produce electricity by transforming light into electricity at an efficiency of less than 2% (Green, 1990).

Pearson, Chapin and Fuller developed the first modern silicon cell in 1954 as a result of the significant development of the techniques used to manufacture crystal. The efficiency of this cell was about 6% (Chapin, Fuller and Pearson, 1954). The first PV product was on the market the next year but was very expensive—around 1500 $/W (1000 £/W). The exorbitant cost prevented this PV technology from becoming an acceptable alternative power source (Kjær, 2005). In spite of this, the invention was adopted by the aerospace industry in 1959 for use in the Vanguard 1 Satellite and successfully operated for 8 years. PV technology was then widely adopted and is now the main source of power for many satellites. For example, NASA launched the Nimbus spacecraft in 1964 with PV arrays that produced 470 W. Two years later, the Orbiting Astronomical Observatory was launched with 1 kW PV arrays. The high level of demand for PV technologies on the part of the aerospace industry has encouraged work to develop these technologies and improve their efficiency. Although the cost is not the issue for aerospace applications, other factors like weight, materials, temperature and efficiency are issues that must be considered (El Chaar, Lamont and Elzein, 2010).

The price of PVs dramatically dropped by about 80% in the 1970s, 100 $/W to 20 $/W (67 £/W to 13.3 £/W). As a result, PV technology use has widely disseminated, and many applications are currently operated by PV power, including offshore signal lights, railroad crossings and highway signs. The University of Delaware (in the United States) is the first university to build a special laboratory devoted to PV technologies. Moreover, the university built the first home powered by PV technology in 1973, connecting it to the grid to sell the extra power (Kjær, 2005).

The United States accelerated the development in PV technologies; by 1980, ARCO Solar (the Atlantic Richfield Company) would be the first group to generate 1 MW from a PV plant. Three years later (in 1983), a 6-MW plant started a new era of megawatt-scale PV usage. In the same year, PV production reached 21 MW worldwide. During this period, another success was achieved in 1985 with the increase in efficiency of the silicon PV cell to 20% (Kjær, 2005).

Starting in the 1990s, many programs were created to encourage people to use PV as their main power source; these programs included the German "100,000 roofs" PV program and the Million Solar Roofs initiative in the United States. During this time, the efficiency of the available PV technology increased to 30% for gallium

indium phosphide and gallium arsenide PV types; the CdTe thin-film PV efficiency increased to about 16% (Kjær, 2005). These circumstances helped usher in an era of greatly increased PV usage (as noted earlier, up to 177 GW). This historical review is summarised in the PV evolution timeline shown in Figure 2.1.
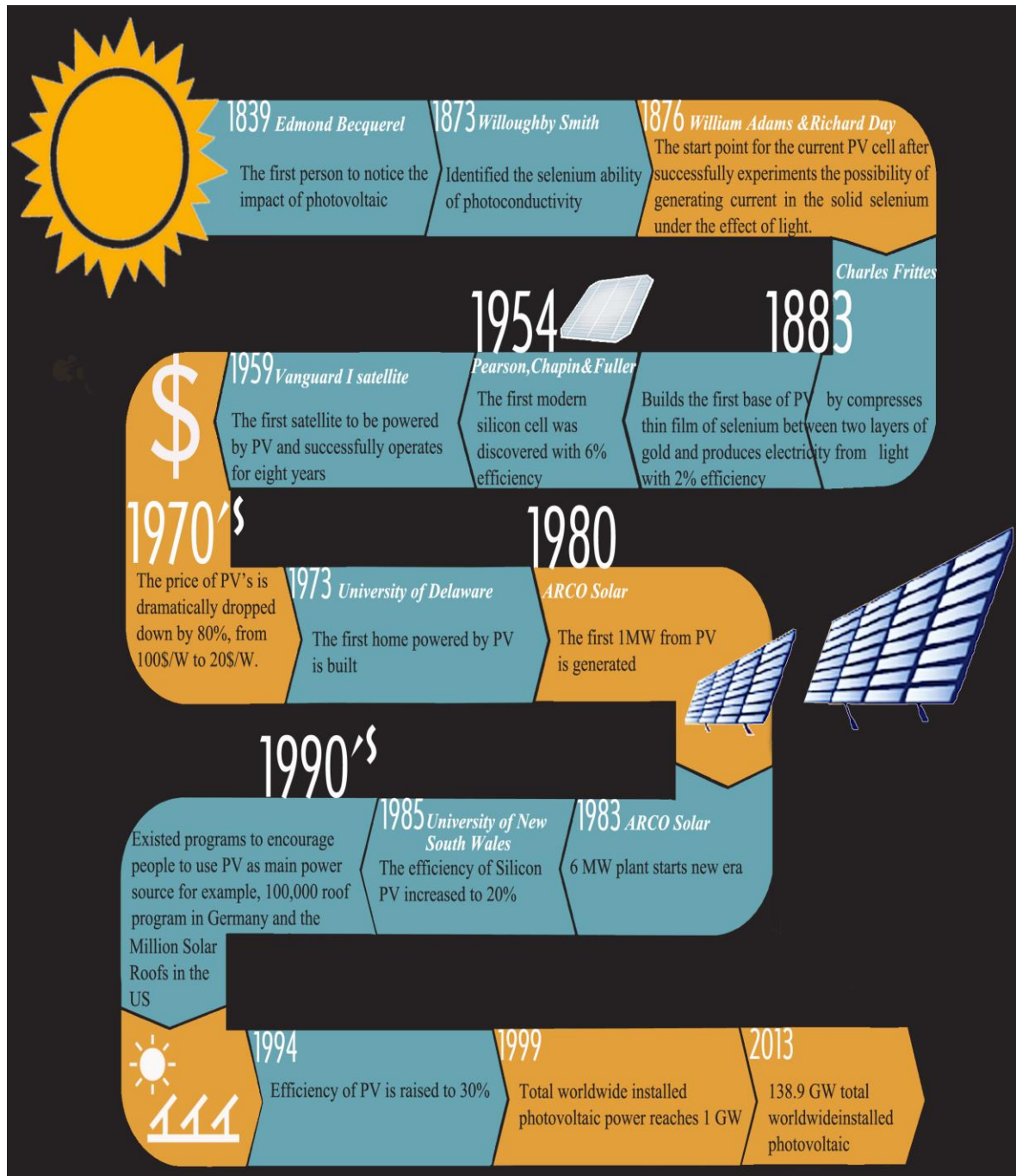
Figure 2.1: PV timeline: the evolution of PV use

2.3   Photovoltaic Model

Photovoltaic cells are the source of power that will be investigated in this thesis and are accordingly subject to detailed analysis. Figure 2.2 shows the equivalent circuit of a PV cell, which simply consists of a DC current source in parallel with a diode connected in series and parallel to two resistances R_s and R_p, respectively (Murtaza *et al.*, 2012)   .

Other published studies have adopted another model with two diodes in parallel with the DC current source, as Figure 2.3 shows (Khalifa and El-Saadany, 2011).
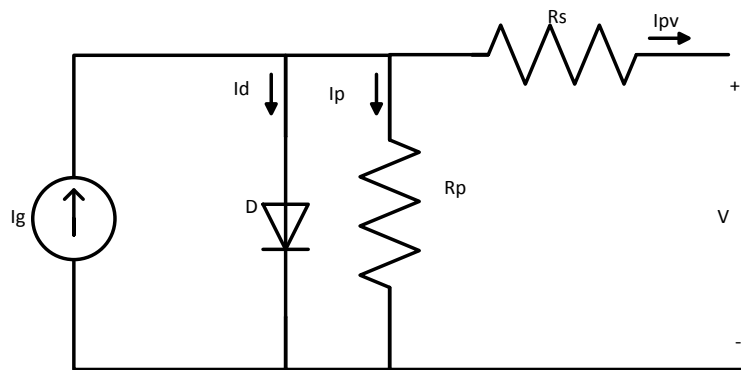
Figure 2.2: PV single diode model.
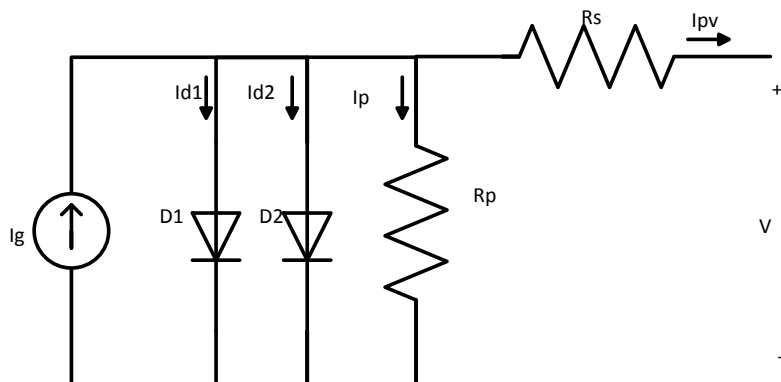
Figure 2.3: PV model with two parallel diodes

The single-diode model is simpler, has an acceptable accuracy and has been selected for study by many researchers (Barchowsky *et al.*, 2012; Khalifa and El-Saadany, 2011)   . On the other hand, for the double-diode model the nonlinearity of the model makes it challenging to develop expressions for the V-I mathematical

model. Due to these challenges, the double-diode model is not considered as frequently in the literature and is rarely implemented (See Appendix A for the mathematical model of the double diode model) (Tsai, Tu and Su, 2008). In response to this, the single-diode model is the approach adopted by this thesis. This model can be represented mathematically by obtaining the relation between I and V of this model:

$$I_{pv} = I_g - I_d - I_p$$

$$I_{pv} = I_g - I_s \left(e^{\frac{q(V+I_{pv}R_s)}{akT}} - 1 \right) - \frac{V+I_{pv}R_s}{R_p} \qquad 2.1$$

where:

I_{pv}: is the cell output current

I_g: is the current from the DC current source (the photogenerated current)

I_s: is the diode saturation current

q: is the electron charge ($1.60217646 \times 10^{-19}$ C)

k: is the Boltzmann constant ($1.3806503 \times 10^{-23}$ J/K)

T: is the diode temperature in kelvins

a: is the diode ideality constant

V: is the output PV voltage

R_s: is the resistance in series

R_p: is the resistance in parallel

The values of R_s and R_p are unknown because the relationship between them cannot be defined (as manufacturers usually consider this information to be secret). Therefore, researchers normally assume different values for them.

Assuming short-circuit current $I_{sc} = I_g$ where I_g is affected by two factors, irradiance and temperature. These factors drive a linear relationship with the current as follows:

$$I_g = \left(I_{sc,n} + K_I \Delta T \right) \frac{G}{G_n} \qquad 2.2$$

where:

$I_{sc,n}$: is the PV short circuit current at nominal conditions (T = 25°C and G = 1000 W/m^2)

K_I: is the current/temperature coefficient

ΔT: is the change in temperature

G: is the solar irradiance level

G_n: is the nominal irradiance level (1000 W/m^2)

Normally, the value of K_I is small, indicating that the PV current is essentially affected by the level of solar irradiance (Murtaza *et al.*, 2012; Khalifa and El-Saadany, 2011)   .

To calculate the reverse saturation current I_s:

$$I_s = I_{sn}\left(\frac{T}{T_n}\right)^3 e^{\left[\frac{q\,E_g}{a\,k}\left(\frac{1}{T_n}-\frac{1}{T}\right)\right]}$$

$$I_{sn} = \frac{I_{sc,n}}{e^{\left(\frac{q(V_{ocn})}{akT_n}\right)} - 1} \qquad 2.3$$

where:

E_g: is the band gap energy of the cell semiconductor

V_{oc}: is the PV open circuit voltage

T_n: nominal temperature in kelvins (298 k = 25 °C)

The temperature is the main influence on PV voltage, and high temperatures reduce the output efficiency of the PV cell.

2.4 Photovoltaic Configurations

PV systems normally consist of many cells that collectively form a module. From there, some modules connect to each other to make a PV panel. A group of such panels is called a *PV array*. These elements can be connected in series or in parallel; the goal of this connection is to obtain higher output power from the PV system. Figure 2.4 shows this process.

The classification of the PV configurations depends on how they are connected to the inverter. The four main types of inverter connections are centralised configuration, string configuration, multi-string configuration, and AC module configuration (Johns, Le and Seeman, 2009).

Cell

Module
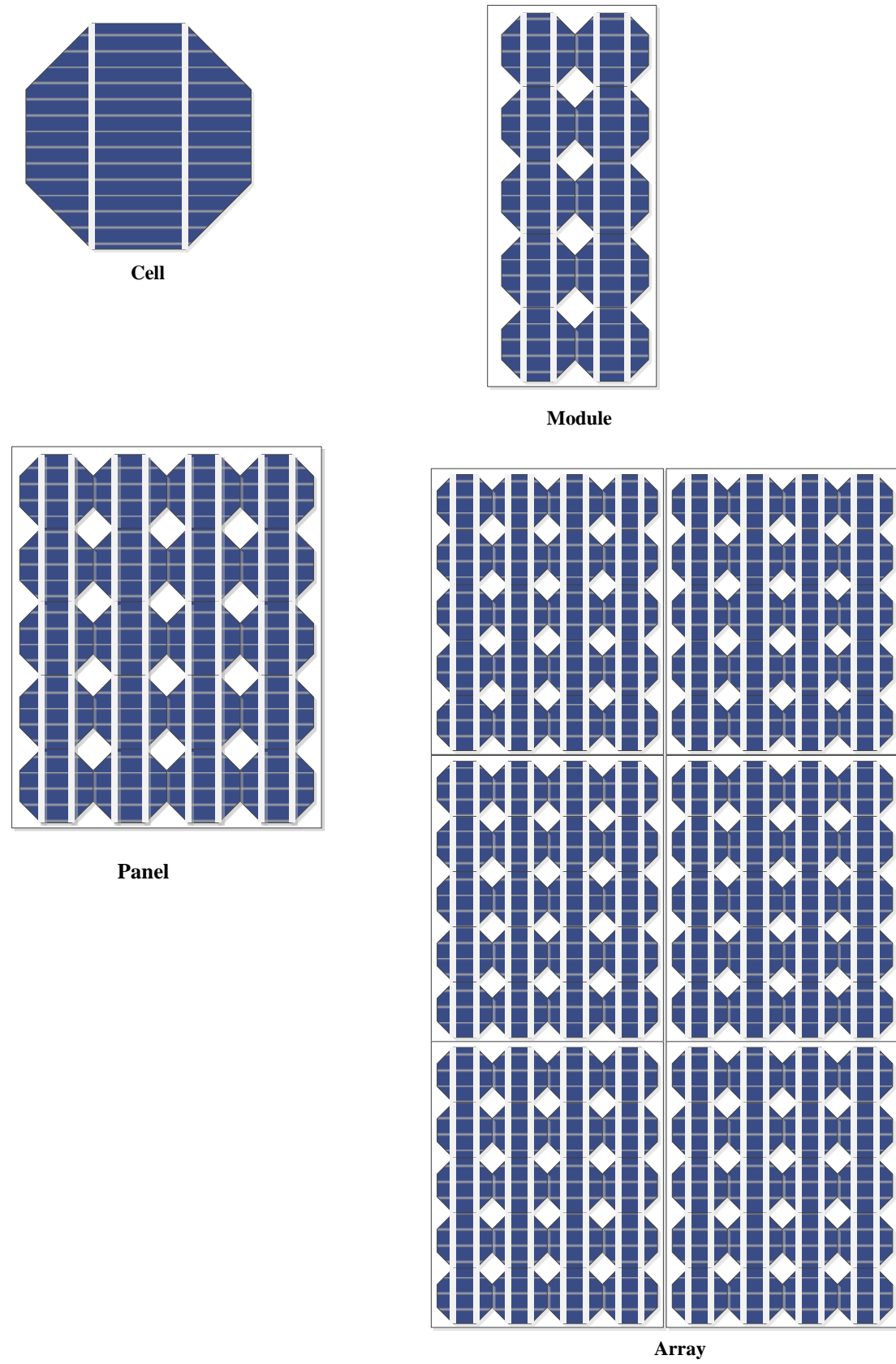
Panel

Array

Figure 2.4: Different elements of a PV system

2.4.1   Centralised PV Configuration

In a centralised PV configuration, only one inverter is used to connect all the PV arrays. Usually, a group of PV panels is connected in series and these series arrays are then connected in parallel to the inverter; see Figure 2.5. A high voltage is generated because of the series connections, avoiding the need for a separate amplification process with this arrangement. The disadvantages of centralised PV configuration include the mismatch between the PV panels, poor efficiency and reliability, the high voltage of the DC cable, losses in string diodes and the limitation of using maximum power point tracking (MPPT) (Johns, Le and Seeman, 2009).
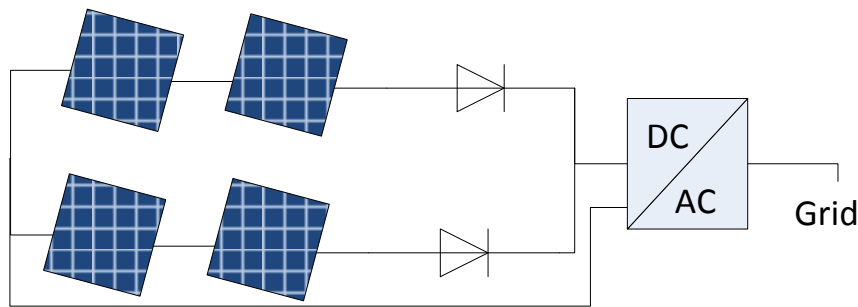
Figure 2.5: Centralised PV configuration

2.4.2   String Configuration

The string inverter shown in Figure 2.6 aims to overcome the disadvantages of the centralised configuration. In the string configuration, PV panels are connected in series to an inverter that then injects the generated power into the grid or the load. MPPT can be used to increase the efficiency of this configuration. As with the centralised module, no diode losses occur. Due to the high voltage at the inverter, a metal–oxide–semiconductor field-effect transistor (MOSFET) or insulated-gate bipolar transistor (IGBT) can be implemented (Johns, Le and Seeman, 2009).
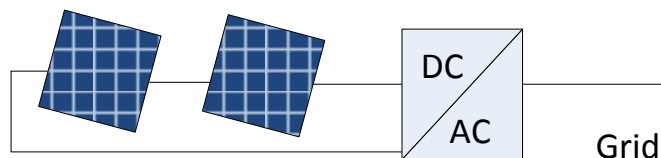
Figure 2.6: String configuration

2.4.3   Multi-string Configuration

The multi-string configuration, shown in Figure 2.7, has the ability to apply the MPPT on each individual string, making the configuration more efficient than the string configuration but at additional cost. The DC-DC converters afford this option with the value of being able to combine strings at different power rates or connection methods (Johns, Le and Seeman, 2009).
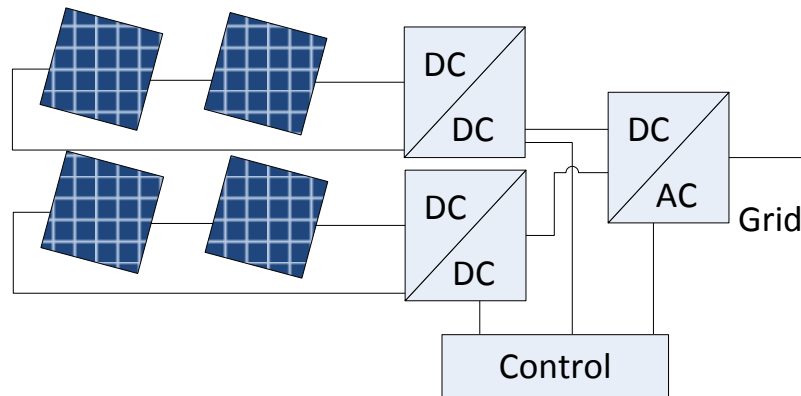
Figure 2.7: Multi-string configuration

2.4.4   AC module Configuration

The AC module Figure 2.8, is the combination of a PV and an inverter in one device. Each PV has its own MPPT, overcoming the mismatch between PVs that is considered a major problem with each of the previous configurations and leading to a more efficient PV system. Although the AC module is costly, it is definitely worthwhile to consider it as part of a mass production process and could help reduce prices overall. This solution is perfect for residential applications where weather conditions are more likely to affect the surfaces of the PV cells and panels. The output of this integrated module comes with a plug that can be easily connected to any device, with no need to consult an expert or an individual with technical prowess to perform the connections (Johns, Le and Seeman, 2009).
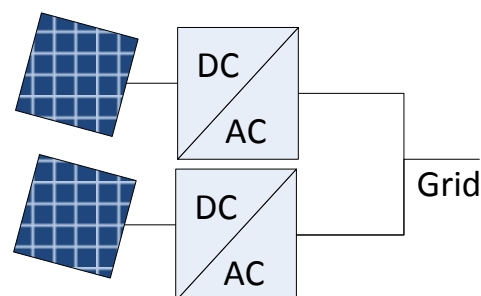
Figure 2.8: AC module configuration

2.5   General Comparison of PV Configurations

Table 2-1 gathers the four PV configurations discussed in the previous section and compares them on four factors: MPPT, voltage level, diode losses and mismatch losses.

Table 2-1: Comparison of the different PV configurations

PV Configuration	MPPT	Voltage level	Diode losses	Mismatch losses
Centralised	NO	HIGH	YES	YES
String	Limited	HIGH	NO	YES
Multi-String	YES	L & H	NO	YES
AC-Module	YES	LOW	NO	NO

2.6   Maximum Power Point Algorithms

The use of renewable energy resources has grown considerably during the past four decades. Photovoltaic energy, one of these sources, is free and can be transformed easily to electricity. One of the main obstacles to the use of PV energy is its high cost and low conversion efficiency. The output power of a PV system is nonlinear and is affected by weather conditions, irradiation and temperature. Figure 2.9 shows the power–voltage (P–V) characteristics of the PV, including the clear nonlinearity between the operating voltage and the output power. This figure also shows that only one exact operational point exists where the PV exhibits ideal behaviour and delivers maximum power. Therefore, maximum power point tracking (MPPT) was invented to extract the maximum power from each PV array. Figure 2.10 shows the utilisation of the MPPT in the PV system (Hussein *et al.*, 1995)   .

Together with low conversion efficiency, MPPT has encouraged researchers to conduct studies in order to detect the maximum power point (MPP) at different weather conditions. It is self-explanatory that the output of a PV panel changes with changes in the weather. Figure 2.9 shows the P–V characteristics of a typical PV unit for several irradiance levels.

Many methods have been introduced to track the MPP. These methods can be classified in several ways depending on their complexity, the measurements required, cost, tracking speed and other factors. In some cases, the method used may not be the most effective method in general applications, but could be the most efficient technique for specific application (Ngan and Tan, 2011).
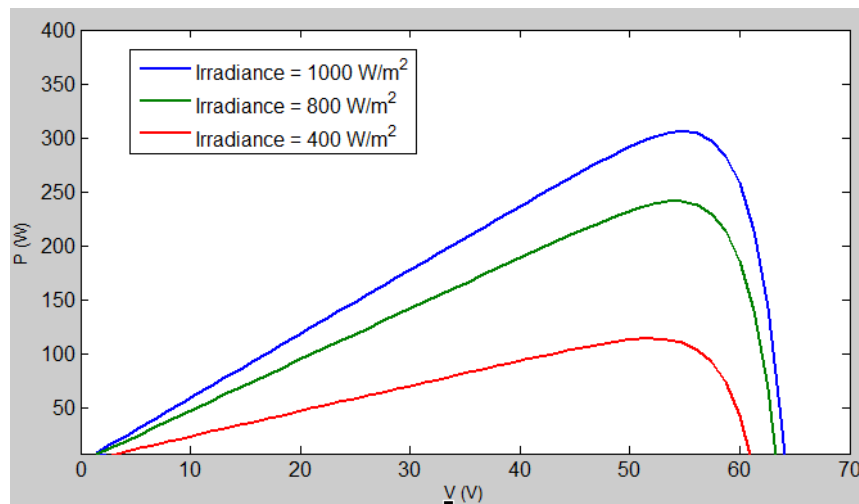
Figure 2.9: P–V Characteristics of PV module at different irradiance
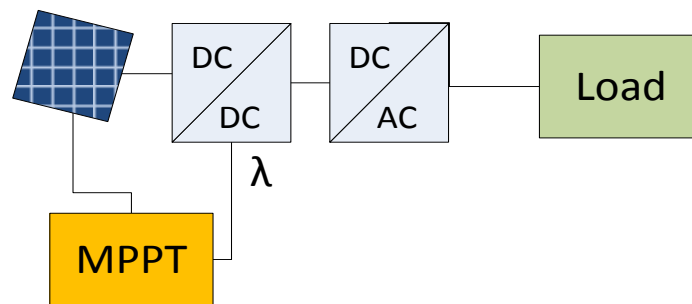
Figure 2.10: A block diagram showing MPPT implementation

2.6.1   Perturb and Observe Algorithm

The Perturb and Observe (P&O) algorithm, which only measures the Voltage (*V*) and Current (*I*) of the PV array, is the most common one used because of its simplicity and low-cost implementation (Salas *et al.*, 2006)   . The P&O algorithm captures the MPP by perturbing the operating voltage and calculating the output power at that point, then comparing it with the previous value. If the new power value is higher, the tracking is in the correct direction and the perturbation process will continue at the same direction. Conversely, if the power measured at the new

operating point decreases so that the MPP is not tracking with (behind) the current voltage, the tracking process should be reversed for the next perturbation (Jung *et al.*, 2005)   (Femia *et al.*, 2005)   . Figure 2.11 shows how the P&O method works.
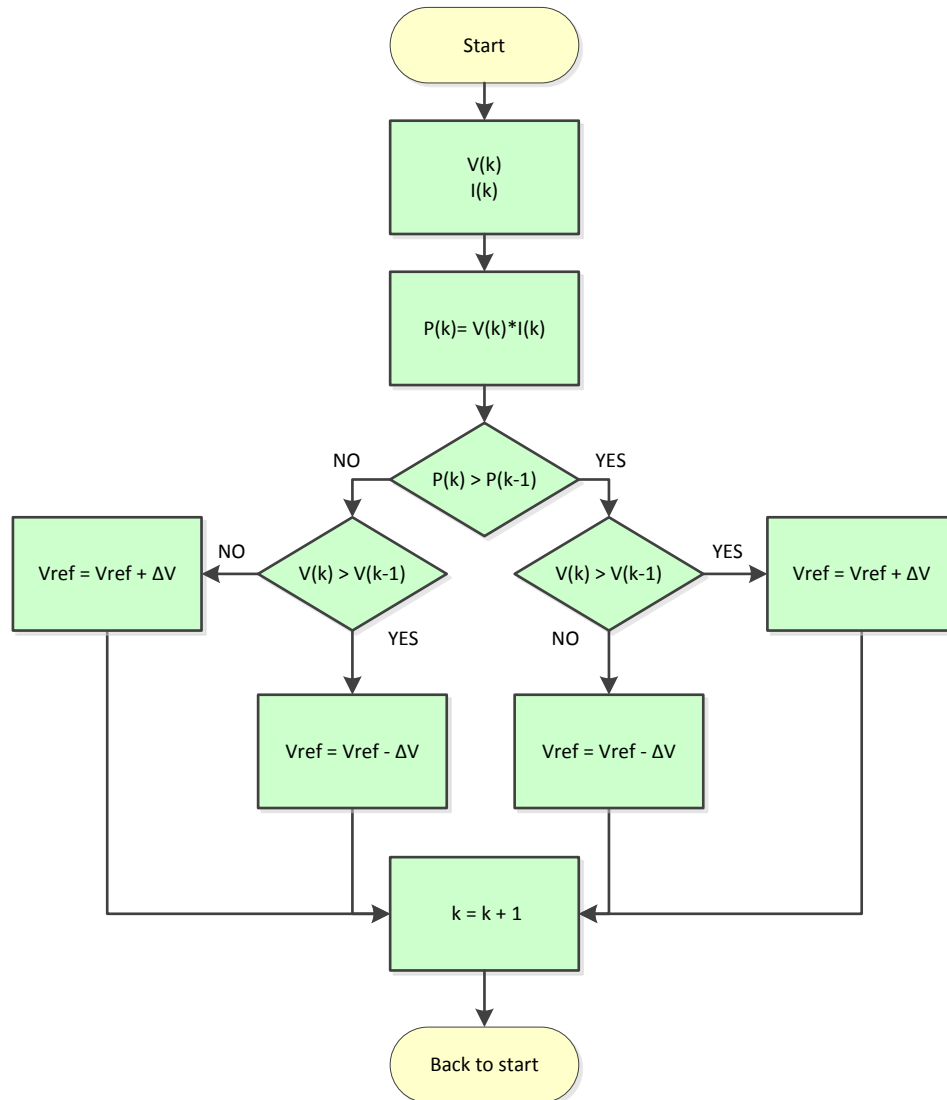
Figure 2.11: P&O algorithm (Femia *et al.*, 2005)

Perturb and observe methods have two primary drawbacks. The first is the oscillation around the MPP at steady state, which wastes energy (Wu *et al.*, 2003)   . Using a small perturbation value helps minimise the energy losses attributable to oscillation, but significantly slows the tracking progressions. Improved versions of P&O methods exist to overcome this oscillation problem. For example, one study suggested a changeable perturbation rate that starts high and decreases as it converges on the MPP (Xiao and Dunford, 2004). A pair of other studies suggested variable

values for the perturbation introduced with the P&O method (Al-Amoudi and Zhang, 1998) (Hua and Lin, 2001).

The second disadvantage is the low quality tracking during rapidly changing weather conditions. The MPPT moves away from the real MPP due to the quick change in the weather conditions as Figure 2.9 shows how the operating point moves when the irradiance level changes instantly from 400 W/m^2 to 1000 W/m^2 (Femia *et al.*, 2005)   . The algorithm cannot verify if the new output power value is higher because of the new irradiation amount or because of the value of the new duty cycle. For example, if the perturbation at a point 'k' is on the left side of the MPP, the next perturbation will decrease the duty cycle towards the MPP:

$$d(k + 1) = d(k) - \Delta d \qquad\qquad 2.4$$

For example (and using 2.4) Figure 2.12 shows that the operation point moves from point 'A' at time k to point 'B' at $k + 1$ if the irradiance is constant. However, if the irradiance is changed (increased), the operation point at $k + 1$ will be 'C' instead of 'B'. In this case, the algorithm will behave normally and the tracking process will not be confused because both values ('B' and 'C') are less than 'A', so the tracking will revert back toward the MPP with the positive duty cycle value. The next perturbation will increase the voltage toward the MPP:

$$d(k + 1) = d(k) + \Delta d \qquad\qquad 2.5$$

Figure 2.13 shows another example where the P&O method may provide confounding results. According to (2.5), at a constant irradiance the operation point moves from 'A' to 'B' so the perturbation after that will approach 'A' to the MPP. On the other hand, if the irradiance is changed rapidly the output power curve will shift up and the new operation point at $k + 1$ will be 'C'. The problem is that the algorithm is not able to account for the changing weather; it cannot differentiate between a new output power value that is the result of changes in the duty cycle versus changes in the irradiance. In other words, the algorithm does not know if the value at $k + 1$ is point 'B' or 'C'. In this case, the algorithm has moved from 'A' (positive value) to 'C' (a higher positive value), so it will keep going in the same direction, moving away from the MPP. The P&O here is confused by the fact that the higher value of 'C' exceeds that of 'A'; this is caused by the rapid changes in irradiance. To summarise this

problem, the algorithm is not intelligent enough to differentiate between the potential causes of increases in power.
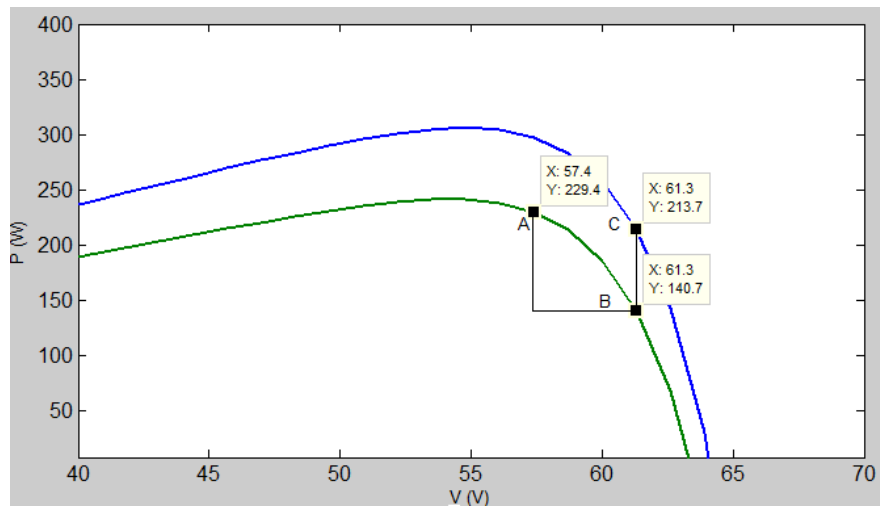
Figure 2.12: Losing the MPP with rapid changes in weather conditions
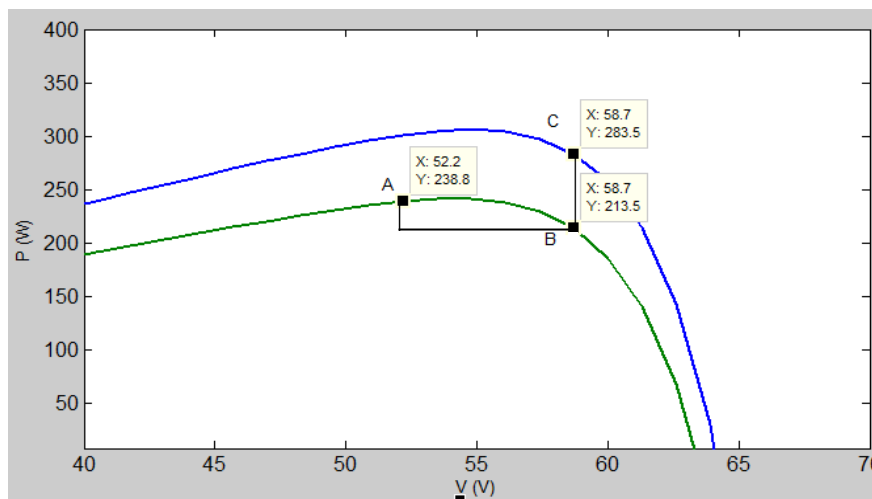
Figure 2.13: Losing the MPP with rapid changes in weather conditions

2.6.2   Incremental Conductance

The incremental conductance method, one of the most commonly used MPPT techniques, is based on the fact that the derivative of the PV power with respect to its output voltage is zero at the MPP. The derivative is positive on the left of the MPP and negative on the right (Alsadi and Alsayid, 2012; Esram and Chapman, 2007), as given by:

$$\frac{dP}{dV} = 0, \ at \ MPP \qquad\qquad 2.6$$

$$\frac{dP}{dV} > 0, \textit{ left of MPP} \qquad\qquad\qquad 2.7$$

$$\frac{dP}{dV} < 0, \textit{ right of MPP} \qquad\qquad\qquad 2.8$$

To make the previous equations (2.6, 2.7, and 2.8) easy, solvable and usable, 2.9 can be used:

$$\frac{dP}{dV} = \frac{d(IV)}{dV} = I + V\frac{dI}{dV} = I + V\frac{\Delta I}{\Delta V} = 0 \qquad\qquad 2.9$$

From Equation 2.9, we can rewrite equations (2.6, 2.7 and 2.8) as follows:

$$\frac{\Delta I}{\Delta V} = -\frac{I}{V}, \textit{ at MPP} \qquad\qquad\qquad 2.10$$

$$\frac{\Delta I}{\Delta V} > -\frac{I}{V}, \textit{ left of MPP} \qquad\qquad\qquad 2.11$$

$$\frac{\Delta I}{\Delta V} < -\frac{I}{V}, \textit{ right of MPP} \qquad\qquad\qquad 2.12$$

The incremental conductance is able to track the MPP by knowing the instantaneous value of the PV's current and voltage and compare it with the incremental conductance, as shown by Equations (2.10), (2.11) and (2.12). The algorithm adjusts itself by setting the power converter duty cycle, which controls the array voltage by increasing or decreasing it as needed until the MPP is reached. When the array delivers at the MPP, the tracking process stops and the operation remains steady until a change in the current is sensed, indicating that atmospheric changes have taken place. At that time, another tracking cycle starts and continues until the MPP is reached once more.

The user adjusts the interval between each increment. A small interval allows for accurate tracking, but with longer tracking time. On the other hand, a larger interval leads to quicker tracking, but with less accuracy near the MPP and the drawback of oscillation (Esram and Chapman, 2007). A solution to this problem is by dividing the tracking into two stages. During the tracking at the first stage, a different method is used to allocate the operation near the MPP; the second stage applies the

incremental conductance method with lower incremental values to provide accuracy around the MPP (Kobayashi, Takano and Sawada, 2006; Irisawa *et al.*, 2000)   .

The incremental conductance method demands two sensors to measure the instantaneous values for the voltage and current. Furthermore, this tracking method can be applied using a digital signal processor (DSP) and microcontroller, which have the ability to save the current and past values and make the proper decision based on the algorithm in Figure 2.14 (Kuo, Liang and Chen, 2001).
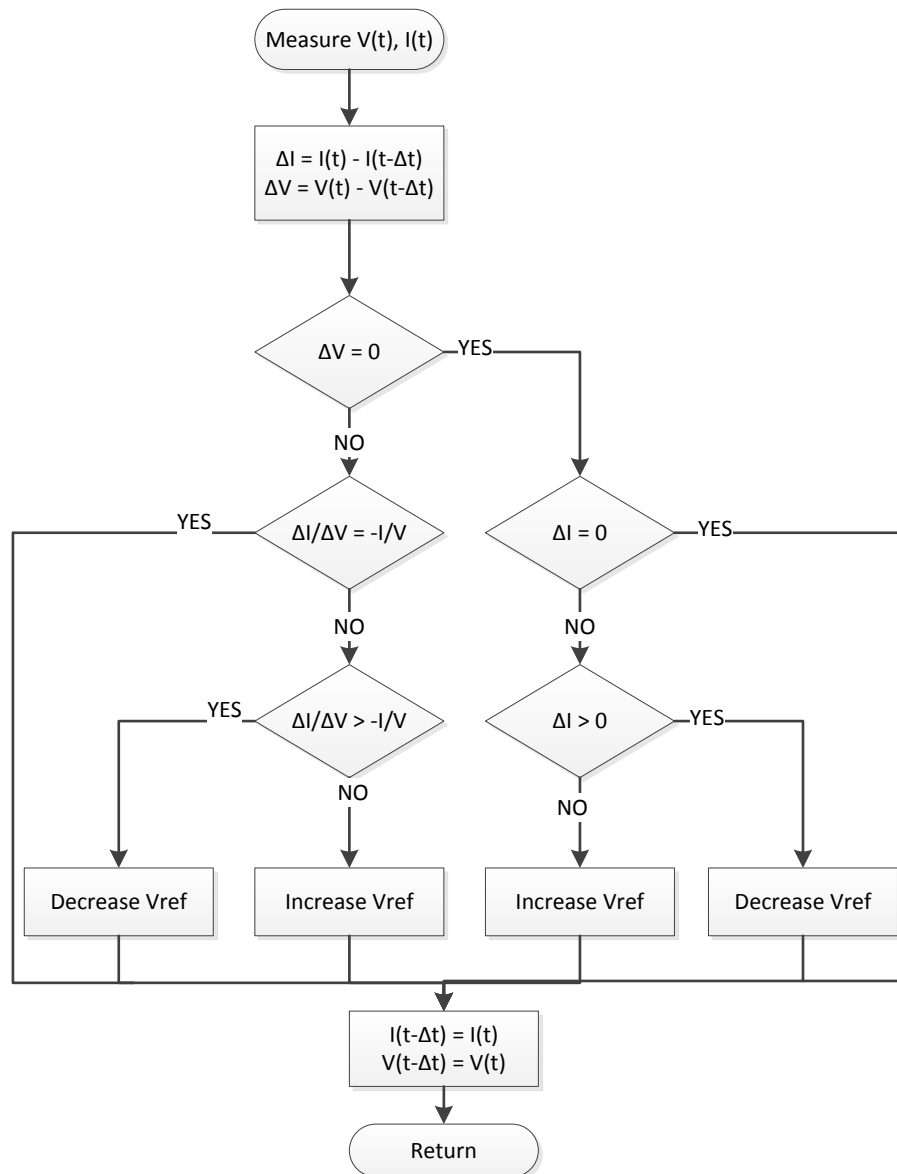
Figure 2.14: Flowchart of the Incremental Conductance method

2.6.3   Fractional Short-circuit Current

This method is based on the fact that the PVs' I_{mpp} and I_{sc} share a near-linear relationship even if the weather conditions are changing (Hart, Branz and Cox Iii,

1984a; Schoeman and Van Wyk, 1982). This relationship is defined by the following equation:

$$I_{mpp} \approx k_1 I_{sc} \qquad\qquad 2.13$$

where k_1 is a constant that can be adjusted depending on the PV characteristics between 0.78 and 0.92 (Esram and Chapman, 2007). I_{sc} is measured regularly to maintain the power delivery at the MPP under changing weather conditions by adding a switch to the circuit to shorten the PV array. This addition adds components and cost to the system; moreover, a power loss occurs each time the switch shorts the circuit. One approach that has been described to overcome these issues is to use the converter switch to obtain the value of I_{sc} (Yuvarajan and Xu, 2003a). Along with the increase in cost, another disadvantage is that the PV array will never operate at the MPP because (2.13) is an approximation. (Noguchi, Togashi and Nakamoto, 2000) invented a way to improve the accuracy of the I_{mpp} value by changing the rate of k_1 based on the current atmospheric conditions. Although the fractional short-circuit current method has the previous enumerated disadvantages, it remains useful because it is easy to implement and economical (Esram and Chapman, 2007).

2.6.4   Fractional Open-circuit Voltage

The PVs' V_{mpp} and V_{oc} share an almost linear relationship whatever the weather conditions are. This insight has driven the existence of a fractional open-circuit voltage method (Masoum, Dehbonei and Fuchs, 2002; Hart, Branz and Cox Iii, 1984a; Schoeman and Van Wyk, 1982). Moreover, this relation between V_{mpp} and V_{oc} has been identified by the following equation:

$$V_{mpp} \approx k_2 V_{oc} \qquad\qquad 2.14$$

where k_2 is a constant factor that varies from one PV to another depending on its characteristics and on the weather conditions. The value of k_2 is between 0.71 and 0.78 according to (Esram and Chapman, 2007) and ranges from 0.7 to 0.8 according to (Ahmad, 2010).

The power losses that occur due to the need to cut power periodically to measure V_{oc} are the main drawback to this method (Ahmad, 2010). One potential solution is to use different PV arrays with the same characteristics and under the same weather conditions, allowing a reference point for the measurement of V_{oc} (Hart,

Branz and Cox Iii, 1984b). Another improvement introduced by this method is the fact that the voltage around the diode is approximately 75% of V_{oc} so V_{oc} does not need to be measured (Kobayashi, Matsuo and Sekine, 2004).

The fractional open-circuit method adjusts the V_{oc} by applying the equation (2.14), although the V_{mpp} is approximated, so MPP practically is never achieved. On the other hand, the simple and cost-effective nature of this technique makes it desirable.

2.6.5 Fuzzy Logic

Fuzzy logic controllers became part of the world of PV technologies as a new artificial intelligence MPPT method and benefit from the introduction of microcontrollers in the PV system (Patcharaprakiti, Premrudeepreechacharn and Sriuthaisiriwong, 2005). This method has the advantage of being able to deal with nonlinear equations and operate with inaccurate inputs. The measurements needed for this method are error (E) and change of error (ΔE). On the other hand, the output is a change of the converter's control signal (Veerachary, Senjyu and Uezato, 2003).

The fuzzy logic method works through three stages: fuzzification, rule-based table lookup and defuzzification. In the first stage, fuzzification, the inputs are converted from numerical to linguistic variables based on a membership function. These variables are adjusted by the user, who may scale it into five levels (as in Figure 2.15). Those levels are: negative big (NB), negative small (NS), zero (Z), positive small (PS) and positive big (PB) (Simoes, Franceschetti and Friedhofer, 1998). For more accuracy, some researchers have adapted a seven-level input and output membership function (Patcharaprakiti, Premrudeepreechacharn and Sriuthaisiriwong, 2005).
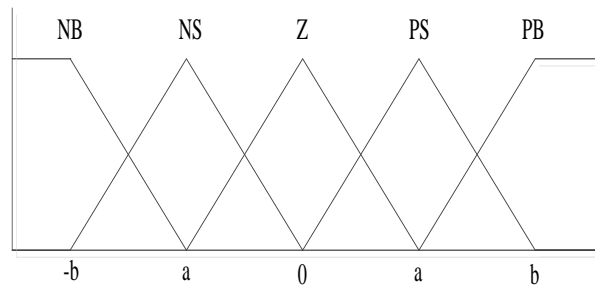
Figure 2.15: Membership function of the fuzzy logic controller

Based on the fact that at MPP dp/dv = 0, the following equations have been adapted by (Khaehintung *et al.*)   :

$$E(n) = \frac{P(n) - P(n-1)}{V(n) - V(n-1)}$$ 2.15

$$\Delta E(n) = E(n) - E(n-1)$$ 2.16

where ΔE and E are converted to linguistics variables in the fuzzification stage after calculation. In the second stage, the action required is taken based on a rule table (see Table 2-2). The controller output is a duty cycle change (ΔD) of the DC-DC converter (Won *et al.*, 1994)   .

Table 2-2: Fuzzy logic rule base table as shown in (Won, Kim et al. 1994)

E \ ΔE	NB	NS	ZERO	PS	PB
NB	ZERO	ZERO	NB	NB	NB
NS	ZERO	ZERO	NS	NS	NS
ZERO	NS	ZERO	ZERO	ZERO	PS
PS	PS	PS	PS	ZERO	ZERO
PB	PB	PB	PB	ZERO	ZERO

Justifying the rule-based table and the membership function is dependent on the knowledge and experience of the user. In the last stage, defuzzification, the output is transformed to a numerical base again, as in Figure 2.15. This output changes the duty cycle and force the PV to operate at the MPP.

One clear disadvantage of the fuzzy logic model is that successful implementation relies on the amount of knowledge of the expert who sets up the

membership function and the rule-base table. In (Patcharaprakiti, Premrudeepreechacharn and Sriuthaisiriwong, 2005), an adaptive fuzzy logic controller was proposed based on a learning mechanism to regularly change the membership function and the rule base table; which showed higher performance than the conventional method. Another improved version adapts two different membership functions that experimentally show better tracking performance (Veerachary, Senjyu and Uezato, 2003).

2.6.6   Neural Networks

Neural networks are another type of artificial intelligence MPPT technique that use microcontrollers to great advantage. As with a fuzzy logic controller, neural networks consist of three stages or layers: input, output, and hidden layers between these layers where the processing takes place (block diagram is shown in Figure 2.16). The user has the flexibility to choose the number of nodes in each stage. For input variables, the user may choose the PV's V and I, the temperature, or any other wanted data. After these inputs are processed in the hidden stage, the output most likely is a duty cycle signal to control the power converter and change the operating voltage to be as close as possible to the MPP (Esram and Chapman, 2007).
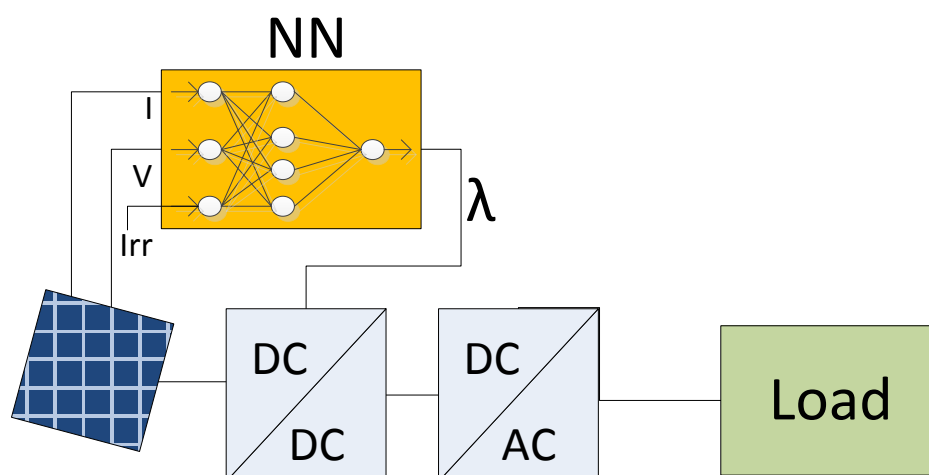
Figure 2.16: Neural network method

The neural network method needs to be well trained to perform at a high quality and operates at the MPP. This training happens on a long run where all the PV data is recorded continuously over months or even years into the neural network database. The relationships between the inputs and outputs are obtained and recorded. The result of this training is the algorithm in the hidden layer where every link between the points is weighted precisely. Each PV array has its unique characteristics, so the neural network controller must be trained for each array separately. Moreover, the weather conditions and age of the PV array are changeable factors that affect the characteristic of the array; therefore, neural networks should be trained regularly to maintain high quality tracking (Hussein *et al.*, 2002; Sun *et al.*, 2002; Hiyama, Kouzuma and Imakubo, 1995)   .

2.6.7 Current Sweep

The current sweep method periodically draws the PV's current waveform and uses that waveform to operate the PV array at the MPP. The *Vmpp* is computed and driven from that curve. This operation takes about 50 ms and no power is delivered at that time. The chosen function for the current waveform is proportional to its derivative, as in

$$i(t) = f(t) = k4 \, \frac{df(t)}{dt} \qquad\qquad 2.17$$

where k4 is constant.

The output power of the PV array is;

$$p(t) = v(t) \times i(t) = v(t) \times f(t) \qquad\qquad 2.18$$

At the MPP the derivative of *P* should equal zero:

$$\frac{dp(t)}{dt} = v(t) \frac{df(t)}{dt} + f(t) \frac{dv(t)}{dt} = 0 \qquad\qquad 2.19$$

By putting the value of *f(t)* into equation (2.12) so:

$$\frac{dp(t)}{dt} = \left(v(t) + k4 \, \frac{dv(t)}{dt} \right) \frac{df(t)}{dt} = 0 \qquad\qquad 2.20$$

Assuming the derivative of *f(t)* does not equal zero on the sweep waveform and by dividing equation (2.20) by *df(t)/dt* so:

$$\frac{dp}{di} = v(t) + k4\frac{dv(t)}{dt}$$
2.21

the only solution for equation 2.17 is

$$f(t) = C\ e^{\frac{t}{k4}}$$
2.22

where C is a selected to be the maximum current of the array and k4 is a negative value. The current can be measured by discharging a capacitor. This method cannot track the MPP continuously, but it does so periodically and the interval time can be adjusted as requested. Another consideration is that the increase of the output power should be greater than the losses in power due to the sweeping and manipulating of the PV current (Esram and Chapman, 2007; Bodur and Ermis, 1994).

2.6.8 Ripple Correlation Control (RCC)

Normally a DC-DC power converter is connected to any PV array to track the MPP and step up the voltage. However, these switching pulses generate current and voltage ripple in the array. As a result, the output power of the PV array is affected and contains some ripple. This MPPT method relies on the advantages of the existence of the ripple by calculating the derivative of the PV time-varying power $\dot{p}$ with PV time-varying current $\dot{i}$ or voltage $\dot{v}$ with respect to time t. The MPP is located where the power gradient equals zero (Midya *et al.*, 1996)   .

If a boost converter is used, the PV current will increase and the voltage will decrease whenever the duty cycle increases. Consequently, the value of the duty ratio is:

$$d(t) = -k_3 \int \dot{p}\,\dot{v}\ dt$$
2.23

or

$$d(t) = k_3 \int \dot{p}\,i\ dt$$
2.24

where k_3 is a positive constant (Esram and Chapman, 2007).

An experiment with an analog circuit showed fast and accurate tracking for the RCC under fluctuating weather conditions. Another positive element of RCC is

the independence of the PV's characteristics, making it easily applicable for any PV (Midya *et al.*, 1996)   .

2.6.9   DC Link Capacitor Drop Control

This method is applicable for PVs that are connected in parallel with an AC line, as Figure 2.17 shows. The boost converter duty ratio is given by:

$$d = 1 - \frac{V}{V_{link}} \qquad\qquad 2.25$$

where V is the PV's operating voltage and V_{link} is the voltage around the capacitor. By keeping V_{link} constant, this technique optimised the duty cycle to export higher current from the PV and maximise power delivery. In comparison to some of the other MPPT methods, this method does not require advanced computing skills or power calculations. Rather, the method can easily be implemented using analog amplifiers and logic unit (Kitano, Matsui and Xu, 2001).
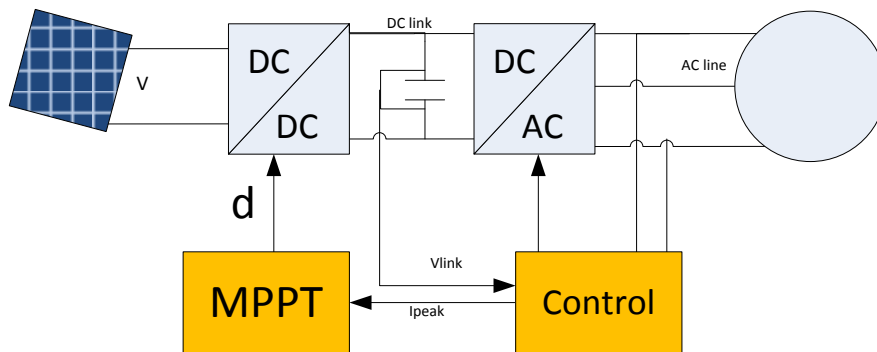
Figure 2.17: Block diagram of DC link capacitor drop control technique

2.6.10 Load Current Maximization

This MPPT method is based on the fact that maximising the power at the load maximises the PV output power. The load could be a voltage or current source, a resistive load or a mix of different types. If we take the voltage source, the battery, as an example, the voltage remains constant and the charging current must be maximised until the PV operates at the MPP. For current sources, the same process is required but through controlling the output voltage. This technique when used with any load

types works best with only one sensor to maximise the power delivery of the PV. Usually a feedback controller is used with this technique to control the converter and the operation is near the MPP, but never at the MPP (Arias *et al.*, 2004; Enslin and Snyman, 1992b)   .

2.6.11 *dp/dv* Feedback Control

Simply, this method benefits from the advantage of the microcontroller and DSP in dealing with complex calculations, affording the opportunity of computing the *dp/dv* curve from the PV characteristics curve. In addition, the MPPT can be conducted by feeding the curve back to the converter and applying some control to drive *dp/dv* to zero (Hou *et al.*, 2004; Bhide and Bhat, 1992)   . Shaping the curve can be done using different techniques. In (Bhide, Bhat 1992), a few cycles are computed and stored; each cycle has a unique sign. Then, the MPP is reached after the controller optimises the duty ratio depending on these signs ordering the converter to either increase or decrease. Sugimoto and Dong (1997) adapted a linearisation-based approach in order to form the *dp/dv* curve. Another methodology is adapted by (Hou *et al.*, 2004; Chiang, Chang and Yen, 1998)   where they converted the collected data and used a subsequent digital division of *P* and *V* trying to estimate *dp/dv*. The tracking time is around 10 milliseconds (Sugimoto and Dong, 1997).

2.7   Comparison of Different MPPT Techniques

To summarise the MPPT techniques, Table 2-3 compares all the techniques that presented in this chapter. The comparison includes the MPPT ability to spot the exact MPP, the need for regular adjusting, the tracking speed, technology used, complexity and finally the sensed variables.

Table 2-3: Comparison of the MPPT techniques

MPPT Technique	Exact MPPT	Regular adjusting	Tracking speed	Analog or Digital	Complexity	Sensed variables
Perturb and Observe	Yes	No	Differs	Both	Low	V, I
Incremental conductance	Yes	No	Differs	Digital	Medium	V, I
Fractional short-circuit current	No	Yes	Medium	Both	Medium	I
Fractional open-circuit voltage	No	Yes	Medium	Both	Low	V
Fuzzy logic	Yes	Yes	Fast	Digital	High	Varies
Neural network	Yes	Yes	Fast	Digital	High	Varies
Current sweep	Yes	Yes	Slow	Digital	High	V, I
Ripple Correlation Control	No	No	Fast	Analog	Low	V, I
DC link capacitor drop control	No	Yes	Medium	Both	Low	V
Load current maximisation	No	No	Fast	Digital	Low	V, I
dp/dv feedback control	No	No	Fast	Digital	Medium	V, I

2.8 Summary

This chapter provided a general view of PV history, the mathematical model, the existing configuration and the MPPT algorithms. First, a brief historical view about the foundation and development of the PV was presented. Second, the PV cell was analysed and mathematically modelled, followed by justification of the various PV configurations, with advantages and disadvantages presented to each configuration. A comparison table enabling side-by-side comparison of the configurations concluded this portion of the chapter. In the chapter's last part, MPPT was reviewed, including its definition, purpose and the different algorithms implemented. Each of the most useful methodologies is presented and supported by flowcharts or diagrams. Finally, a comparison table sums up the important information about the MPPT algorithms. Chapter 3 discusses the PV converter topologies.

Chapter 3

PV Converter Topologies

Chapter 3. PV Converter Topologies

3.1 Overview

This chapter covers one of the main components of the PV systems, the DC-DC power converter. This section illustrates the importance of studying the power converter, the objectives of using them and the different types of converter being used. Then, each type is discussed from many vantage points, including functionality, block diagrams, mathematical models, and so forth. Finally, a comparison of the different types of converter in accessible (tabular) form is presented, and the chapter closes with a summary.

3.2 PV Converter Topologies

The high demand for PV cells and arrays as sources of energy has encouraged researchers to work on developing the technology and making it more reliable, cheap, and highly efficient (Blaabjerg, Chen and Kjaer, 2004). One potential course of action for maximising efficiency would be to study an entire PV system and maximise the efficiency of each single component. Figure 2.11 shows the block diagram of the PV system, which consists of a PV panel, an MPPT unit, a DC-DC converter, and the AC-DC converter.

The PV's output power is changed by weather conditions (Zhao *et al.*, 2012) . Additionally, the output voltage is sometimes very low when the source is a single or a few PV panels. Therefore, the DC-DC converter plays a major part in the PV system configuration, executing the roles of stepping up and regulating the voltage, tracking the MPPT and delivering the maximum preserved power (Zhao *et al.*, 2012; Khalifa and El-Saadany, 2011; Skretas and Papadopoulos, 2009)   .

Stepping the voltage up or down through the converter is usually achieved by controlling the switch's on and off time. In addition, this control can be conducted at a normal or high frequency. The ratio between T_{on}, when the converter's switch is closed, and T_{off}, when the converter's switch is open, is called the *converter's duty cycle*. Therefore, the duty cycle can be calculated from Equation 3.1.

$$D = \frac{T_{on}}{T_{off} + T_{on}} = \frac{T_{on}}{T} \qquad\qquad 3.1$$

In an ideal situation, the output power equals the input power; however, in practice power loss is expected due to switching loss (Hart, 2011; Enrique *et al.*, 2007)   .

Generally speaking, three different types of power converters are most frequently used within a given PV system: a buck converter, a boost converter, and a buck-boost converter (Mocci and Tosi, 1989).

3.2.1   Buck Converter in a PV System

A buck converter is a device which steps down the input voltage and gains a lower output voltage. Both input and output are DCs and share the same polarities (Simonsen, 2009). Figure 3.1a shows the buck converter circuit.
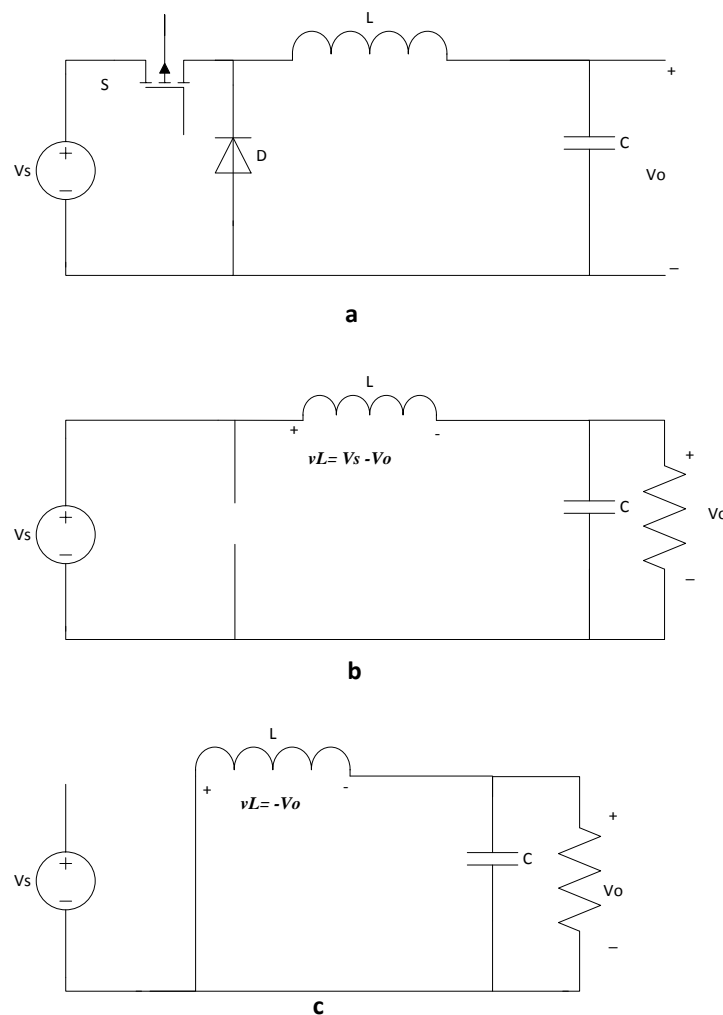
Figure 3.1: Buck converter circuit

As Figure 3.1a shows, the switch is connected to an LC low-pass filter, which aims to minimise the output fluctuating. However, the value of L and C must be picked sensibly to achieve the optimal design. Moreover, the diode in the circuit offers an easy path for the stored energy in the inductor to be released when the switch is open (Hart, 2011).

To clearly analyse the buck converter, the circuit will be represented twice depending on the switch status. The inductor current will be evaluated and the relationship between the converters' input and output will be studied. However, these assumptions are to be considered beforehand:

1. The capacitor has a huge volume.
2. The converter functions at steady state.
3. The inductor has a continuous current.
4. The switching period is T_s, and DT_s is the time when the switch is ON and $(1 - D)T_s$ is the time when the switch is OFF.
5. All components are ideal.
6. Input voltage is V_s, and output voltage is V_o, and both are constant.

When the switch is on, the equivalent circuit is shown in Figure 3.1b; the inductor current will linearly increase as V_s continues to supply the load. In this case the diode is reverse-biased and no energy will go through it. The equivalent circuit will look like Figure 3.1c when the switch is off. The stored current in the inductor will pass through the diode, which acts as a forward-biased diode in this case, causing the current to decrease. The voltage across the inductor is

$$v_L = L \frac{di_L}{dt} \hspace{4cm} 3.2$$

and

$$v_L = V_s - V_o \quad \textit{if the switch is On} \hspace{2cm} 3.3$$

$$v_L = -V_o \quad \textit{if the switch is Off} \hspace{2.5cm} 3.4$$

The early assumption that the converter functions at steady state requires that the inductor current be the same at the beginning and end of the switching cycle, and

the changing of the inductor current remains the same for both switching states (Hart, 2011; Simonsen, 2009).

$$(\Delta i_L)_{on} = -(\Delta i_L)_{off} \qquad\qquad 3.5$$

By combining equations 3.2, 3.3 and 3.4 into equation 3.5 the equation can be represented as:

$$(\frac{V_s - V_o}{L})DT_s = -\frac{V_o}{L}(1 - D)T_s$$

$$(V_s - V_o)DT_s = V_o(1 - D)T_s \qquad\qquad 3.6$$

Therefore the relationship between the input and output voltage is:

$$V_o = V_s D \qquad\qquad 3.7$$

where: D is the duty cycle.

The output voltage of the buck converter is equal or less than that of the input voltage depending on the value of the duty cycle. From this, it can be said that the buck converter is like a transformer where the duty cycle (rather than the turns ratio) controls the output (Hart, 2011; Simonsen, 2009). From this output control, and by neglecting the power losses within the converter, the input and output power can be defined by the following equation:

$$P_s = P_o$$

$$V_s I_s = V_o I_o$$

$$\frac{V_o}{V_s} = \frac{I_s}{I_O} = D \qquad\qquad 3.8$$

The inductor is used to store the power generated because of the flowing current. This maintains continuous output as long as possible. Hence, the design of the buck converter must take in consideration the value of the inductor in order to maintain the continuous mode of operation. Moreover, the design must not neglect the inductor's peak current and frequency in order to avoid saturation of the inductor. Knowing the inductor current ripple is key to determining the inductor value (Hart, 2011; Rogers, 1999b).

$$(\Delta i_L)_{on} = \left(\frac{V_s - V_o}{L}\right) D T_s = \left(\frac{V_s - V_o}{Lf}\right) D, \quad where \ f = \frac{1}{T_s}$$

Combining the value from equation 3.7:

$$\Delta i_L = \frac{V_o(1 - D)}{Lf}$$

$$L = \frac{V_o(1 - D)}{\Delta i_L f} \qquad\qquad 3.9$$

The other component that needs to be handled carefully in designing the buck converter is the capacitor. In this case, the baseline assumption was to use a high-value capacitance so the output voltage remained constant. It also acts as a sink for the voltage ripple and unwanted harmonics. The impedances of the capacitor are equivalent series resistance (ESR), equivalent inductance (ESL) and capacitance (C). The voltage ripple can be calculated from (Hart, 2011; Rogers, 1999b) as follow:

$$\Delta V_o = \frac{T_s \, \Delta i_L}{8C}$$

and for the switch-off state:

$$\Delta i_L = -\frac{V_o}{L}(1 - D)T_s \quad therefore;$$

$$\Delta V_o = \frac{V_o(1 - D)}{8CLf^2}$$

$$C = \frac{(1 - D)}{8\frac{\Delta V_o}{V_o}Lf^2} \quad or \ = \frac{\Delta i_L}{8\Delta V_o f} \qquad\qquad 3.10$$

A buck converter is commonly adopted in PV systems. It was used with a modified P&O MPPT and showed decent performance (Wu, Shen and Wu, 2009). In another study, (Farivar, Asaei and Rezaei, 2010) used a buck converter that exhibited both a high level of performance and accurate results. Moreover, a buck converter has proven to be a good choice for PV technologies connected to a grid as well as for standalone systems (Villalva, Gazoli and Ruppert Filho, 2009; Arias *et al.*, 2004; Hussein *et al.*, 1995; Enslin and Snyman, 1992b)   .

3.2.2   Boost Converter in a PV System

A *boost converter* is a device which step-up the input voltage and gains a higher output voltage. The input and output of the boost are DCs and the output keeps its polarity (Simonsen, 2009). Figure 3.2a shows the circuit of the boost converter.
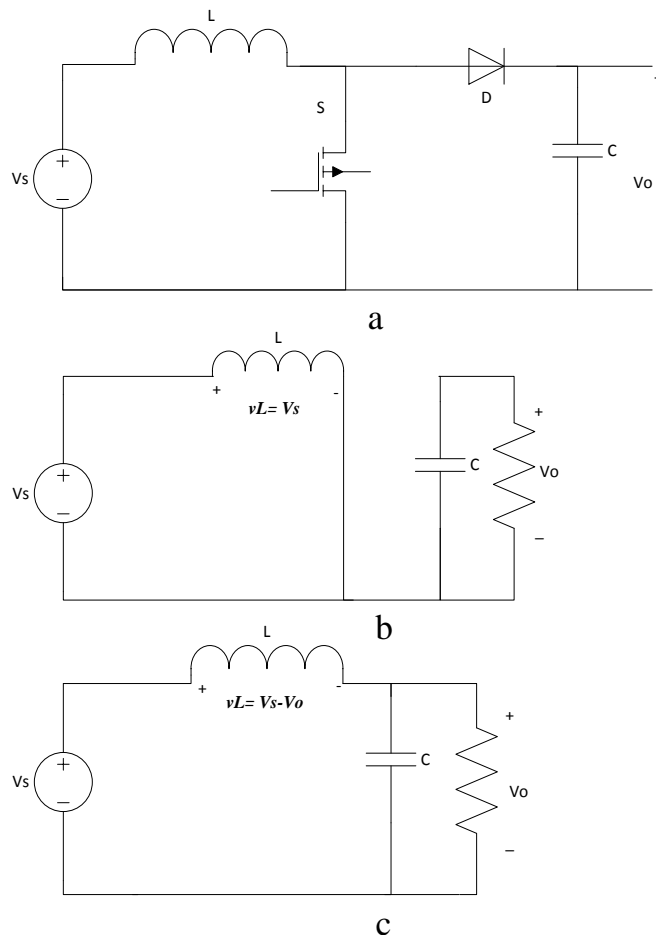
Figure 3.2: Boost converter circuit

To understand the functionality of the boost converter, the circuit must be critically analysed and mathematically modelled whether the status of the switch is on or off. However, before analysing each scenario a number of assumptions need to be illustrated (Hart, 2011; Simonsen, 2009):

1. The converter operates in steady-state mode.
2. The switching period is T_s, and DT_s is the time when the switch is ON and $(1-D)T_s$ is the time when the switch is OFF.
3. The capacitor has a very large value.

4. The inductor current is continuous.

5. All components are ideal.

6. Input voltage is V_s and output voltage is V_0; both are constant.

Both circuits are analysed by examining the inductor current and voltage. Therefore, when the switch is closed (Figure 3.2b), the diode operates on a reverse-bias so the current will go through the inductor and to the source. The voltage across the inductor is:

$$v_L = V_s = L\frac{di_L}{dt} \quad or \quad \frac{V_s}{L} = \frac{di_L}{dt}$$

<div align="right">3.11</div>

As equation 3.11 shows, the change rate of the inductor current is constant and increases linearly as long as the switch remains closed. This change can be represented by equation 3.12:

$$\frac{\Delta i_L}{\Delta t} = \frac{\Delta i_L}{DT_s} = \frac{V_s}{L}$$

<div align="right">3.12</div>

The rate at which the inductor current changes when the switch is on is given by:

$$(\Delta i_L)_{on} = \frac{V_s DT_s}{L}$$

<div align="right">3.13</div>

On the other hand, when the converter switch is off, Figure 3.2c (the output) is supplied from the input source and the energy stored in the inductor. The diode acts in a forward-biased scenario, which offers a path for the inductor current to be released as the stored energy is transferred away (Simonsen, 2009). In this case, the inductor voltage is:

$$v_L = V_s - V_o = L\frac{di_L}{dt}$$

$$\frac{di_L}{dt} = \frac{V_s - V_o}{L}$$

<div align="right">3.14</div>

As equation 3.14 shows that the changing of the inductor current is constant, this change decreases linearly while the switch is off. This current can be calculated as:

$$\frac{\Delta i_L}{\Delta t} = \frac{\Delta i_L}{(1-D)T_s} = \frac{V_s - V_o}{L}$$

$$(\Delta i_L)_{off} = \frac{(V_s - V_o)(1-D)T_s}{L} \qquad\qquad 3.15$$

As it is supposed in the beginning that the converter is in the steady state mode, the total change in the current must be zero (as equation 3.5) shows). By combining equation 3.13) and (3.15) into equation (3.5):

$$\frac{V_s D T_s}{L} = -\frac{(V_s - V_o)(1-D)T_s}{L}$$

$$V_s D = -(V_s - V_o)(1-D)$$

Finding V_0

$$V_s D = -V_s + V_s D + V_o - V_0 D$$

$$0 = -V_s + V_o - V_0 D$$

$$V_s = V_o(1-D)$$

$$V_o = \frac{V_s}{1-D} \qquad\qquad 3.16$$

The inductor is used to store the power generated by the flowing current. This maintains continuous output for as long as possible. Hence, the design of the boost converter must consider the value of the inductor in order to maintain the continuous mode of operation. Moreover, the design must not neglect the inductor's peak current and frequency to avoid saturation. Knowing the inductor changing current is key in determining the inductor value (Hart, 2011; Rogers, 1999a).

$$(\Delta i_L)_{on} = \frac{V_s D\, T_s}{L} = \frac{V_s D}{Lf}, \qquad where\ f = \frac{1}{T_s}$$

$$L = \frac{V_s D}{\Delta i_L f} \qquad\qquad 3.17$$

The other component that requires careful handling in designing a boost converter is the capacitor. The assumption made is to use a high value for the capacitance so the output voltage remains constant. The capacitance also acts as a sink for the voltage ripple and unwanted harmonics. The impedances of the capacitor are equivalent series resistance (ESR), equivalent inductance (ESL) and capacitance (C). The voltage ripple can be calculated from the following equation (Hart, 2011; Rogers, 1999a)

$$\frac{\Delta V_o}{V_o} = \frac{DT_s}{RC} = \frac{D}{RCf}$$

Therefore:

$$C = \frac{D}{R\frac{\Delta V_o}{V_o}f} \qquad\qquad 3.18$$

The boost converter has seen widespread adoption in PV systems and. It helps extracting the maximum power of the PV array and increasing the output voltage to match the high voltage level of the grid (Khalifa and El-Saadany, 2011). It has high efficiency because it only contains a single switch and maintains an MPPT under different atmospheric conditions (Kumari and Babu, 2011). It is difficult to identify all studies that have used boost converters in PV grid-connected or stand-alone applications; some of these studies include (Ngan and Tan, 2011; Ahmed and Shoyama, 2010; Yuvarajan and Xu, 2003b)

3.2.3   Buck Boost Converter in a PV System

This type of converter incorporates both the buck and the boost converters. The output voltage can be either greater than or less than the input voltage. The input and output polarity are opposite each other (Hart, 2011; Skretas and Papadopoulos, 2009). The circuit of the buck boost converter is shown in Figure 3.3a.
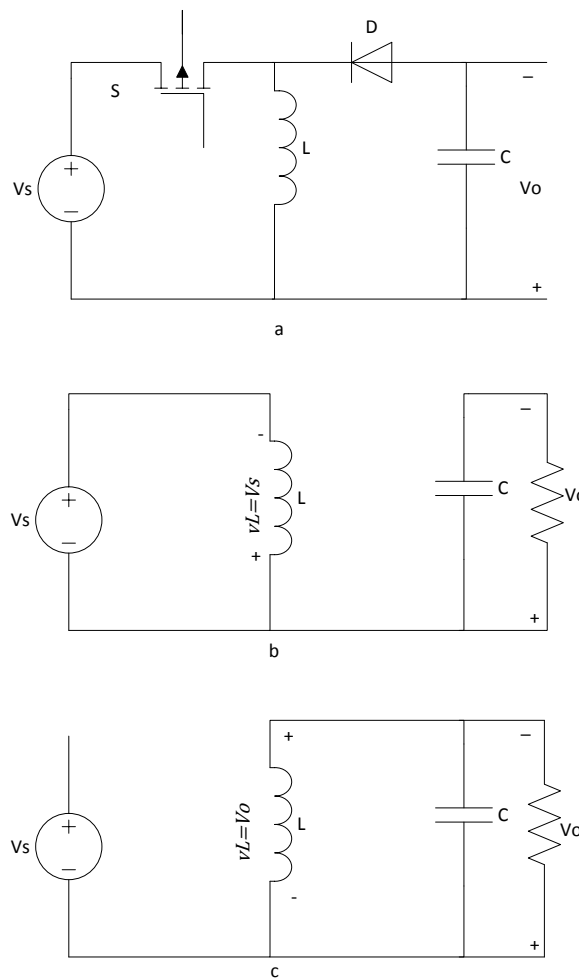
Figure 3.3: Buck boost converter circuit

To fully understand the functionality of the buck boost converter, it is better to investigate the two different states of the converter with respect to the switch position. For each state, the inductor current and voltage will be analysed. The assumptions that must be considered in the context of this experiment are as follows (Hart, 2011):

1. The converter is running in a steady-state mode.

2. The inductor current is continuous.

3. The capacitor has a huge value.

4. The switching period is T_s, and DT_s is the time when the switch is ON and $(1-D)T_s$ is the time when the switch is OFF.

5. Input voltage is V_s and output voltage is V_0 and both are constant.

6. All components are ideal.

When the switch is closed, equivalent circuit in Figure 3.3b, the diode will act with a reverse bias and the current flows from the source to the inductor. The inductor

current will rise slowly as long as the switch is closed. The voltage across the inductor is

$$v_L = V_s = L\frac{di_L}{dt}$$

$$\frac{V_s}{L} = \frac{di_L}{dt} \qquad\qquad 3.19$$

As equation 3.19 shows, the change in the inductor current is constant, and the ratio increases linearly while the switch is on. Therefore, the equation becomes like

$$\frac{\Delta i_L}{\Delta t} = \frac{\Delta i_L}{DT_s} = \frac{V_s}{L}$$

The linear change of the inductor current is

$$(\Delta i_L)_{on} = \frac{V_s DT_s}{L} \qquad\qquad 3.20$$

On the other hand, when the switch is off (equivalent circuit Figure 3.3c) the inductor will start releasing its current, which will decrease gradually through the diode, which acts in a forward-biased mode to the load. The inductor voltage in this situation is:

$$v_L = V_o = L\frac{di_L}{dt}$$

$$\frac{V_o}{L} = \frac{di_L}{dt} \qquad\qquad 3.21$$

As with the previous case, equation 3.21 shows a linear changing rate in the inductor current. This change can be represented by

$$\frac{\Delta i_L}{\Delta t} = \frac{\Delta i_L}{(1-D)T_s} = \frac{V_o}{L}$$

Therefore the changing rate of the inductor current is

$$(\Delta i_L)_{off} = \frac{V_o (1-D)T_s}{L} \qquad\qquad 3.22$$

As this analysis is for the steady-state mode, the inductor current should be zero for every single period. By calling equation 3.5 and applying equation 3.20 and 3.22:

$$\frac{V_o\,(1-D)T_s}{L} = -\frac{V_s DT_s}{L}$$

Finding V_0

$$V_o = -V_s\left(\frac{D}{1-D}\right) \qquad\qquad 3.23$$

The inductor is used as a location for storage of the power generated because of the flowing current. This maintains continuous output as long as possible. Hence, the design of the buck boost converter must consider the value of the inductor in order to maintain the continuous mode of operation. Moreover, the design must not neglect the inductor's peak current and frequency to avoid saturation. Knowing the changing current of the inductor is key to determining the inductor value (Hart, 2011; Rogers, 1999a).

$$(\Delta i_L)_{on} = \frac{V_s DT_s}{L} = \frac{V_s D}{Lf}, \qquad where\ f = \frac{1}{T_s}$$

$$L = \frac{V_s D}{\Delta i_L f} \qquad\qquad 3.24$$

The other component that needs to be handled carefully in designing the buck boost converter is the capacitor. A high value was used for the capacitance so that the output voltage remained constant. It also acts as a sink for the voltage ripple and unwanted harmonics. The impedances of the capacitor are equivalent series resistance (ESR), equivalent inductance (ESL) and capacitance (C). The voltage ripple can be calculated from the following equation (Hart, 2011; Rogers, 1999a):

$$\Delta V_o = \frac{V_o DT_s}{RC} = \frac{V_o D}{RCf}$$

Therefore,

$$C = \frac{V_o D}{R\Delta V_o f} \qquad\qquad 3.25$$

Designs involving a buck boost converter have not been widely utilised in PV systems compared to those utilising a buck or boost converter. It is used with an adaptive neural-network MPP technique to supply a DC motor that has previously shown good results in another study (Hussein *et al.*, 2002)   . A buck-boost

converter with two switches is also a proven high-efficiency system (Chomsuwan, Prisuwanna and Monyakul, 2002)

3.2.4   Ćuk Converter in a PV System

Another converter type is the Ćuk converter, named after its inventor, Slobodan Ćuk (Middlebrook and Cuk, 1970). This converter can increase or decrease the input DC voltage, and the output polarity is reversed with respect to the input.

Functionally, the Ćuk converter acts as a buck-boost converter, but unlike all the previous converters discussed earlier in this chapter the responsible part of transferring energy in the Ćuk converter usually is the capacitor instead of the inductor. Figure 3.4a shows the Ćuk converter circuit.
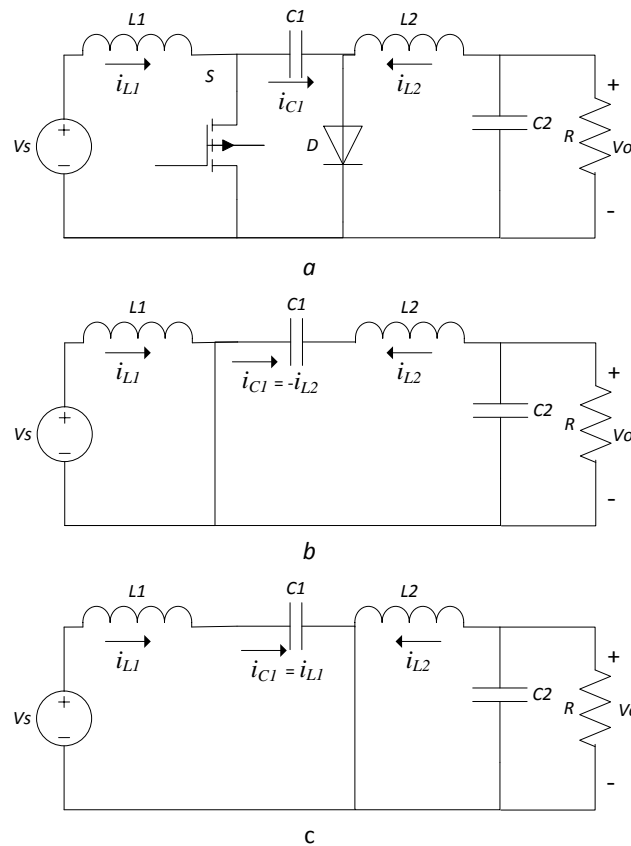
Figure 3.4: Ćuk converter equivalent circuits

For better understanding of the Ćuk converter, a deeper analysis is desired. However, before starting such a step some assumptions must be stated. These assumptions are (Hart, 2011):

1. All inductors are critically large in volume with a constant current through them.

2. Capacitors are huge and their voltages are constants.

3. The circuit operates in a steady state and the waveforms are periodic.

4. The switching period is T_s, and DT_s is the time when the switch is ON and $(1 - D)T_s$ is the time when the switch is OFF.

5. All components are ideal.

First, as the energy is transferred from input to output in the Ćuk converter through the capacitor C1, application of Krichhoff's voltage law for the outer circuit yields:

$$V_s - V_{L1} - V_{c1} + V_{L2} - V_o = 0$$

However, the inductor voltage is zero for the steady state. Therefore,

$$V_{c1} = V_s - V \hspace{4cm} 3.26$$

With the assumption that the waveforms are periodic, the average capacitor current should be zero:

$$(\Delta i_{c1})_{on} + (\Delta i_{c1})_{off} = 0 \hspace{3cm} 3.27$$

For the circuit in which the switch is 'on', Figure 3.4b, the diode is in a reverse-bias mode, and the stored power in the capacitor will be transferred to the output through the inductor L2. In this case,

$$(i_{c1})_{on} = -I_{L2} \hspace{4cm} 3.28$$

On the other hand, when the switch is off, as with the circuit in Figure 3.4c, the diode operates in a forward bias state due to the amount of current in the two inductors. In this case,

$$(i_{c1})_{off} = I_{L1} \hspace{4cm} 3.29$$

By applying equation 3.28 and 3.29 into equation 3.27 with respect to the switch time on and off:

$$[(i_{c1})_{on}]DT + [(i_{c1})_{off}](1 - D)T = 0$$

$$I_{L2}DT = I_{L1}(1 - D)T$$

$$\frac{I_{L1}}{I_{L2}} = \frac{D}{1 - D} \hspace{4cm} 3.30$$

As the input and output power are equal in the Ćuk converter:

$$P_s = P_o$$

$$I_{L1}V_s = -I_{L2}V_o$$

$$\frac{I_{L1}}{I_{L2}} = -\frac{V_o}{V_s}$$

$$V_o = -V_s \left(\frac{D}{1-D}\right) \qquad\qquad 3.31$$

Unlike the previous converters, the Ćuk converter has two inductors L_1 and L_2 and two capacitors C_1 and C_2. However, the output parameters C_2, L_2 and R are treated as being the same as those in the buck converter, and the inductor current is drawn from the same equation as for the buck converter. Hence, the formula to calculate the proper value of C2, which is responsible for adjusting the output voltage ripple, is likewise the one used in the buck converter (Hart, 2011).

$$\frac{\Delta V_o}{V_o} = \frac{(1-D)}{8C_2 L_2 f^2}$$

$$C_2 = \frac{(1-D)}{8\frac{\Delta V_o}{V_o}L_2 f^2} \qquad\qquad 3.32$$

On the other hand, the value of C1 can be selected by knowing the voltage ripple through this capacitor driven according to the following equation:

$$C_1 = \frac{V_o D}{R\Delta V_{c1} f} \qquad\qquad 3.33$$

The inductor is used to store power generated by the flowing current. Continuous output is maintained as long as possible. Hence, the design of the Ćuk converter must consider the value of the inductor to maintain the continuous mode of operation. Moreover, the design must not neglect the inductor's peak current and frequency to avoid saturation. Knowing the inductor's changing current is key to determining. However, as mentioned earlier the difference between this power converter and the previous types is the exciting current of the two inductors. To pick a

suitable value of L1, the voltage across the inductor while the switch is closed is represented by the following equation (Hart, 2011; Rogers, 1999a):

$$V_s = L_1 \frac{di_{L1}}{dt}$$

The time interval while the switch is closed is DT_s; therefore,

$$L_1 = \frac{V_s DT_s}{\Delta i_{L1}} = \frac{V_s D}{\Delta i_{L1} f} \qquad\qquad 3.34$$

The last component that needs to be handled carefully in designing the Ćuk converter is the output inductor L2. Similar to the derivation of the value of L1, the value of L2 will be driven from the inductor voltage equation while the switch is closed (Hart, 2011).

$$v_{L2} = V_s = L_2 \frac{di_{L2}}{dt}$$

The time interval while the switch is closed is DT_s; therefore,

$$L_2 = \frac{V_s DT_s}{\Delta i_{L2}} = \frac{V_s D}{\Delta i_{L2} f} \qquad\qquad 3.35$$
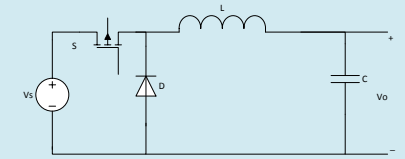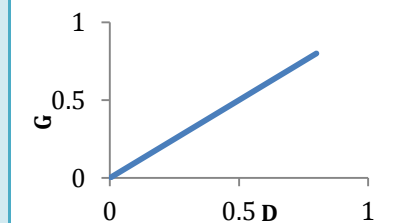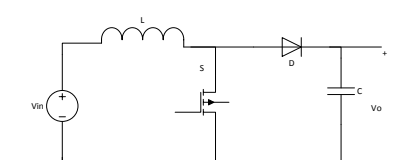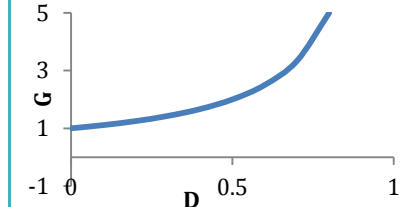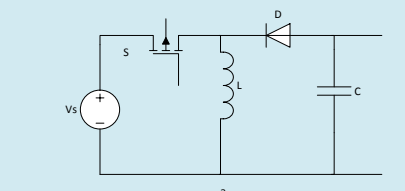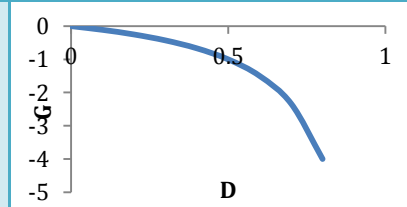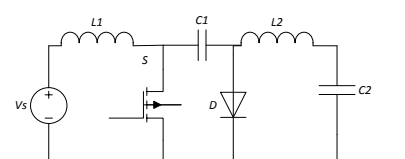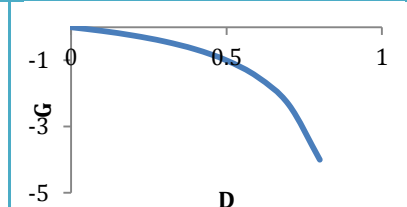
3.3   Comparison of Power Converters in a PV System

Several references have noted that many different converter topologies can be used in certain situations. (Enslin and Snyman, 1992a) used a buck converter but argued that other converter topologies could also have been used. Furthermore, the result of applying a specific boost converter and examining it proves that any converter topology can be used within similar applications (Femia *et al.*, 2005)   . When applying MPPT with two different converters, the boost converter shows a higher efficiency than does the buck converter; this also suggests adding the buck converter back after the boost in case the output voltage is higher than the desired voltage, rather than using only one buck converter with the MPPT (Glasner and Appelbaum, 1996). Another study states that both the buck and boost converters are suitable for MPPT; however, the boost converter is most frequently used in existing

systems. Boost converter implementation is a must, especially if the PV system is small and the output voltage is low, in order to step it up to be delivered to the grid or load. Furthermore, this supports the previous statement that the boost converter has higher efficiency than the buck converter for varying the duty cycle (Simonsen, 2009).

Table 3-1 summarises the differences between the four DC-DC power converters discussed earlier in this chapter. The table contains the circuit diagram, the gain and its relation to the duty cycle, the switch voltage stress and the inductor average current, for the four converter possibilities (buck, boost, buck-boost and Ćuk converter).

Table 3-1: Comparison between the power converter types

Type	Circuit	Gain $(G) = V_o/V_s$	D Vs G	Voltage stress of switch (V_{switch}/V_s)	Inductor average current
Buck		D		1	$I_L = \dfrac{1}{G} I_s$
Boost		$\dfrac{1}{1-D}$		G	$I_L = I_s$
Buck boost		$-\left(\dfrac{D}{1-D}\right)$		$G+1$	$I_L = -\left(\dfrac{1-G}{G}\right) I_s$
Ćuk		$-\left(\dfrac{D}{1-D}\right)$		$G+1$	$I_{L1} = I_s$ $I_{L2} = -\left(\dfrac{1-G}{G}\right) I_s$

3.4 Summary

The aim of this chapter is to review the DC-DC converter topologies. The four topologies (buck, boost, buck-boost and Ćuk converters) are discussed. First, the buck functionality is explained and the circuit analysis supported by the circuit diagram is delineated. Additionally, the boost, buck-boost and Ćuk converters all are discussed in detail and their modes of operation explained. Additionally, the merits and drawbacks of each type are presented. Moreover, the implementations of these converters in PV applications are shown. Finally, a comparison table between the different converters is displayed. The proposed PV configuration is presented in the next chapter (chapter 4).

Chapter 4

The Proposed PV Inverter Configuration

Chapter 4. The Proposed PV Inverter Configuration

4.1 Overview

In Chapter 2, all existing PV configurations were critically reviewed and the most useful MPPT techniques were investigated. Furthermore, in Chapter 3, the different DC-DC power converters were critically reviewed and each one was analysed and modelled. In this chapter, the proposed PV inverter system configuration is presented. The proposed system is optimised in order to gain the highest efficiency. This optimisation includes different parts of the system from selection of the appropriate MPPT techniques to the power converter topologies and the control signals. Based on the analysis in Chapters 2 and 3, the new system is presented in this chapter. Each part is analysed and investigated in detail.

4.2 The State-of-the-art PV System

In Chapter 2, the different PV inverter configurations are presented. Nowadays, there are four types of configuration; centralised configuration, string configuration, multi-string configuration and AC module; see Figure 4.1.
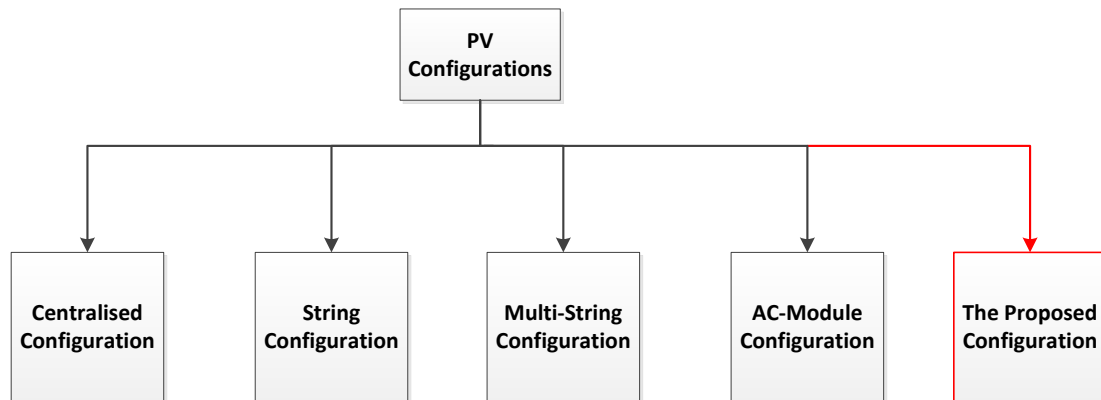
Figure 4.1: The PV configurations

The discussion in Chapter 2 covered the advantages and disadvantages of each configuration. The AC-module is the latest configuration introduced and is considered superior for rooftop PV systems and small applications, as this configuration has no step-up stage.

On the other hand, the multi-string configuration suffers from some drawbacks, such as the mismatch between the panels of each string. Certainly the effect of this problem is lower than that of the string configuration, but it is still considered a disadvantage.

The high demand on PV installation around the world leads to more research on how to maximise PV system efficiency. Additionally, as the literature shows that the number of PV configurations is limited and each individual configuration has its pros and cons, the variety of PV configurations must be taken into account carefully when proposing an optimal configuration, as is done in section 4.3 below.

4.3   The Proposed PV Inverter System Configuration

Since the existing PV inverter configurations are limited (four configurations), a need for optimal configuration is desirable. In addition, the variety of the PV systems configurations provides greater advantages in expanding the implementation of PV technology. Low energy efficiency (conversion efficiency) has always been one of the main weaknesses of this technology. Therefore, the new configuration must consider the importance of the system's efficiency. Decreasing the switching losses should improve the overall efficiency.

The applications of PV installation are diverse and some of the current configurations can be applied in one or two applications only. Given this, a configuration that could be used for several different applications would be worth devising.

Flexibility is an attribute that also leads to a system being preferred by users. In this context, flexibility means the possibility of adding further panels to the current system, or removing panels due to damage.

This study proposes a new PV integration that aims to promote the PV system's output to a new, higher level. The system components are to be designed, simulated and tested. Furthermore, the design has benefited from the ability to modify some of the circuit components, which is explained in detail later in this chapter.
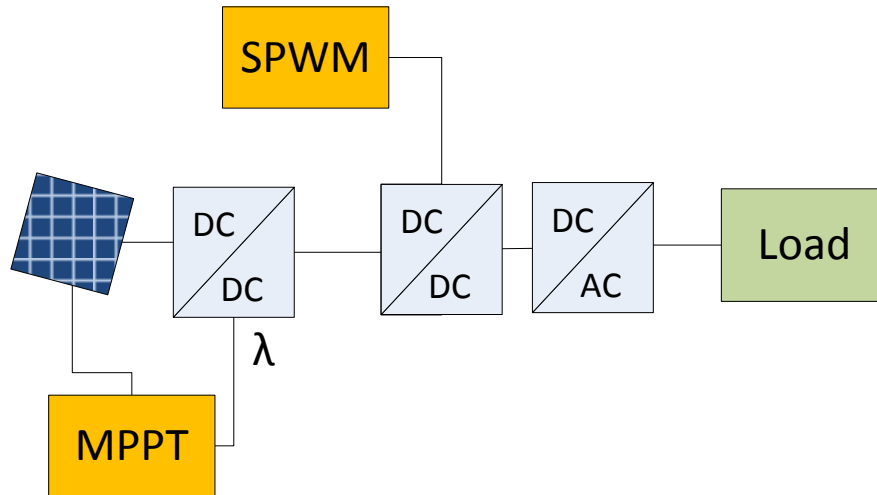
Figure 4.2: Block diagram of the proposed PV configuration

The proposed configuration, shown in Figure 4.2, consists of a PV system, two DC-DC converters, two control units and an inverter. The following sections present detailed descriptions for each component.

4.4   The PV System

In the centralised configuration, all the PVs are connected together in parallel and series into a single inverter. While in the string layout, the PV panels are all connected in series and to the load through an inverter. Furthermore, the multi-string layout adds a DC-DC converter stage at the end of each string, which then connects to an inverter. Finally the AC module connects the PV alone directly to the inverter. The output power of each module is about 100-300 W.

The PV system in the proposed configuration can be a string, multi-string or a combination of parallel and series panels. The variety of options for different PV connections gives this configuration advantages over other existing configurations. This maintains the flexibility factor, which is sought to optimise the proposed configuration.

The PV output is directly affected by the weather conditions, with any sudden atmospheric change reflected straight away in the output values. Any sudden atmospheric change is reflected straight away in the output values. In addition, temperature and irradiance are two main factors that must be accounted for while testing the system.

The PV system in the Matlab/Simulink model is a combination of multi PVs connected in series and parallel. The aim is to assess the configuration's ability to handle a large-scale power system.

4.5   Maximum Power Point Tracking Technique

Chapter 2 reviewed the most utilised MPPT techniques described in the literature. The present thesis selected a single technique that is believed to be the most appropriate option given the configuration. Selection was based on the factors: ease of implementation, simplicity, tracking speed, accuracy and efficiency.

Both fractional open-circuit voltage and short-circuit current methods are simple, easy to implement and cheap, with the main disadvantage of these two methods being the power loss due to the regular shutting off of the PV terminal. Moreover, the fact that the PV does not operate at the exact MPP is another drawback for both of them. They both depend on the PV characteristics to adjust the value of the fractional constant, and this value needs to be tuned at regular intervals. Both the fractional open-circuit voltage and the short-circuit current methods are sub-optimal in the proposed system for these reasons.

Artificial intelligence methods (such as fuzzy logic and neural networks) demonstrate a quicker tracking response compared to traditional tracking methods. However, considerable experience and knowledge is needed to design and build a fuzzy logic methodology compared to the previous methods. An additional drawback to the fuzzy logic method is that it shows an oscillation around the MPP.

Neural networks require training so that they make optimal decisions; such training may take from one month to years. Each PV has its individual characteristics that affect the output of the neural network; therefore, the network should be trained for the exact PV. Moreover, as both methods rely on the characteristics of the PV array or panel they are being used in, they need to be regulated so often because of the influence of aging on the PV technology. Finally, these methods are complex and difficult to implement and maintain (Reisi, Moradi and Jamasb, 2013; Esram and Chapman, 2007). For these reasons, fuzzy logic and neural network systems were ultimately not implemented in the proposed system.

The perturb and observe method is one of the most popular MPPT techniques in use and has been discussed in most papers about MPPT. Its concept is simple and can be implemented easily. The cons of this method are poor tracking under rapidly changing weather conditions and oscillation around the MPP.

In comparison to the other methods, incremental conductance has shown a good tracking character. Furthermore, incremental conductance is inexpensive to implement and does not depend on the PV characteristics. Additionally, incremental conductance demonstrates a higher accuracy in selecting the MPP with more stability at the operating point; it does not need regular adjusting or detailed knowledge for its initial set up.

The algorithm is simple for incremental conductance. The inputs are the PV current and voltage; a comparison is then performed between the instantaneous conductance (I/V) to the incremental conductance ($\Delta I/\Delta V$) while the maximum operating point is at ($\Delta I/\Delta V = -I/V$). The whole flowchart is shown in Figure 2.14. Moreover, a digital signal processor (DSP) is used in implementing this method, which has the ability to carry on the comparison process, recall the previous values, and make decisions.

In the proposed system, a decision table matrix, Table 4-1, is created to determine the way in which an MPPT method is selected. Within this table, a list of factors for consideration in choosing suitable algorithms is placed in the first row. In addition, in the first column of Table 4-1 the list of the MPPT algorithms is positioned. Each of these algorithms is given a score between 1 to 5 for each factor. These scores are given from literatures survey on MPPT; the values are subsequently multiplied by the weight of each factor (Narendiran, 2013; Barchowsky *et al.*, 2012; Murtaza *et al.*, 2012; Villalva, Gazoli and Ruppert Filho, 2009; Faranda, Leva and Maugeri, 2008; Esram and Chapman, 2007) .

Table 4-1 shows the details of the decision matrix model. According to the table, the incremental conductance algorithm has the highest score of all the algorithms; it is therefore the adopted MPPT method in this thesis. The inputs of this unit are the PV's current and voltage; the output is a duty cycle correction. Figure 4.3 provides a chart of the decision table matrix scores.

Table 4-1: Decision Matrix Table to select the MPPT algorithm

MPPT Algorithm Selection Factors	Weight	P&O	Incremental Conductance	Open-circuit voltage	Short-circuit current	Fuzzy logic	Neural Network
Ease of implementation	5	5	4	5	4	1	1
Simplicity	5	5	5	5	5	1	1
Tracking Speed	3	3	3	3	3	4	4
Accuracy	3	2	3.5	2	2	4	4
Cost Effectiveness	4	4	4	5	5	1	1
Efficiency	4	2.5	4	2	2	5	5
Total		91	96.5	93	88	58	58
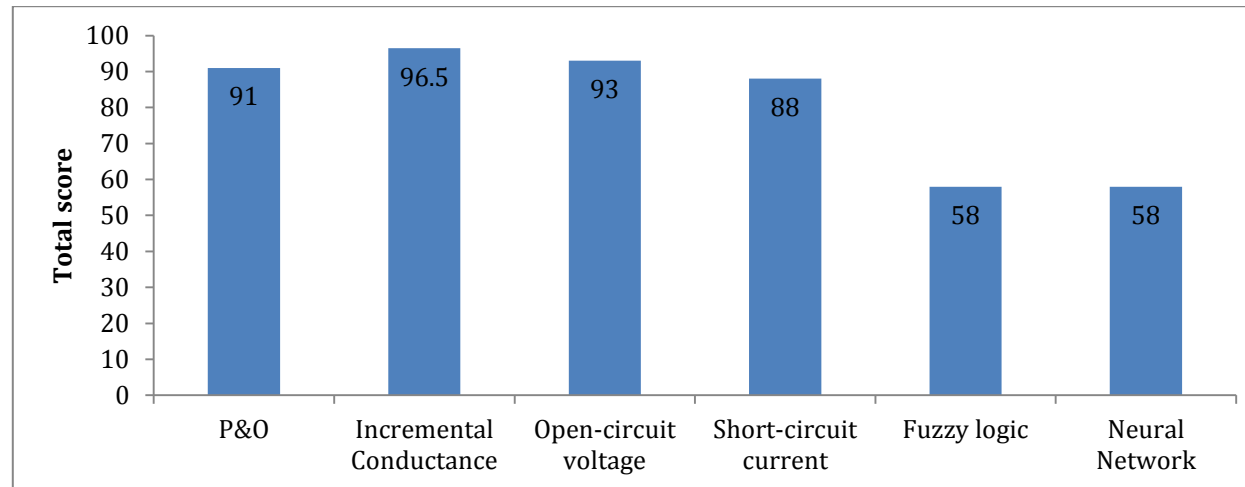
Figure 4.3: Relative scores (after weighting) of the MPPT techniques; incremental conductance has the highest score

4.6   MPPT DC-DC Power Converter

As Figure 4.2 shows in the proposed layout of the system, the PV is connected to a DC-DC converter. This converter here is called the *MPPT converter* in order to differentiate it from the second DC-DC converter (which will be explained later). This converter aims to extract the maximum power from the PV whatever the weather conditions are. The duty cycle of this converter is produced by the MPPT algorithms that control the converter's switch. This control signal is the normal PWM signal.

Many power converters can be used with the MPPT unit. For example, buck, boost, buck-boost and Ćuk converters have been utilised within the PV system. An implementation of the boost converter is carried using PSPICE and the boost circuit; input and output voltages are shown in Figure 4.4 and Figure 4.5, respectively. Likewise, Figure 4.6 and Figure 4.7 show the buck converter circuit and its signals. Additionally, the buck-boost circuit is presented in Figure 4.8 and the voltage signals are shown in Figure 4.9. Finally, a review discussion about each type is presented in Chapter 3 including the utilization of each converter in previous works.

Control of the Ćuk converter is considered difficult and sometimes results in operational instability. Moreover, the Ćuk converter suffers from low reliability because it uses electrolysed capacitors, which are 30% less reliable than non-electrolysed capacitors and add costs (Knight, Shirsavar and Holderbaum, 2006; United States of America: Department of Defense, 1991). From the efficiency point of view, this converter has more elements, leading to higher cost and power dissipation.

However, a decision matrix model is carried to support the process of selecting the MPPT converter. The decision is made according to factors including:

- Efficiency
- Utilisation in PV application
- Reliability
- Ease of control
- Number of components (cost)
- Switching loss

These factors are placed in the first row and given a specific positive weight except in the case of the last two factors, which are given negative values as they are considered disadvantages of the device. The four types of power converters are placed in the top column. These types have been evaluated, with a value between 1 and 5 given to each factor. The summation of these values multiplied by the weight of each factor is calculated for each power converter. The converter of the highest summation is the chosen solution.

Table 4-2: Decision Matrix Table to choose the best converter

DC-DC Converter Selection Factors	Weight	Buck	Boost	Buck-Boost	Ćuk
Utilisation in PV application	4	4	5	5	5
Efficiency	5	3	4.5	4	3
Reliability	4	4	4	3	1
Ease to control	3	2	3.5	2	2
No. of components	-1	3	3	5	5
Switching loss	-4	3	2	3	4.5
Total		38	58	41	22

With respect to Table 4-2, the chosen DC-DC converter in this thesis is the boost type, which has the highest sum according to the selection parameters. Additionally, the boost steps up the voltage level, which might be needed in some applications. Another advantage of the boost over the buck is that the current in the boost is actually very smooth because it is driven from the inductor while in the buck an input capacitor is needed to minimise the current ripple. Lastly, the free-wheel diode in the boost converter protects the PV system from the reverse current that can occur when the PV is not delivering power (for example, with the absence of light).
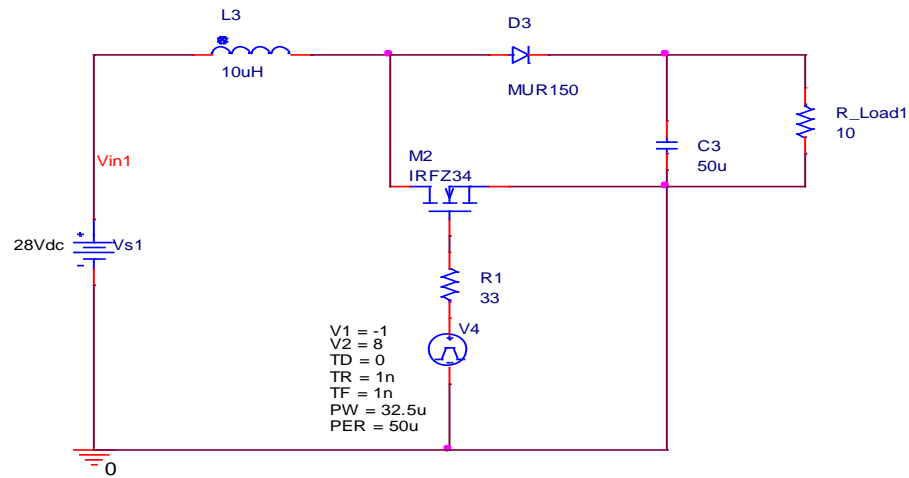
Figure 4.4: Boost converter circuit in PSPICE
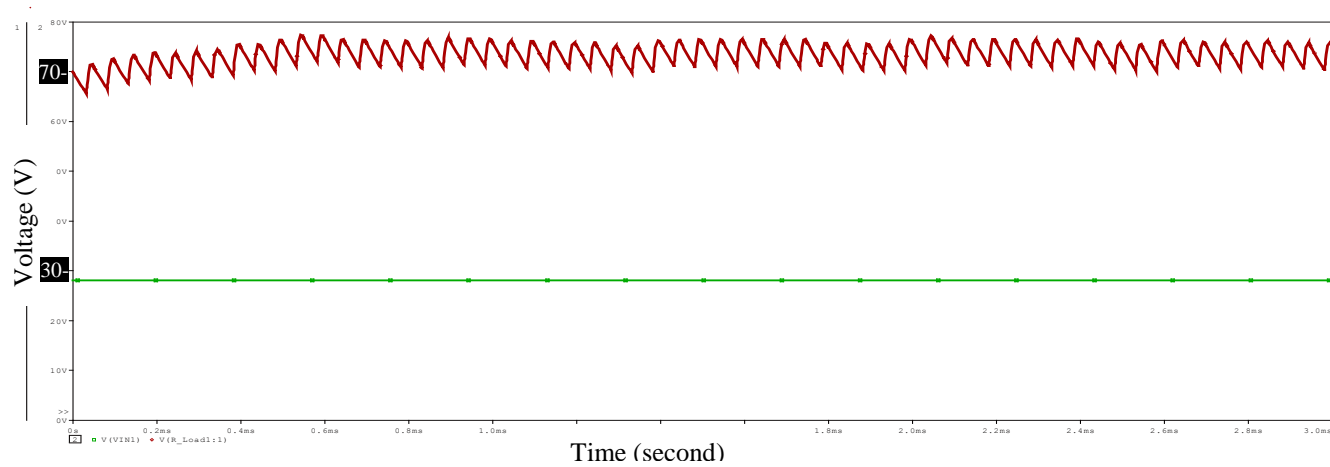
Figure 4.5: The input (green) and output (red) voltage of the boost converter
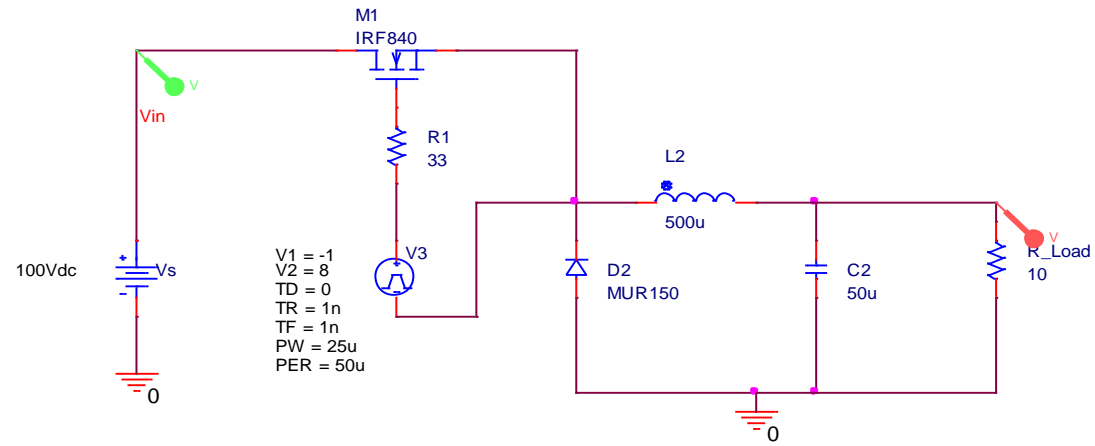
Figure 4.6: Buck converter circuit in PSPICE
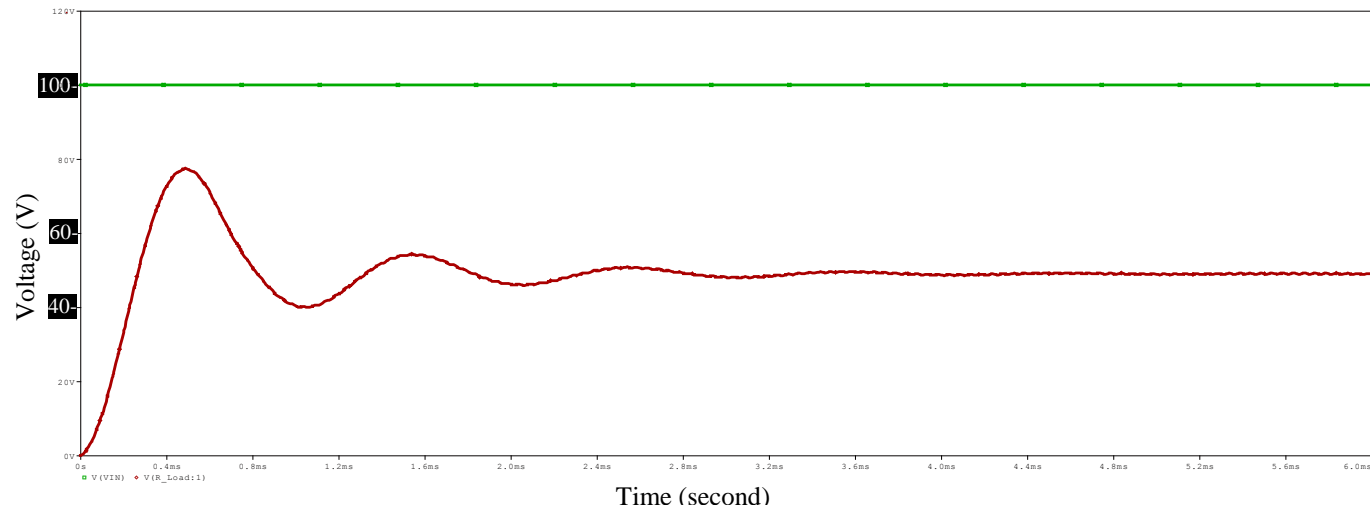
Figure 4.7: The input (green) and output (red) voltage of the buck converter
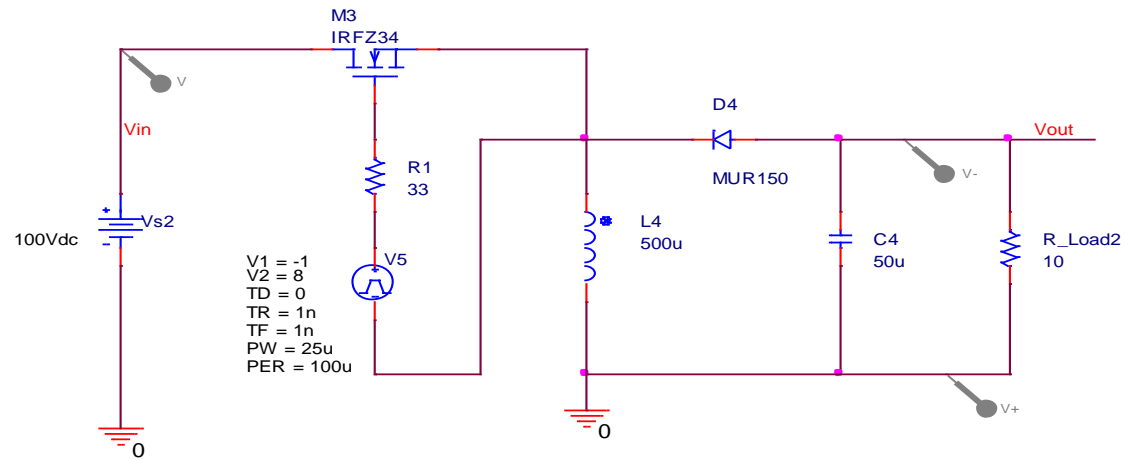
Figure 4.8: Buck-boost converter circuit in PSPICE
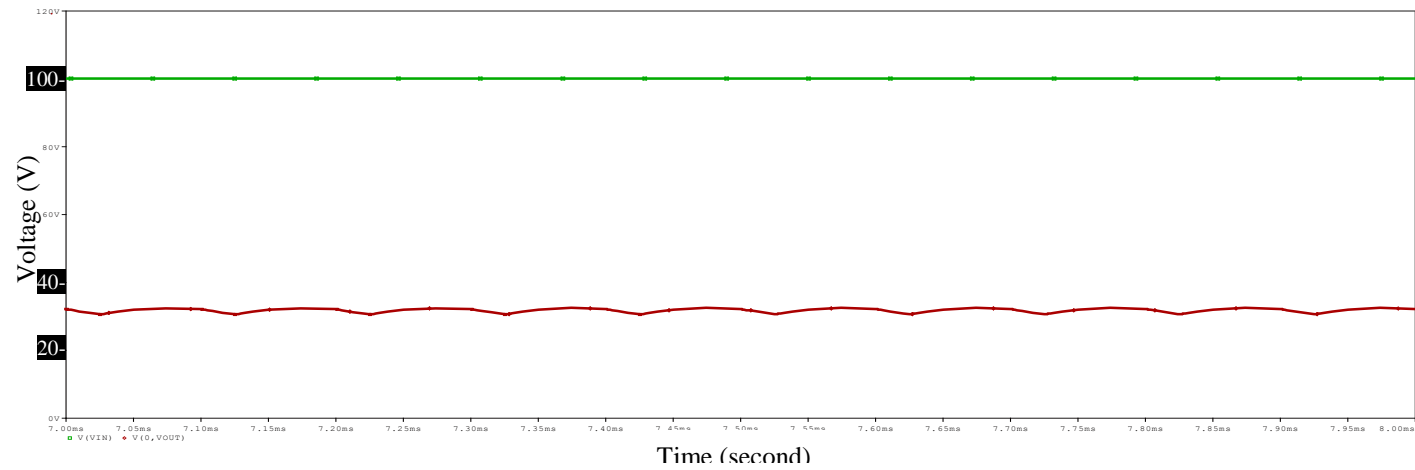
Figure 4.9: The input (green) and output (red) voltage of the buck-boost converter

4.6.1 MPPT Boost Converter Design

The functionality of the boost converter is provided in detail in Chapter 3. This includes the design considerations and equations needed to design any boost converter. Here, all those equations will be recalled in order to design the MPPT boost converter for the proposed system shown in Figure 4.10. The input values are taken from the chosen PV system data sheet.
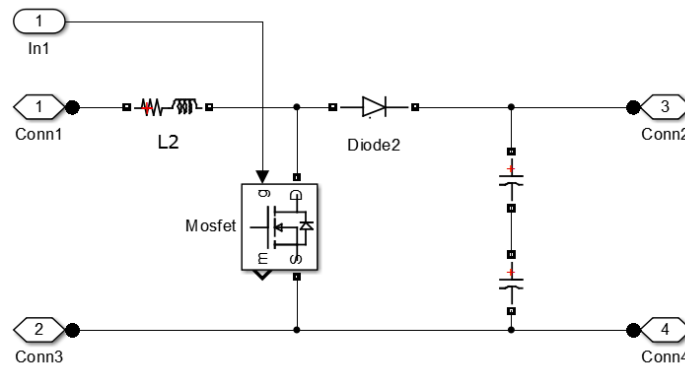
Figure 4.10: MPPT boost converter

4.6.1.1 Output Capacitor

The converter's output capacitor is used to eliminate the output voltage ripple and also supplies the load when the switch is closed. Therefore, it is affected by factors such as voltage ripple, maximum output voltage, duty cycle, load and frequency. Thus, the value of this capacitor can be calculated from the following equation

$$C_{min} = \frac{D}{\frac{\Delta V_o}{V_o} \times f \times R}$$

f	20 kHz
$\frac{\Delta V_o}{V_o}$	0.001
D	0.625
R	30 Ω

Therefore,

$$C_{min} = \frac{0.625}{0.001 \times 20000 \times 30}$$

$$C \geq 1 \, mF$$

The duty cycle here is selected at 0.625 and the selected capacitor in this system is chosen to be 6 mF in order to get a maximum ripple voltage of 0.1%.

4.6.1.2 Inductor Selection

The inductor is used in the boost converter for energy storage. Additionally, it controls the desired output-current ripple. An inverse relationship exists between the volume of L and the switch frequency. Therefore, increasing the frequency allows the use of a smaller inductor size, although using very high frequency can lead to switching loss. Moreover, the boost converter must operate at a continuous mode, which can be assured by selecting the proper value of L, which is capable of providing a continuous current to the load. The minimum inductor value at the given frequency is therefore:

$$L_{min} = \frac{V_s \times D}{\Delta i_L \, f}$$

f	20 kHz
V_s	300 V
D	0.625
Δi_L	4 A

$$L_{min} = \frac{300 \times 0.625}{4 \times 20000}$$

$$L_{min} = 2.3 \, mH$$

The inductor value of the proposed system is chosen to be higher than the calculated minimum value at 6 *mH*.

4.6.1.3 Diode Specification

The diode is another part of the boost circuit that blocks the reverse current from the load to reach the source when the switch is closed. The diode should provide a path for the current to flow from the source to the load when the switch is open.

Therefore, the diode selection should maintain the diode's forward current, which is the maximum load current.

$$I_D = I_{o\ max} = 400\ A$$

In this equation, the I_D is the diode's average forward current, and $I_{o\ max}$ is the maximum output current.

The forward voltage drop of the Schottky diode is around 0.3V where other diode types have a higher forward voltage drop rating, indicating that the power drop is lowest for the Schottky diode. Additionally, the Schottky diode is the fastest among the ultra-fast and standard rectifier diodes. Therefore, the Schottky diode has the highest efficiency amongst other diodes (Hart, 2011; Hauke, 2009).

The power consumed within the diode can be calculated from the following equation:

$$P_D = I_D \times V_D$$

where V_D is the forward voltage drop around the diode.

4.6.1.4   Converter Switch

The last component of the MPPT boost converter is the power switch. This switch steps up the input voltage by frequently switching on and off. Different types of transistors can be used in this converter, including MOSFET, a bipolar junction transistor (BJT), and an insulated-gate bipolar junction transistor (IGBT). Furthermore, each of these transistors has its own characteristics and specifications. In fact, MOSFET has the ability to handle a heavy load, with a voltage rating that reaches 1500V and a maximum current of 600A. Moreover, MOSFET has another advantage in that it can be run with an ultra-high frequency (a hundred megahertz). On the other hand, IGBT is another transistor that might be implemented that is commonly used instead of BJT, which is not typically used in recent applications. Additionally, the IGBT has higher voltage and current ratings than the MOSFET, which is not the case in this application. However, the IGBT can operate at a maximum frequency of 100 kHz while the MOSFET here operates at 20 kHz. Finally the voltage drop around the IGBT, which results in higher power loss, is considerably higher than with the MOSFET (Hart, 2011).

4.7 Voltage Reshaping Converter

The second converter in the proposed configuration is the SPWM controlled DC-DC converter. It is connected between the MPPT converter and the DC-AC inverter and aims to convert the input DC voltage to a rectified sine wave output voltage. This converter manages this function through controlling the switching pulses, which in this case are rectified sine wave modulation signals (SPWM) instead of normal pulses width modulation (PWM) signals.

In the proposed system, the second converter is a boost converter. The design of this converter's components must take into consideration the input and output voltage and the current rates. In addition, choosing the value of each component should help in obtaining the output rectified sine wave shape. All design parameters are evaluated in the following subsections.

4.7.1 Design of the Parameters

Using the conventional boost equations to select the values of the inductor L and capacitor C of this converter is the first step. However, this converter should be able to reshape the voltage wave as well. This extra function demands proper selection of each of these components. The minimum inductor value at the given frequency is therefore:

$$L_{min} = \frac{V_s \times D}{\Delta i_L \, f}$$

f	1000 Hz
V_s	800 V
D	0.64
Δi_L	4 A

$$L_{min} = \frac{800 \times 0.64}{4 \times 1000}$$

$$L_{min} = 128 \, mH$$

The inductor value of the proposed system is chosen to be higher than the calculated minimum value at $500 \, mH$.

4.7.1.1 Output Capacitor Selection

The output capacitor in a converter is set to smooth the output voltage from unwanted voltage ripple. Additionally, in this converter it helps to maintain the output voltage as a pure half sine wave as possible. Therefore, the goal is to avoid the distortion in the output wave by smartly choosing the size of the capacitor.

The relationship between the capacitor size and the harmonic distortion is driven at 1000 Hz switching frequency. While the inductor is constant at 500 mH, the capacitance was increased gradually from a very low value (0.6 µF) to (0.5 mF) and the total harmonic distortion (THD) is measured at each point. A representation plot of this relation is drawn and shown in Figure 4.11. It is noticed that the THD decreases as far as the capacitor volume is increasing in an inverse relation till a breaking point. After the breaking point, the relationship between capacitance and THD becomes a direct relationship where the THD increases with the increase in the capacitor volume. Thus, the goal is to pick the capacitor that guarantees the voltage delivery at the minimum THD.
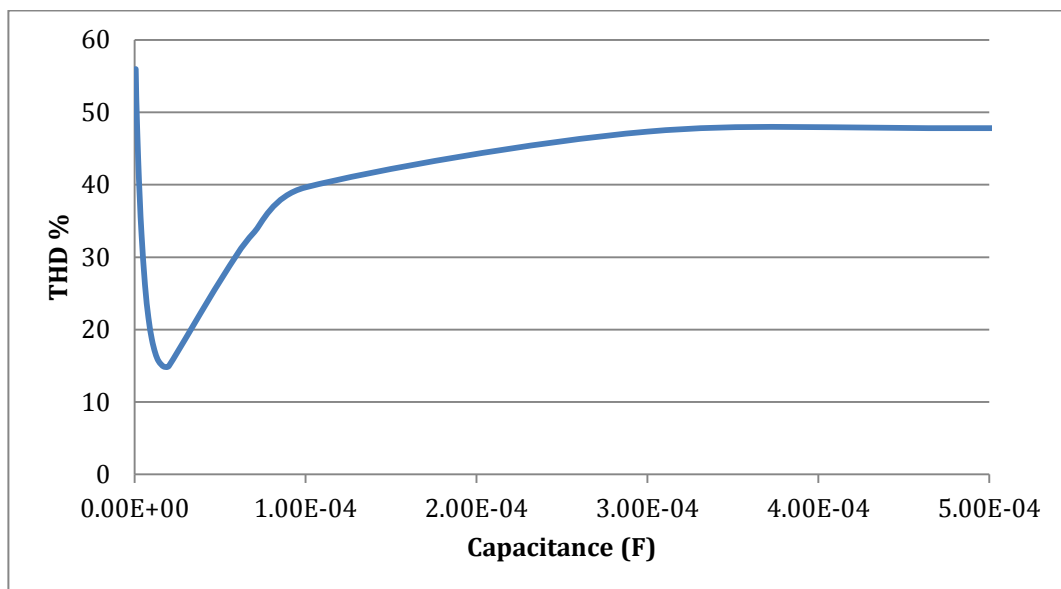
Figure 4.11: Capacitance (in farad) vs Total Harmonic Distortion
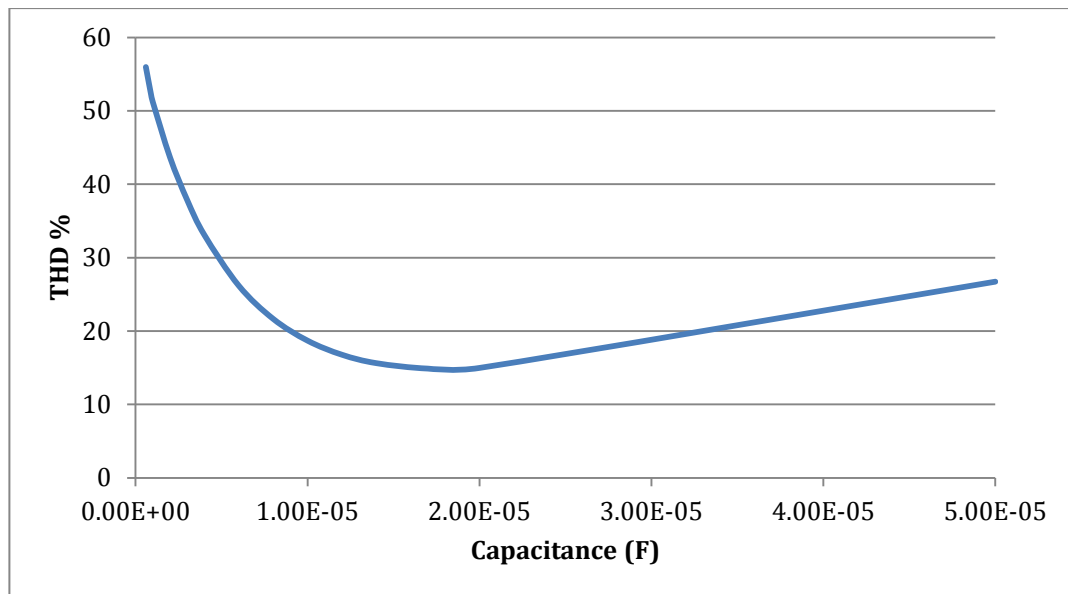
Figure 4.12: Capacitance (in farad) vs Total Harmonic Distortion

Since the target is to obtain the output voltage with the minimum THD, a detail of Figure 4.11 focusing on the area with the lowest THD value is presented in Figure 4.12. This area is between the capacitance values of 10 - 22 µF. In order to accurately obtain this value, an equation depicting the relationship between C and THD is needed. As Figure 4.11 shows, the relationship between C and THD is nonlinear; for this reason, it is likely impossible to drive the curve's equation manually. In a situation like this, Matlab software is very useful and provides the necessary tools to analyse the collected data and generate the appropriate mathematical model.

The collected data in the Matlab file has been plotted. In addition, the 'Curve Fitting' tool in Matlab is applied to work out the equation that fits the plotted data. This tool has a variety of mathematical equations for different types of curves, including polynomial, exponential, power and rational polynomial model equations. Additionally, Matlab allows the user trying these different mathematical models to compare them and implement the most suitable model. Once the fitting curve is shown, the mathematical model appears with all of its coefficients.

The rational polynomial type is the mathematical model that could best fit the collected data. Moreover, by controlling the model's number of coefficients, the user

can obtain different fittings. Accordingly, seven models are generated for the collected data in order to capture the model with the minimum possible error.

The accuracy of the mathematical model is calculated by the Curve Fitting tool, which provides the user with the values of different factors that enable the user to select the model of best fit. These factors are:

- The sum of squares due to error of the fit 'SSE'.
- The square of the correlation between the response values and the predicted response values 'R-square'.
- The degrees of freedom adjusted R-square 'Adj R-sq'
- The root mean squared error or standard error 'RMSE'
- The number of coefficients in the mathematical model '#Coeff'

The curve-fitting window shows a table of all fits and the values of each of the previous factors.

Table 4-3 shows the seven solutions (1-7), their types and the accuracy factors. The best three solutions (solution 2, solution 6, and solution 7) are highlighted, and extracted in Table 4-4 for closer comparison and examination.

Table 4-3: Numbers of possible fits and their accuracy factors

Fit name	Data	Fit type	SSE	R-square	DFE	Adj R-sq	RMSE	#Coeff
Solution 1	X vs. Y	rat53	3.08E+03	0.2299	12	-0.2835	16.0122	9
Solution 2	X vs. Y	rat52	24.099	0.994	13	0.9907	1.3615	8
Solution 3	X vs. Y	rat52	489.3268	0.8775	13	0.8116	6.1352	8
Solution 4	X vs. Y	rat52	489.3268	0.8775	13	0.8116	6.1352	8
Solution 5	X vs. Y	rat52	2.30E+03	0.4242	13	0.1142	13.3023	8
Solution 6	X vs. Y	rat52	212.424	0.9445	12	0.9122	4.2074	8
Solution 7	X vs. Y	rat55	32.6779	0.9941	10	0.9881	1.5388	11

Table 4-4: Accuracy comparison for the best 3 solutions

Fit Name	SSE	R-square	RMSE	Adj R-sq	#Coeff
	Best fit = closer to 0	Best fit = closer to 1	Best fit = closer to 0	Best fit = closer to 1	Best fit = less #
Solution 2	24.09	.994	1.361	.9907	8
Solution 6	212.42	.944	4.207	.9122	8
Solution 7	23.68	.994	1.539	.9881	11

According to Matlab, the closer SSE and RMSE are to zero, the more likely the model is to have high predictive accuracy, with accuracy decreasing as these two factors increase in value. On the other hand, the perfect fit should have the value of R-square at one, the optimum, or very close to it. The other factor is the number of coefficients; even though a higher number would increase the value of R-square, it could results in an over-fit model. The Adj R-sq is actually considered the best indicator of the fit quality. A high level of differentiation between the Adj R-sq and R-square indicates there are too many coefficients for the model.

Regarding to Table 4-4, the best two fits are solutions 2 and 7. Both share the same R-square rate at 0.994, while the R-square rate for solution 6 is slightly lower. In addition, the SEE of solution 6 is considerably higher than the other two fits—this is the primary reason for excluding this solution. Each of the other fits likely shares the same SSE and RMSE rates. However, solution 2 has the higher Adj R-sq rate and a lower number of coefficients; therefore, it is chosen as the best mathematical model for selecting the value of the converter's capacitor.

The function that fit the collected data with the least error is shown in Figure 4.13.
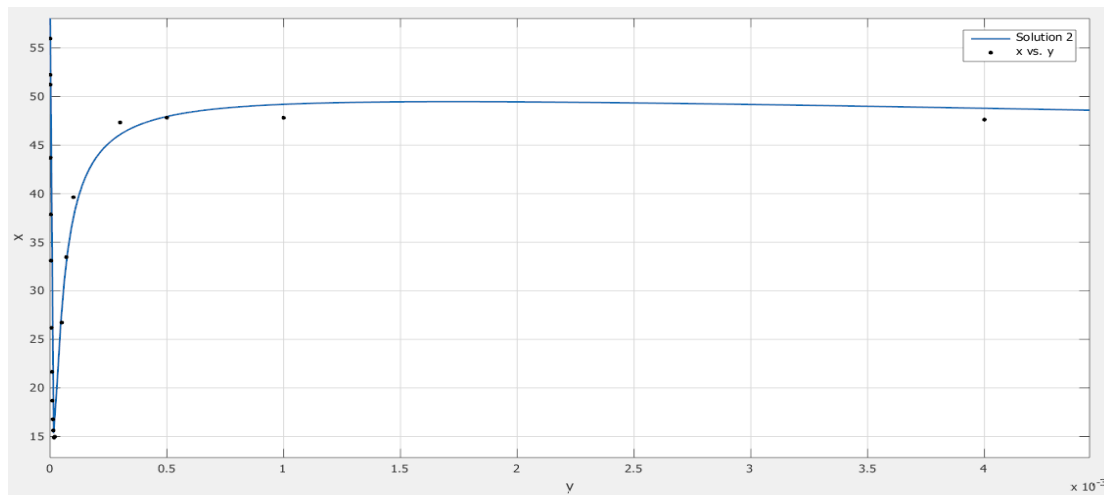
Figure 4.13: Curve fitting of the collected data of C vs THD

4.7.1.1.1 The Mathematical Model

The curve-fitting tool produces the mathematical model that represents the curve in Figure 4.13. This model is a fifth-degree rational polynomial with eight constants:

$$f(x) = \frac{p_1 x^5 + p_2 x^4 + p_3 x^3 + p_4 x^2 + p_5 x + p_6}{x^2 + q_1 x + q_2}$$

The values for these eight constants are given in the table below:

$p_1 =$	0.4084
$p_2 =$	-2.988
$p_3 =$	-525.2
$p_4 =$	51.28
$p_5 =$	-0.0009194
$p_6 =$	-1.171e-08
$q_1 =$	1.297e-05
$q_2 =$	1.963e-10

To find the value of the suitable capacitor for the proposed converter, the mathematical model is solved in Microsoft Excel. To validate the model, a curve for a long series of capacitor rates is plotted and compared to the curve from the collected data shown earlier. Both curves are shown in Figure 4.14.
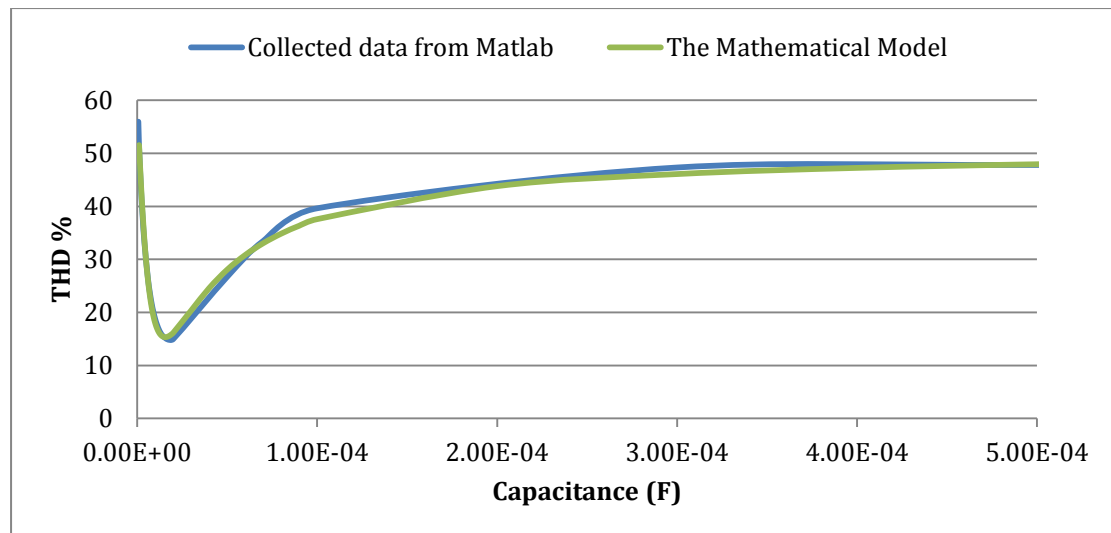
Figure 4.14: Mathematical model vs Collected data

The minimum THD for this curve is at 15.3%; the capacitance at this value is 16×10^{-6} F.

Table 4-5 shows the rates of the whole components of the reshaping converter.

Table 4-5: The second converter's circuit parameters

Parameter	Symbol	Value
Input Voltage	V_{in}	800 V
Output Voltage	V_{o2}	2200 V
Rating Power	P	100 kW
Frequency	f_2	1000 Hz
Capacitor	C	$16{\times}10^{-6}$ F
Inductor	L	500 mH
Load	R	30 Ω

4.7.2   Principle of Operation

Normally, a boost converter is used to step up the input voltage by controlling the switch pulses. These control pulses are usually generated from a PWM source that operates at a selected duty cycle. The output voltage level can be controlled by changing the value of the duty cycle. Generally, both the input and output of the power boost converter are flat DC voltage. However, in the proposed system, this particular boost converter aims to redraw the voltage shape from a flat DC to a (most likely) rectified sine wave. Instead of the usual PWM signal, the switch of the converter receives an unusual control signal, a rectified sinusoidal waveform (SPWM), which helps fulfil the aim the converter is utilised for. The output is reshaped into an almost-rectified sine wave signal and stepped up since it is the main function of the boost converter.

4.8   Rectified SPWM Controller

Normally, a boost converter is controlled by a PWM signal. However, this thesis proposes a rectified sinusoidal pulse width modulation (SPWM) source to control the second boost converter in the proposed configuration. It delivers the on and off sequences to the switch gate, allowing the power to be delivered through the converter. The reason for applying this type of control signal is to obtain the desired output voltage—in this case a rectified sine wave.

A SPWM consists of a combination of two waveforms—the carrier and the reference waveform. The carrier waveform is a high-frequency triangular wave, for

example 1000 *Hz*, which is the converter operation frequency. The reference waveform is a 50 *Hz* rectified sine wave. Both waves are merged and the output of this combination is delivered to the switch gate. Figure 4.15 shows the pulse generator circuit.
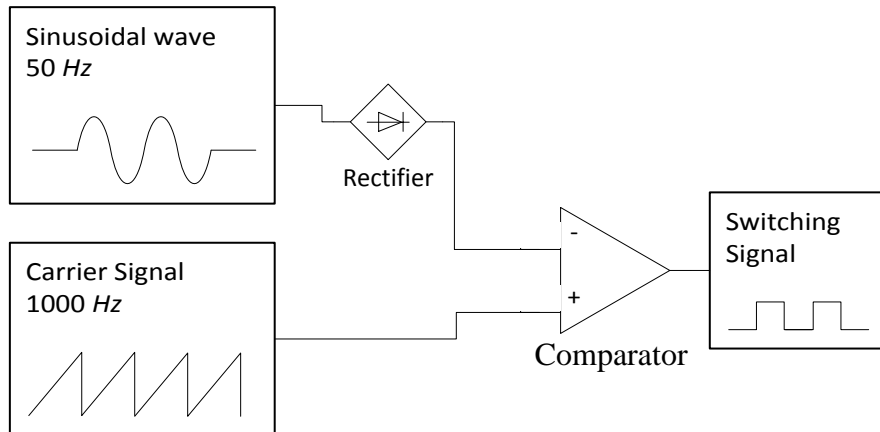
Figure 4.15: Rectified SPWM generator

The carrier signal and the reference waveform are shown in Figure 4.16, where it can be seen that the carrier frequency is very high compared to the reference waveform. The output voltage carries the reference waveform frequency (in this case, 50 Hz). On the other hand, the high frequency of the carrier signal helps to obtain a smoother output wave with a lower level of distortion.

The output pulses are values of zero and one (Figure 4.16). It is important to know that the output value is one when the carrier signal amplitude is greater than the sine wave; otherwise, it is zero.
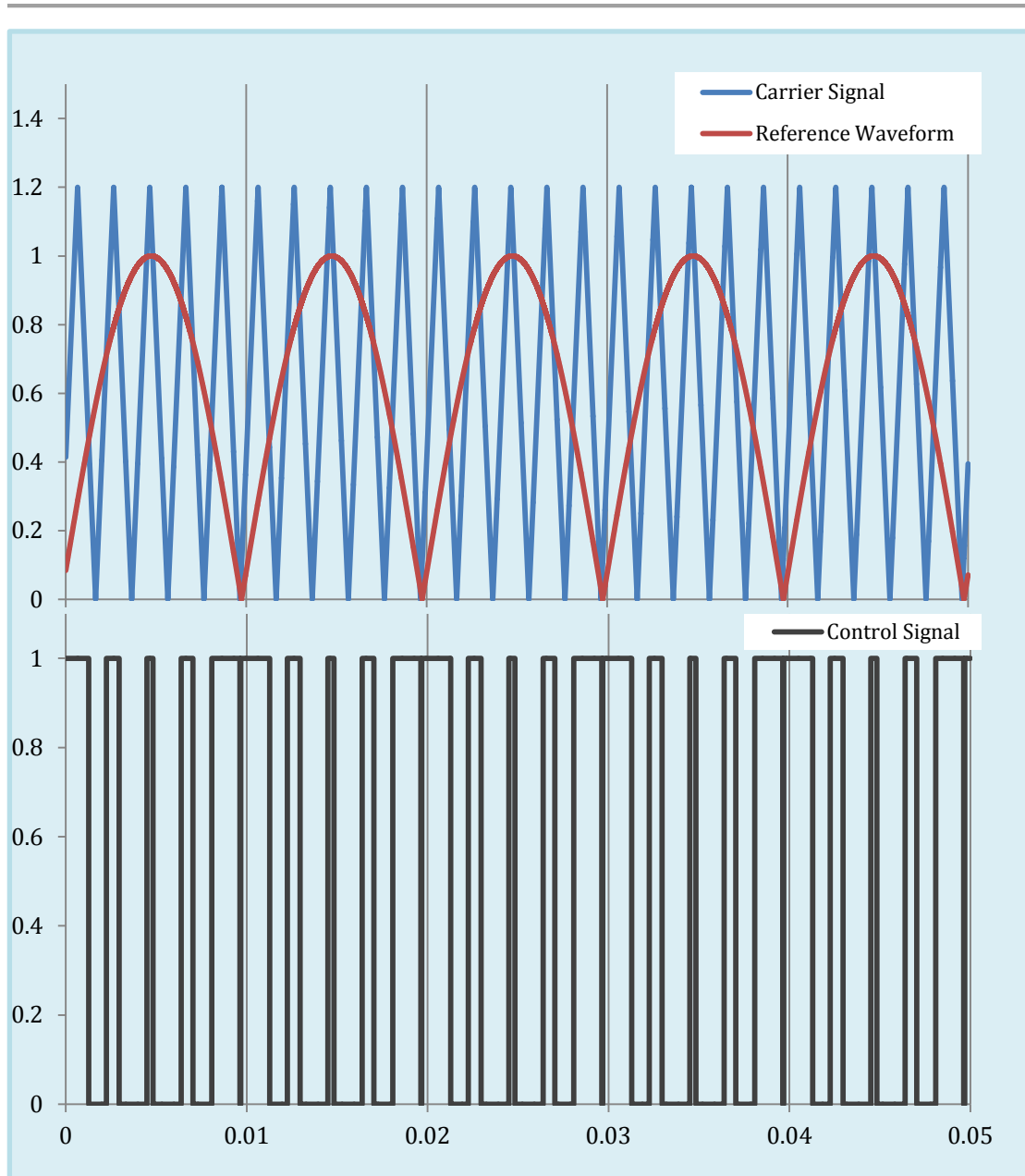
Figure 4.16: Input and output signals of rectified SPWM

4.9   Output Filter

The ideal output voltage would be a fine sine wave with a THD of 0%. However, the inverting interface in the proposed system produces a distorted sinusoidal waveform with around 15% THD. This percentage is higher than the acceptable IEEE practice standard for electrical power systems, so (even though it is still manageable) the THD should be reduced to match the IEEE standard, or even to

a value below the standard cut-off (see Table 4-6). This standard limits the voltage THD and each single harmonic value according to the voltage level. These limits get lower as the voltage level goes up and vice versa. The different categories in the IEEE 2014 THD standard are presented in Table 4-6. As the output voltage of the system presented in this thesis is 2 kV, the acceptable THD and individual harmonic values are 5.0% and 3.0%, respectively (IEEE-519, 2014).

Table 4-6: IEEE voltage harmonic standards

V	Single harmonic	THD
$V \leq 1\ kV$	5.0 %	8.0 %
$1\ kV < V \leq 69\ kV$	3.0 %	5.0 %
$69\ kV < V \leq 161\ kV$	1.5 %	2.5 %
$V > 161\ kV$	1.0 %	1.5 %

In order to decrease the THD from 15%, an inductor-capacitor (L-C) filter has been added to the circuit at the load coupling point. The L-C filter is formatted as shown in Figure 4.17; the capacitor operates as a sink for all high-order harmonics, while the inductor smooths the path for the fundamental frequency to pass through and block the higher frequency component. The values of L and C are calculated from the equation:

$$f = \frac{1}{2\pi\sqrt{LC}}$$

where $f = 100\ Hz$.

The filter aims to eliminate all harmonics of the 3rd order and higher (3rd order at 150 Hz), as the filter allows only the fundamental component to pass through to the load and eliminate all higher order harmonics.

The equation shows that the values of L and C are both unknown. To calculate the value of C, the value of L is assumed. Different inductance values are assumed, with the value of C changed accordingly every time the value changes. The simulation is then carried out and the THD measured. These data are collected and

plotted in Figure 4.18 to depict the relationship between the THD and the filter's inductance.

Table 4-7 shows the value of each component of the filter and the THD for that filter. For clearer explanation, each filter is given a number in the first column. Filter number 10 has the lowest THD at 2.58% and 1.6% for the highest individual harmonic; these are excellent numbers when placed side-by-side with the IEEE standard in Table 4-6. However, any of the other filters with THD lower than 5% can be implemented. The selected L and C values assure that the THD of the delivered voltage is consistent with the standard. Table 4-8 summarises the data of the implemented filter.
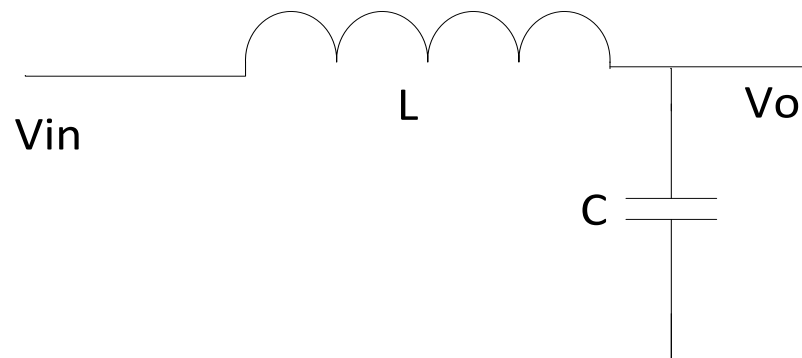
Figure 4.17: Output filter
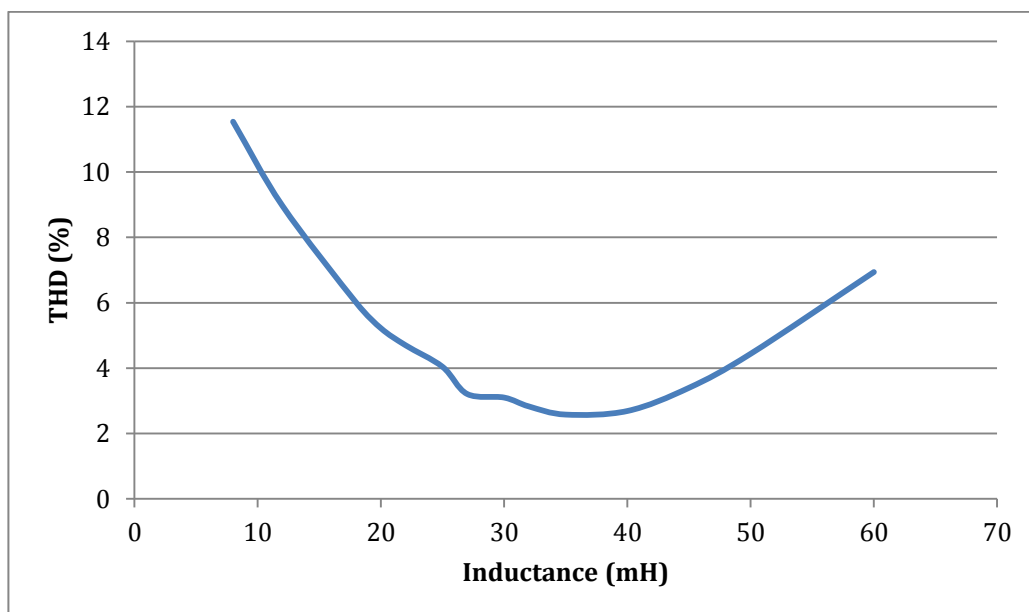
Figure 4.18: THD vs filter's inductance

Table 4-7: THD for different values of L and C

Filter no	L (H)	C (F)	THD (%)
1	8.00E-03	3.17E-06	11.54
2	1.20E-02	2.11E-06	8.97
3	1.80E-02	1.41E-06	6.00
4	2.00E-02	1.27E-06	5.22
5	2.20E-02	1.15E-06	4.70
6	2.50E-02	1.01E-06	4.04
7	2.70E-02	9.38E-07	3.21
8	3.00E-02	8.44E-07	3.1
9	3.20E-02	7.92E-07	2.8
10	3.50E-02	7.24E-07	2.58
11	4.00E-02	6.33E-07	2.69
12	4.50E-02	5.63E-07	3.40
13	5.00E-02	5.07E-07	4.44
14	6.00E-02	4.22E-07	6.94

Table 4-8: The filter data

Inductor (L)	$25\ mH$
Capacitor (C)	$1.01 \times 10^{-6}\ F$
THD	4.04 %
Maximum individual harmonic (5th)	1.60 %

4.10 The DC-AC Inverter

The DC-AC inverter is the other component of the proposed system in Figure 4.2. It is an H-bridge inverter and it connects the output from the second converter to the load. Additionally, it is used to transform the DC voltage to AC voltage and inject it into the load.

Generally, if the H-bridge inverter is controlled by normal-square control at a low frequency (for example, 50 Hz) the output voltage wave will be a two-level square wave (Figure 4.19) This non-sinusoidal wave has high harmonic values, but these could be acceptable for some applications. However, in order to develop a sinusoidal output wave with lower total harmonic distortion (THD) the PWM control

is implemented. This concept shows an improved output voltage shape, but the inverter switches must operate on high frequency. This increases the total loss at the inverter and lowers its efficiency.
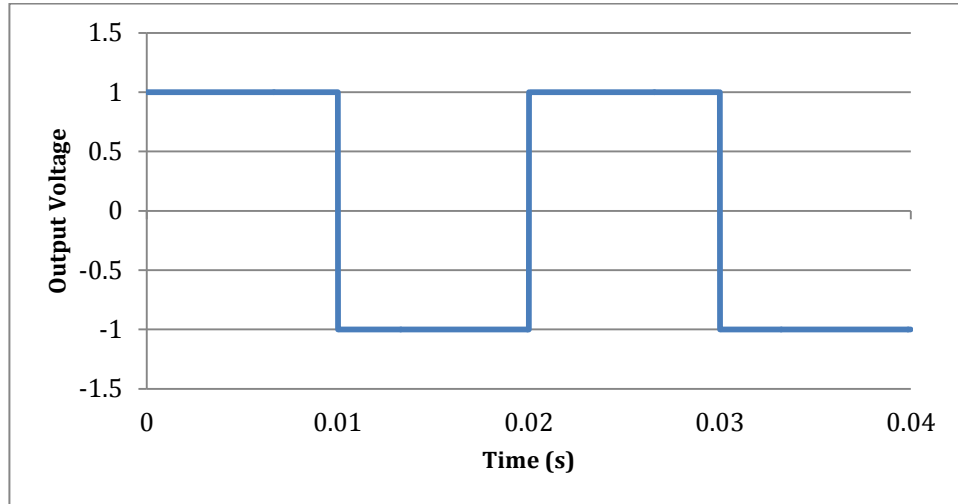
Figure 4.19: H-bridge inverter square output voltage

The multi-level inverter is another topology that is often used to transform DC to AC voltage in PV applications. This topology can be applied into a single H-bridge to obtain a three-level voltage output +V, 0 and -V that still experienced high THD. However, production of multi-level output voltage usually requires more than a single H-bridge for a desired sine-like output with a reduced harmonic component. The operation of this significant number of switches in the circuit at high frequency leads to more switching loss and decreases system efficiency. An example of a 7-level inverter voltage output is shown in Figure 4.20.
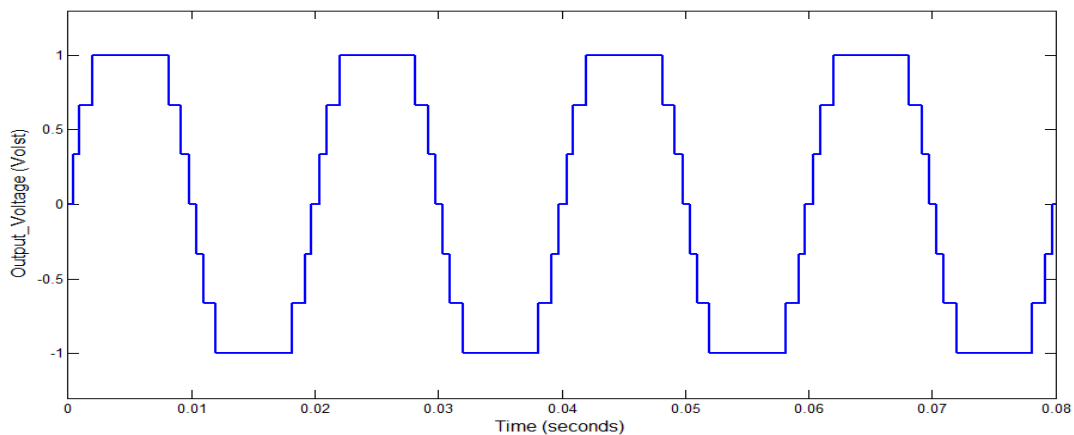
Figure 4.20: Output voltage of a multi-level inverter (7-level)

4.10.1 The Proposed H-bridge

In order to maintain the high efficiency within the proposed system configuration, the loss at the inverter must be kept at a low level or eliminated if possible. Therefore, the inverter in this system is an H-bridge inverter that consists of four IGBT switches as Figure 4.21 shows.
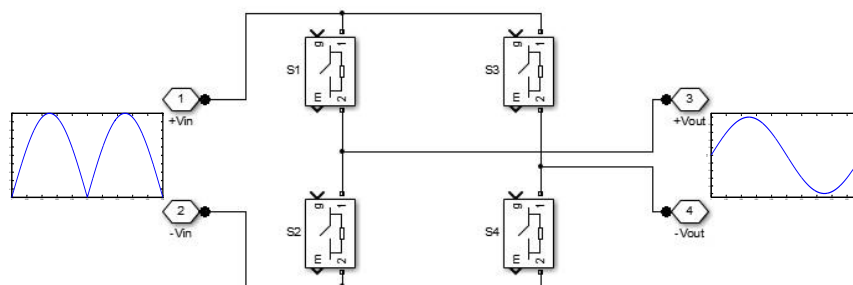
Figure 4.21: The H-bridge inverter

The proposed inverter is superior to other inverter types and provides many advantages. Firstly, it is designed to operate at 50-Hz frequency instead of at a high frequency, significantly decreasing the switching loss. Moreover, the total number of switches is four, whereas in a multi-level inverter (if applied) there are at least eight switches, further reducing the switching power loss. Furthermore, the number of components in the circuit is considerably reduced, dramatically reducing costs. The ease with which this inverter can be controlled is another advantage compared to multi-level inverters.

4.10.2 Principle of Operation

The principle of operation for this H-bridge inverter is simple. The input voltage is a rectified sinusoidal waveform that is produced by the converter in the previous stage. Therefore, the goal with use of this inverter is to flip-flop each half cycle for the sake of earning sinusoidal output voltage. This goal is attained by switching the switches S1, S2, S3 and S4 on and off in a specific order. Normally, S1 and S4 operate at the same time and are fired by the same signal, while S2 and S3 close together when the other switches are open.

Table 4-9 shows these sequences and the output voltage rate.

Table 4-9: The switching sequence of the H-bridge inverter

Switches Closed	Switches Opened	Output Voltage
S1 and S4	S2 and S3	+Vo
S2 and S3	S1 and S4	-Vo

4.11 The Proposed Configuration's Merits

4.11.1 The System Efficiency

The proposed system replaces the multi-level inverter in the PV application by introducing the rectified SPWM converter and an H-Bridge inverter that operates at a low frequency of 50 Hz. The aim of this replacement is to improve the transformation efficiency by decreasing the power losses attributable to the utilisation of a large amount of switches operating at a high frequency. The switching power losses in multi-level inverters are quite high especially since the switches operate at high frequency. The average loss occurring in each diode and switch in the circuit can be calculated by the following equations (Kim *et al.*, 2001)

$$P_{D_{avg.\ sw_{loss}}} = \frac{1}{2\pi} \int_{\alpha}^{\beta} E_{rec} \cdot |i_c| \cdot f_c \, d\theta \quad 4$$

$$P_{S_{avg.\ sw_{loss}}} = \frac{1}{2\pi} \int_{\alpha}^{\beta} (E_{on} + E_{off}) \cdot |i_c| \cdot f_c \, d\theta$$

where:

fc is carrier wave frequency (High Frequency).

E_{rec} is the reverse recovery energy coefficient.

E_{on} is the turn-on switching energy.

E_{off} is the turn-off switching energy.

α is the start angle of interval to appear switching loss over fundamental period.

β is the end angle of the switching interval.

As the equations show, the frequency (*fc*) is a main factor in calculating the loss of each switch and diode. Moreover, multilevel inverters usually operate at high

frequency. Additionally, as these equations are for each individual switch, therefore, the loss is significantly increased with the existence of more switches within the circuit.

On the other hand, the proposed system implements an H-bridge inverter with only 4 switches and 4 diodes at the line frequency 50 Hz. In addition, the system introduces an extra switch at 1000 Hz and a diode within the SPWM converter. A comparison between the proposed system and the existing multi-level inverter has been provided in Table 4-10 to show the number of switches for each inverter topology. The Cascaded H-bridge Multilevel Inverter (CHB-MLI) has been chosen among the other multilevel inverter topologies as it employs a minimum number of switches. The proposed topology is found to have the least number of HF switches compared to the other topologies. Therefore, the proposed system operates at higher performance and lower loss than the system that applies the multi-level inverter topology.

Table 4-10: The number of HF & LF switches and diodes of each inverter topology

	5-level		7-level		9-level		N-level		Proposed	
	Switches	Diodes	S	D	S	D	S	D	S	D
HF	8	8	12	12	16	16	N_S	N_D	1	1
LF									4	4

4.11.2 The Maintenance Cost and Reliability

Decreasing the cost of any system is always a desired goal. The proposed system in this thesis aims toward this goal whenever possible. Moreover, the loss in the switches at high frequency generates heat, causing switch failure (Zhou *et al.*, 2015) . However, operating these switches at a low frequency helps overcome this obstacle.

From the control point of view, each converter of the proposed configuration is controlled individually in order to increase the reliability of the system. Furthermore, the control of the H-Bridge inverter is quite simple and easy to implement compare to the significantly complicated control of the multi-level inverter.

4.12 Summary

In this chapter a new proposed PV inverter configuration is presented. A comprehensive analysis of each component of this configuration is carried out, and a comparison between widely used MPPT methods presented. Moreover, a decision matrix table is presented. The incremental conductance method is the selected method and its flowchart is presented. Additionally, the MPPT converter is chosen based on an analysis carried out using the decision matrix table technique. The boost converter was selected, as it had the highest score among all of the reviewed converters. PSPICE implementation of each converter is presented, and a detailed design process for the MPPT converter is obtained that is supported by the mathematical models. Then, the reshaping converter principle is explained and designed. In addition, the control signals of all power electronics devices in the circuit are clarified. The last component of the configuration is the inverter, which is presented in detail. Finally, the merits of the proposed configuration are illustrated.

The next chapter presents the model of the proposed configuration in Matlab/Simulink and includes all of the simulation results.

Chapter 5

Modelling, Simulation and Implementation of the Proposed PV System Configuration

Chapter 5. Modelling, Simulation and Implementation of the Proposed PV Configuration

5.1 Overview

Chapter 2 illustrated in detail the existing PV inverter configurations along with their advantages and drawbacks. The potential for an improved PV inverter configuration encouraged the author to propose a new configuration, with the intent of designing a high-efficiency PV inverter configuration by carefully selecting and optimising each component. Furthermore, the proposed configuration has lower switching losses compared to the configuration that applied multi-level inverters, with fewer components. Chapter 4 presented all of the configuration's specifications.

This chapter presents the author's proposed model and includes the simulation model and the results of different scenarios. These results should prove the validity and the performance quality of the proposed configuration.

5.2 The Model

Matlab/Simulink sets off the required environment to design the proposed system in Figure 4.2. Figure 5.1 shows the build of the proposed configuration in Matlab/Simulink.
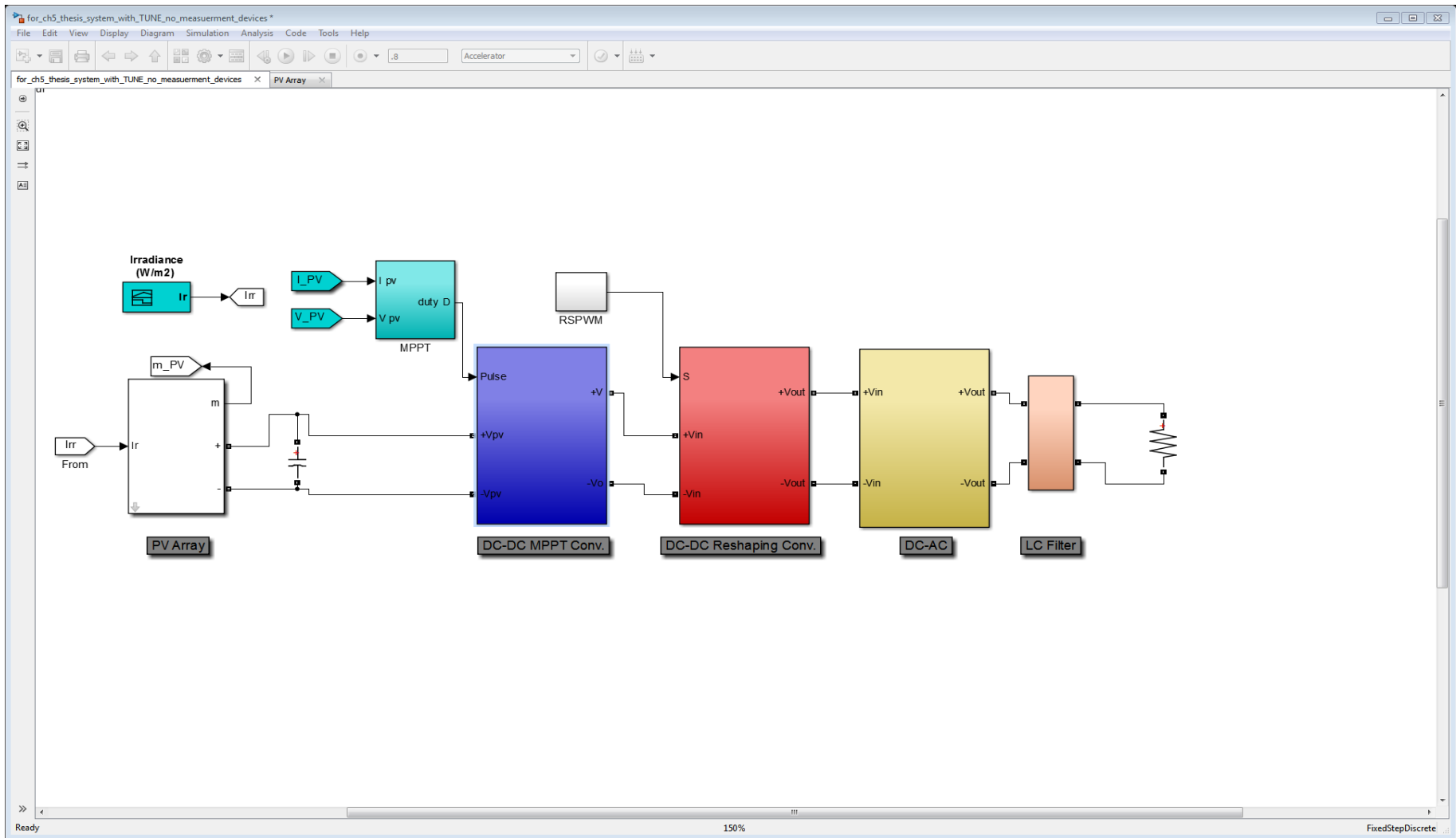
Figure 5.1: The proposed implementation of the PV configuration in Matlab/Simulink

5.2.1 PV Model

The PV cell model is analysed in Chapter 2. This model is implemented in Matlab/Simulink by using a Matlab function box. In this box, the author is able to build the mathematical model by using Matlab codes. However, this model requires actual PV data; these will help to:

- Validate the decision of implementing the single diode PV model.
- Validate the Matlab/Simulink model.
- Show the non-linear relationship between the PV's output current and voltage.
- Examine the impact of the weather conditions on the PV.

This PV model represents the module type SPR-305-WHT manufactured by SunPower (See the datasheet in Appendix B). The parameters of this module are shown in Table 5-1.

Table 5-1: The SunPower SPR-305-WHT PV panel: Parameters

SPR-305-WHT by SunPower	
At Standard Test Conditions (STC) Irradiance $= 1000$ W/m^2 and Temperature $= 25^\circ$ C	
No. of cells per module	96
V_{oc}	64.2 V
I_{sc}	5.96 A
V_{mpp}	54.7 V
I_{mpp}	5.58 A
Series resistance (R_s)	0.038 Ω
Parallel resistance (R_p)	993.5 Ω
Diode ideality constant (a)	1.3

A single panel consisting of 96 cells is modelled using the data from Table 5-1. This model is shown in Figure 5.2 and consists of the PV panel modelled in a Matlab Function, three inputs and an output. The inputs are temperature, irradiance and voltage while the output is the current. The voltage is fed gradually to the PV in order to draw the current-voltage (I-V) and power-voltage (P-V)

characteristics of the PV. The output current is multiplied by the voltage to obtain the PV output power using a Dot box. Furthermore, the model utilises an XY graph box to plot the P-V characteristic and two To Workspace boxes to export the data in case it is needed for further analysis.

The panel is tested under the standard test conditions (STC) of 1000 W/m^2 irradiance and 25°C temperature. Consequently, the P-V characteristic is plotted and shown in Figure 5.3. This panel is designed to deliver a maximum of 305 W output power under these conditions; the plot in Figure 5.3 certifies the accuracy of the chosen mathematical model with a single diode, which is described earlier in Chapter 2.
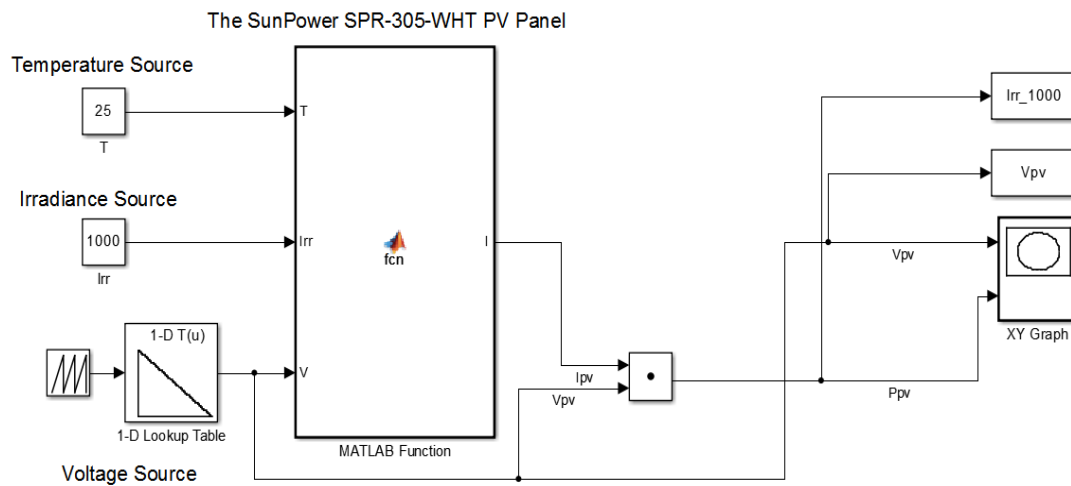
Figure 5.2: The PV panel modelled in a Matlab Function
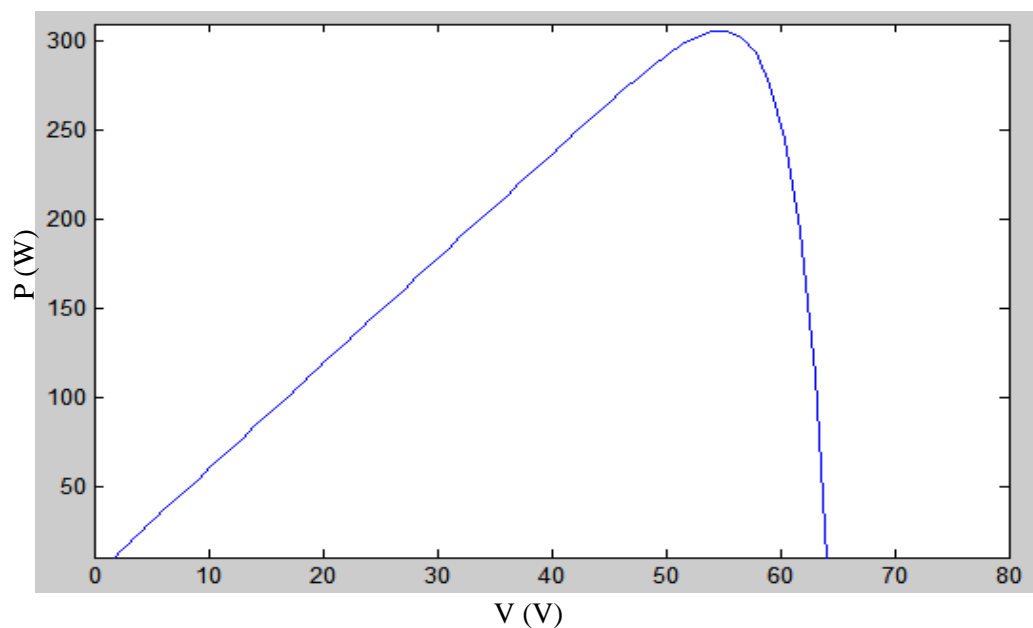
Figure 5.3: P-V characteristic of the SunPower SPR-305-WHT panel
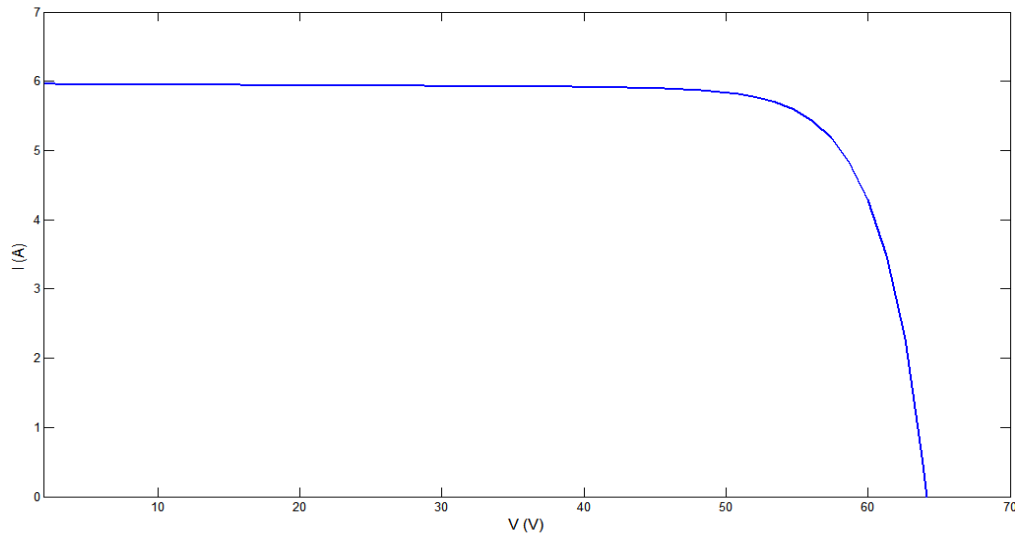
Figure 5.4: I-V characteristic of the SunPower SPR-305-WHT panel

Figure 5.4 shows the relationship between the output current and voltage of the PV at STC. The curve shows that the maximum operating point is around the 'knee' of the curve where the panel delivers its maximum harvested power. However this curve is affected by weather conditions (such as irradiance and temperature) that are certain to influence output power. To obtain that impact, the PV is simulated under various irradiance levels (from 1000 W/m^2 to 200 W/m^2). To prove the accuracy of the Matlab/Simulink model, the I-V curves from the SunPower305 panel's manual are shown in Figure 5.6 and match the curves extracted from the model.
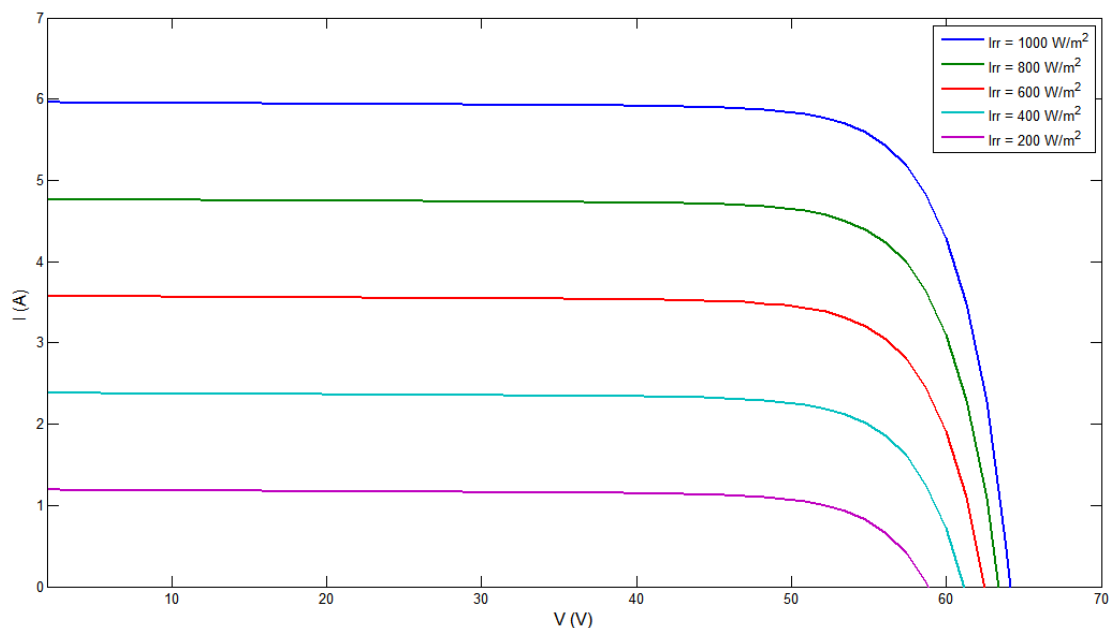
Figure 5.5: I-V curves at different irradiance
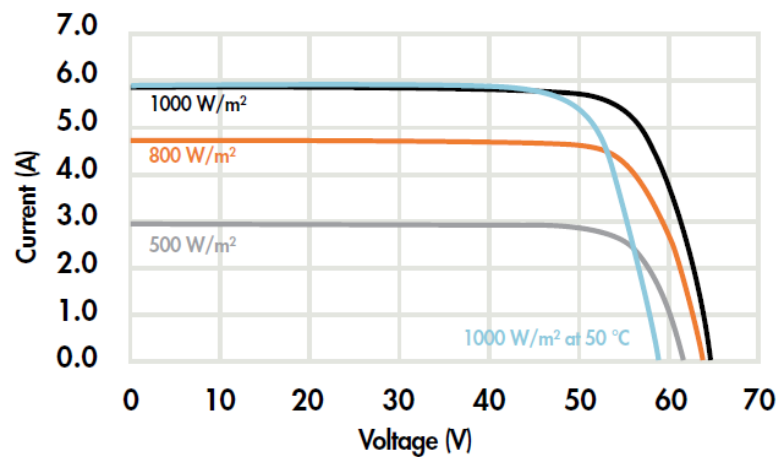
Figure 5.6: I-V curves from the SunPower 305 panel's manual (Appendix B)

On the other hand, tests demonstrated that the performance of the solar panel declines with increases in temperature. Figure 5.7 shows the P-V curves for different temperature levels; it is clear that the PV has high performance when temperatures are low.
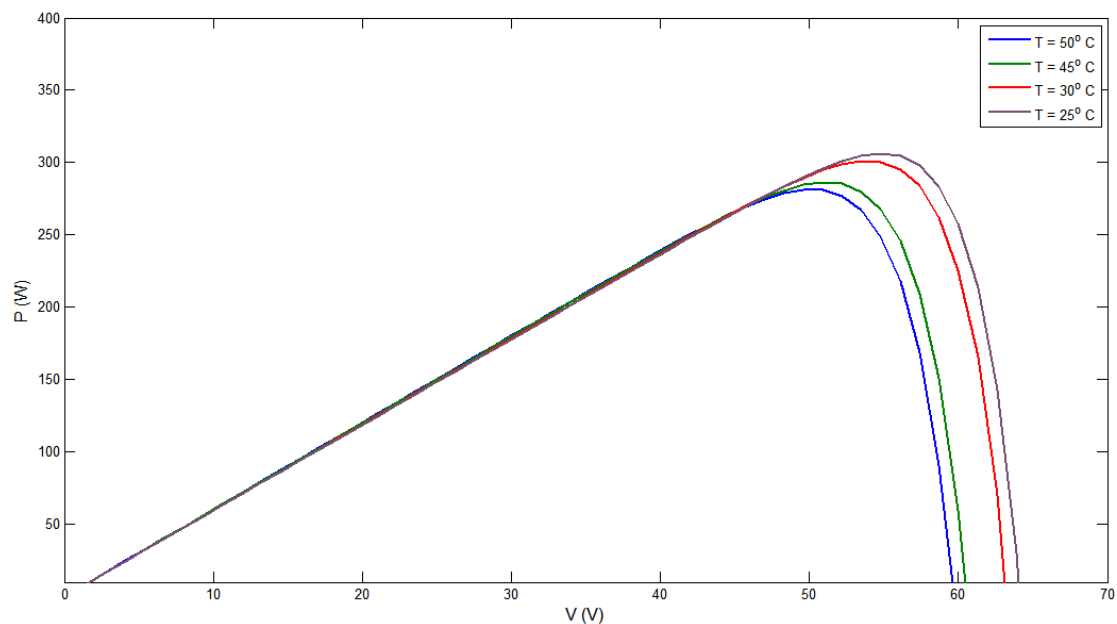
Figure 5.7: P-V curves under various temperatures and fixed irradiance

5.2.2   PV Array

A PV array is used as the energy source in the proposed system. This array consists of multiple panels connected in parallel and series to deliver a higher amount of power and to scale up the size of the system. Additionally, this proposed configuration aims to be implemented in large-scale PV power system.

The array consists of 330 panels distributed in 66 parallel strings; each string contains 5 panels connected in series. Therefore, the total power of these panels equals the summation of each individual PV. Table 5-2 shows the characteristics of this array at STC.

Table 5-2: The PV array characteristics at STC

No. of panels per string	5
No. of parallel strings	66
I_{sc}	393.36 A
V_{oc}	321 V
I_{mpp}	368.28 A
V_{mpp}	273.5 V
P_{mpp}	100.7 kW

The P-V curve of this array is shown in Figure 5.8 and confirms the specification stated in Table 5-2 (that is, the maximum delivered power by the array is around 100 kW at 273.5 V).
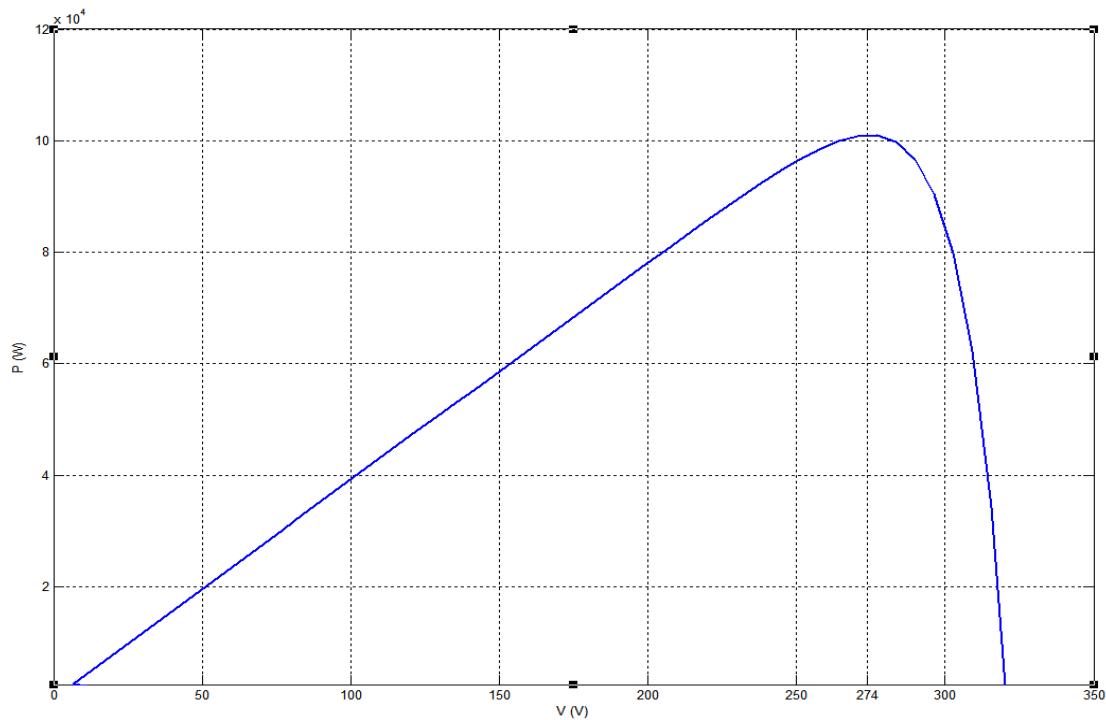
Figure 5.8: P-V characteristics of the PV array

5.2.3   MPPT Unit

The function of the MPPT, as discussed in Chapter 2, is to force the PV to produce its maximum available power under different weather conditions. Moreover, Chapter 2 includes a review of the most implemented algorithms. In addition, Chapter 4 provides a comparison between the algorithms, which was carried out based on the author criteria using the decision table matrix technique. Accordingly, the incremental conductance algorithm is implemented in the system proposed by this thesis.

Sunlight and temperature have a direct effect on the PV's output. Therefore, it is necessary to identify the maximum power of the PV arrays at different irradiances to test the MPPT performance accordingly. The temperature is kept constant at 25° C and the irradiance is changed from 1000 to 250 W/m^2.

Table 5-3 shows the power values at these different irradiances and it can be seen that the PV performance declined dramatically with the absence of light. This relationship is represented in Figure 5.9, which demonstrates the linear relationship between the perceived irradiance and the power produced by the PV array.

Table 5-3: Maximum PV power at different irradiances

Irradiance (I_{rr}) W/m^2	P_{mpp} (kW)
1000	100.7
800	81.28
600	58.52
400	37.9
250	23.1
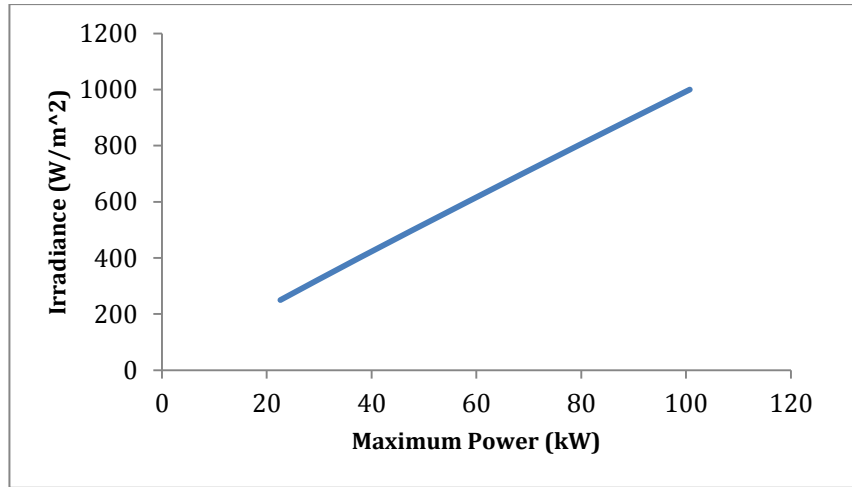
Figure 5.9: I_{rr} vs P_{mmp}

In fact, the irradiance has a direct and obvious impact on the PV current as it is explained in the discussion about the PV model in Chapter 2. Therefore, it is appropriate to recall the equation that describes the relationship between the PV current and perceived sunlight.

$$I_{pv} = \left(I_{pv,n} + K_I \Delta T\right)\frac{G}{G_n} \qquad\qquad 5.1$$

where:

$I_{pv,n}$ is the current at nominal conditions (T = 25°C and G = 1000 W/m^2)

K_I: is the current/temperature coefficient

ΔT: is the change in temperature

G: is the solar irradiance level

G_n: is the nominal irradiance level (1000 W/m^2)

K_I usually has a very low value, which explains the minimal impact of T on the PV's current (Khalifa and El-Saadany, 2011). However, the early assumption is that the temperature remains constant, so the only impact on the current is the irradiance. Equation 5.1 shows that the I_{PV} is proportional to the irradiance where the increase in the irradiance results in extra current to the load.
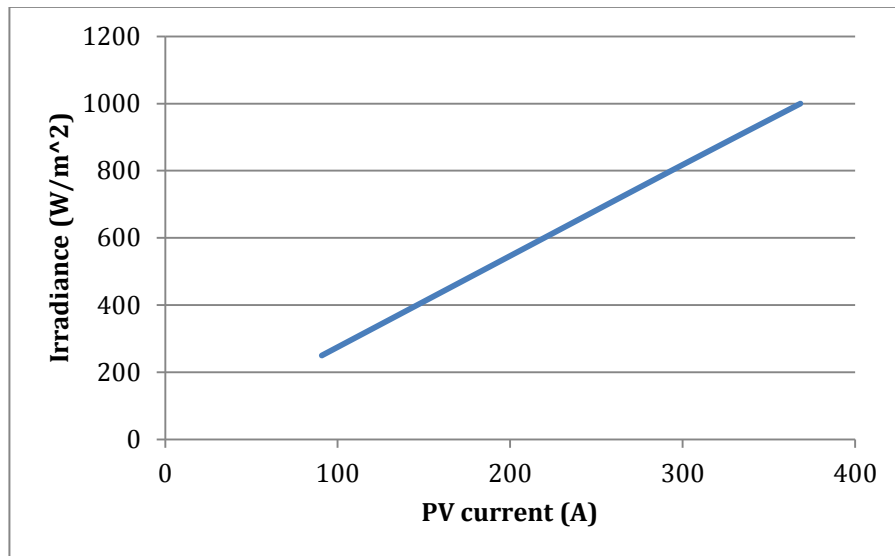
Figure 5.10: PV's current vs Irradiance

5.2.3.1 Simulating the System without the MPPT

To understand the benefits and check the validation of the MPPT, the behaviour of the PV array needs to be clarifies. Normally, the PV energy source operates at a voltage level that is dependent on the load, meaning that the extracted power also varies based on this same load. To examine this, a 30 Ω resistive load is connected directly to the PV panel at STC (see Figure 5.11). The delivered power is recorded around 3.45 kW (as Figure 5.12 shows), while the maximum power stored in the array is 100 kW.
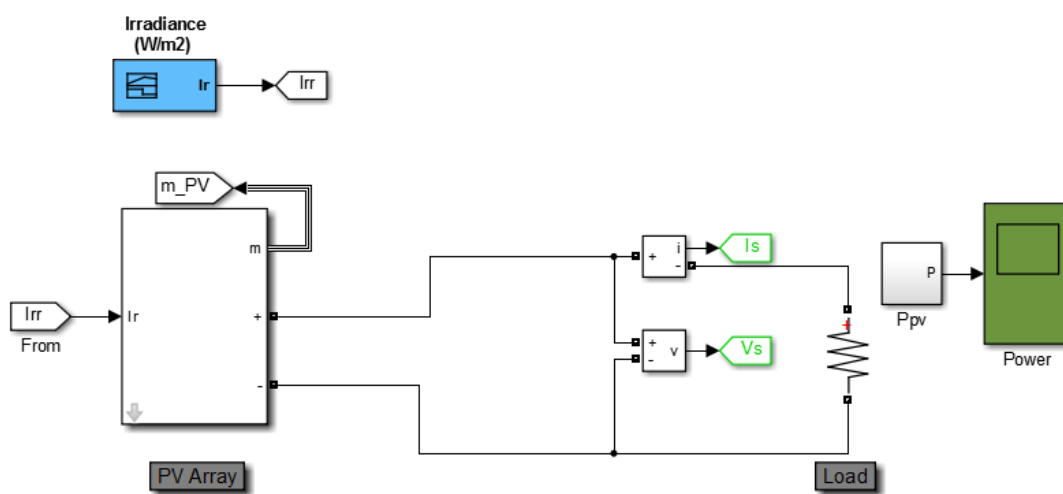
Figure 5.11: The circuit of a PV connected directly to the load
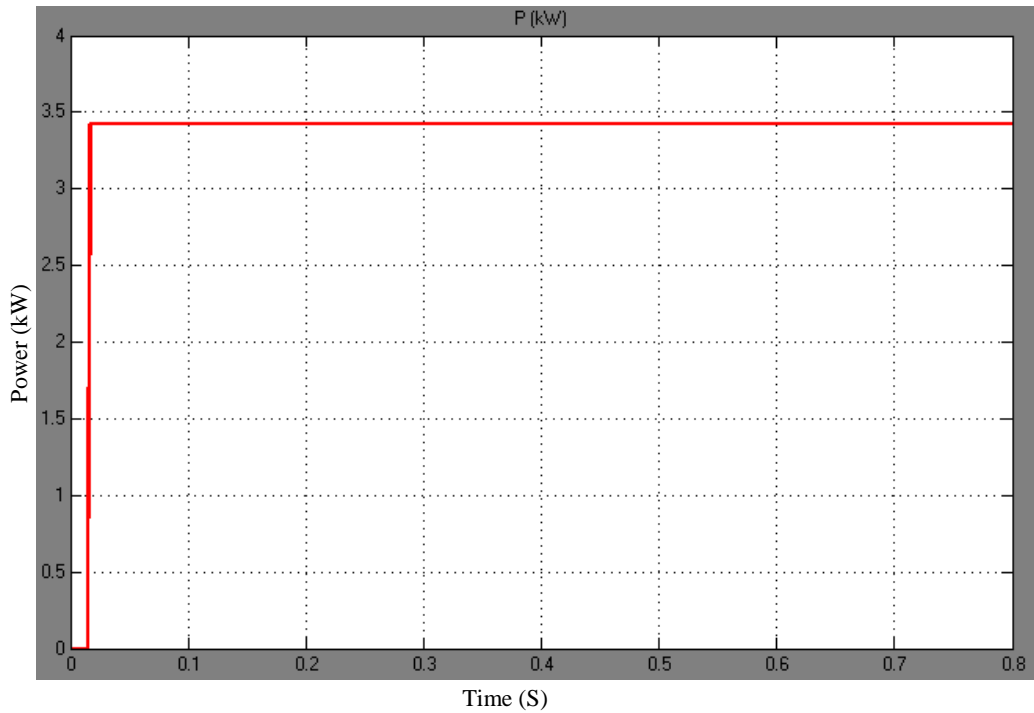
Figure 5.12: PV output power with 30 Ω R$_{Load}$

The simulation has been launched several times, with the load being changed each time. The PV never delivers the maximum power to the load, and Figure 5.13 shows that the amount of delivered power increases as the load decreases. In fact, the maximum power is never delivered because the PV does not operate at the right voltage (V_{mpp} = 273.5 V), meaning that the operating point slides on the P-V curve with respect to the value of the load (see Table 5-4).

Table 5-4: PV output power at different loads

R (Ω)	P (kW)	V$_{PV}$ (V)
0.5	76.28	195.3
1	88.26	297.09
5	20.22	317.96
10	10.21	319.54
30	3.43	320.52
100	1.1	320.86
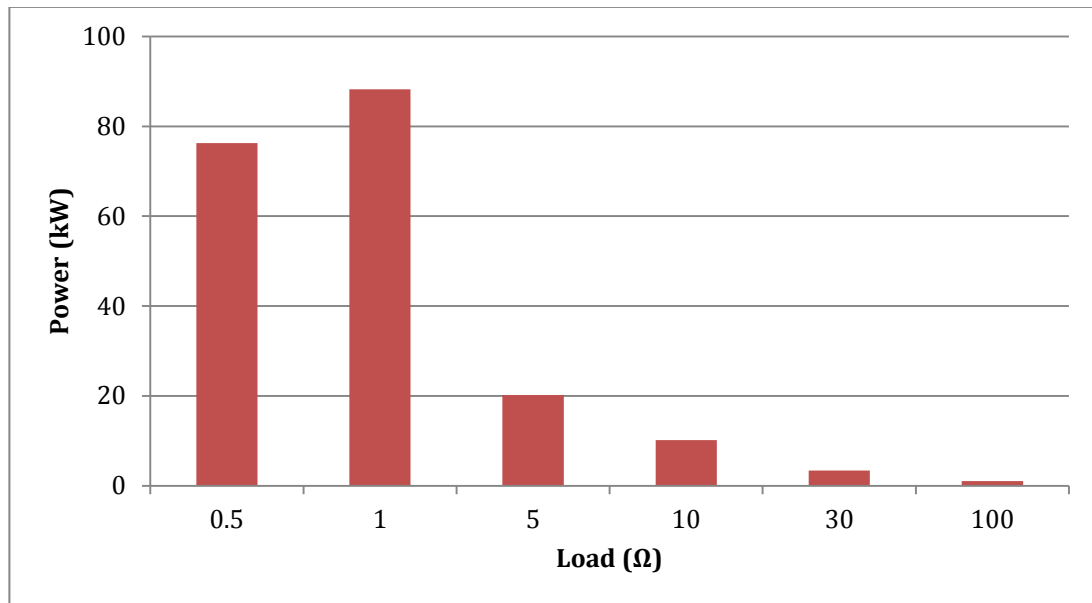
Figure 5.13: P$_{PV}$ vs load

Only a single case exists where the load receives the full stored power within the array. This point can be found by solving equation 5.2:

$$P_{mpp} = \frac{V_{mpp}^2}{R}$$

5.2

where P_{mpp} = 100.7 kW and V_{mpp} = 273.5 V; therefore; R_{mpp} = 0.748 Ω.

The power scope from Matlab/Simulink is shown in Figure 5.14 and the power extracted from the PV array is at its maximum at 100.7 kW.
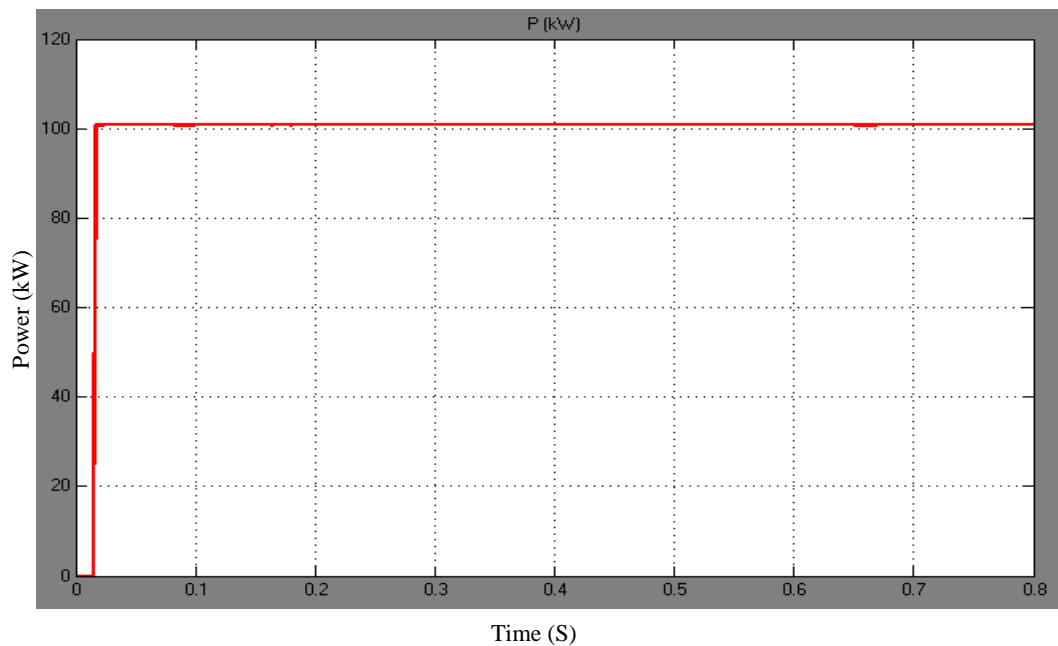
Figure 5.14: PV output power at the optimum load

In conclusion, the simulation of the PV system without adding the MPPT unit proves that a huge amount of the preserved power within the PV is not delivered to the load. The PV in this case serves the load needs only, and any change in the load generates power change, indicating a massive energy loss in the PV system. This evidence clearly shows why this source of energy is considered to be of low efficiency.

5.2.3.2   Simulating the System with an MPPT Unit

The MPPT unit consists of two parts; the MPPT algorithm (the control) and the boost converter. The algorithm receives the voltage and current measurement from the PV and sends the duty cycle correction signal to the converter's switch. The unit should be able to track the MPP at different atmospheric conditions regardless of the load's value. Different scenarios are carried out in order to examine its performance.

The circuit diagram shown in Figure 5.15 consists of the PV array, the MPPT unit (within the black dashed square) and the load. Other measurement devices are connected to either side of the converter and to the display scopes. One scope displays the PV output power and the power at the load, while the other scope displays the operating voltage and the load voltage.

Case I:

Table 5-5 lists the conditions for the first simulation. Note that the irradiance and temperature are set at STC. The aim of this simulation was to examine the functionality of the MPPT unit in delivering the maximum power preserved within the PV.

Table 5-5: Case I simulation data

I_{rr}	T	R	P_{PV} (Expected)
1000 W/m^2	25°C	30 Ω	100.7 kW
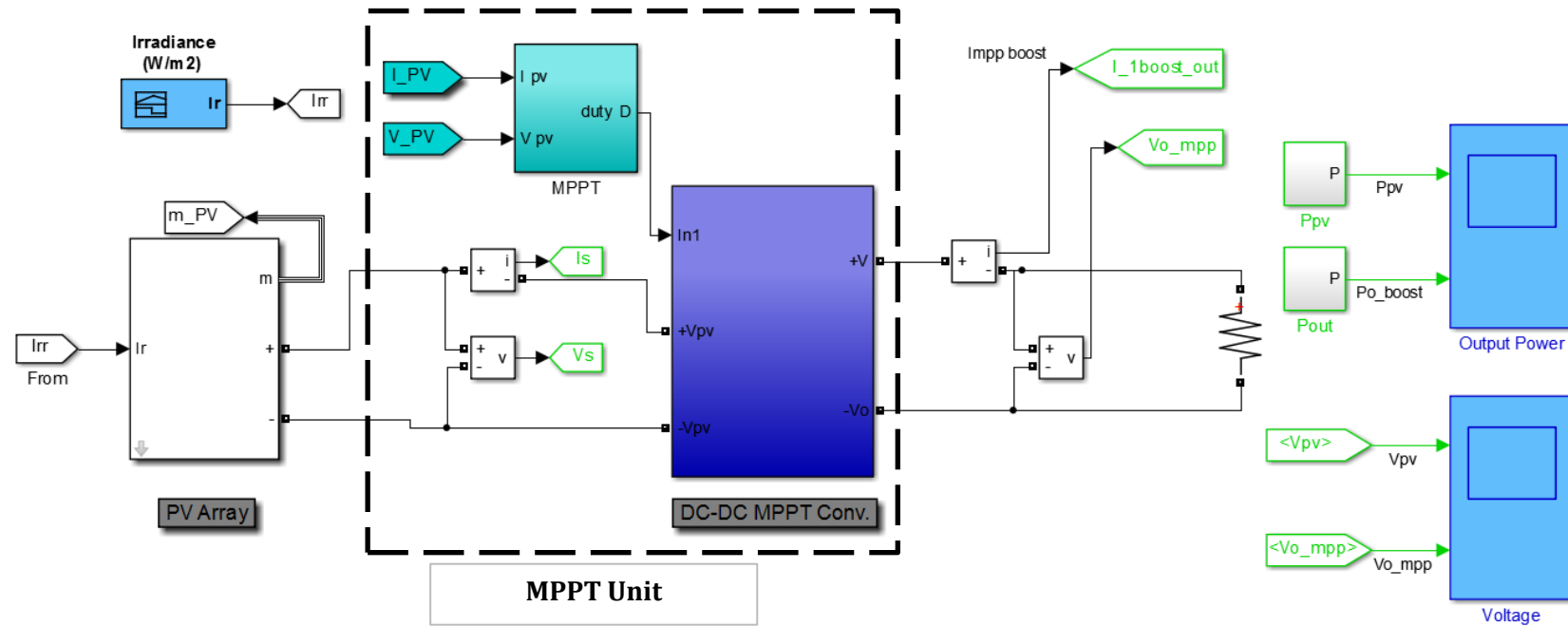
Figure 5.15: The PV array connected to the load through the MPPT unit

The simulation is run for these conditions and the voltage and power outputs of the PV array are 280 V and 100 kW, respectively. The produced power is a bit below the maximum that could be generated at this level of irradiance, but exhibits very low variance. Figure 5.16 shows the PV operating voltage and power.
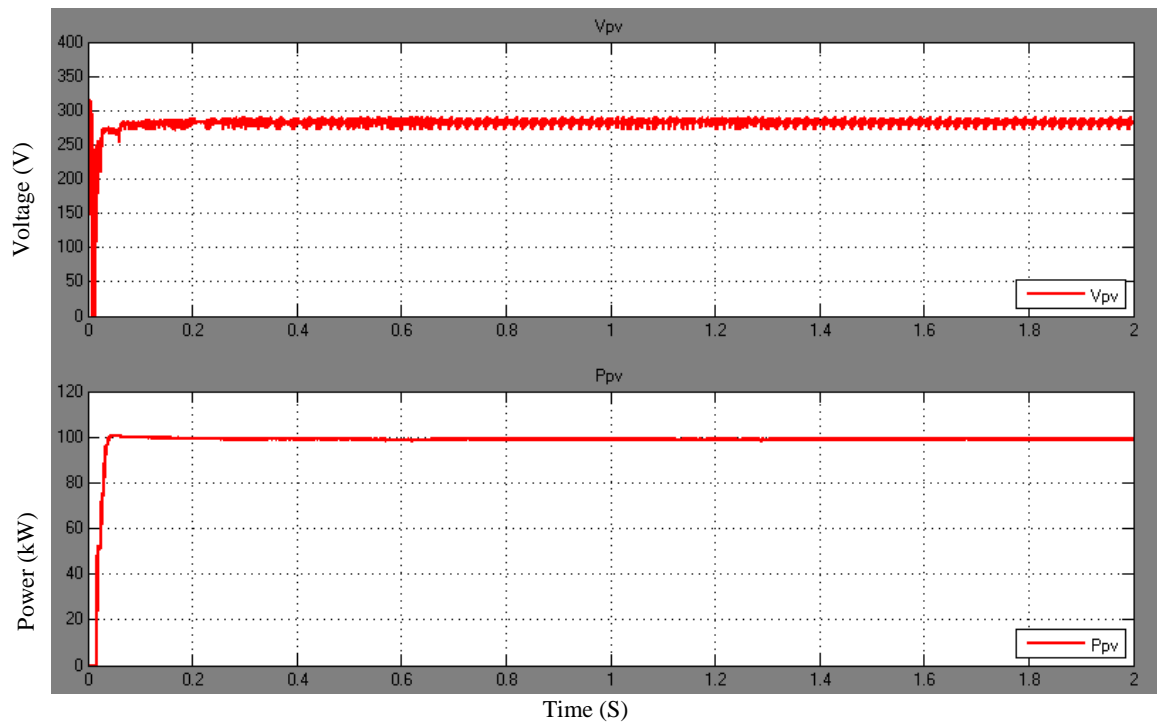
Figure 5.16: PV operating voltage and output power.
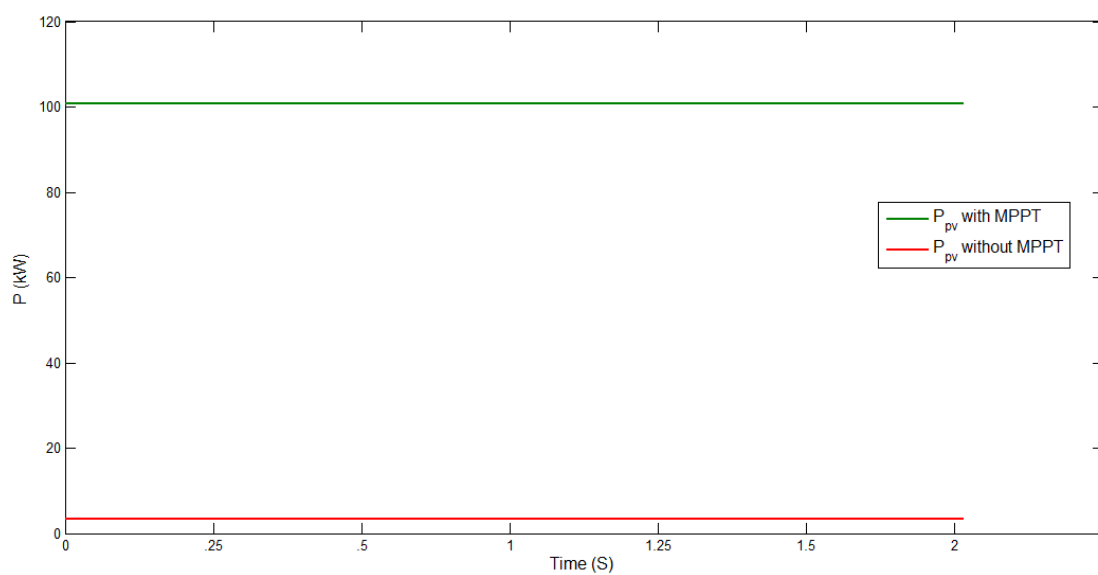
Figure 5.17: PV output power with and without the MPPT at 30Ω load

A quick comparison for the delivered power from the array when it is connected to a 30 Ω load with and without the MPPT unit is shown in Figure 5.17. Even though both are tested at the same conditions, the gap between the two values is enormous—about 97 kW of wasted power. Therefore, utilising the chosen MPPT algorithm in Chapter 4 improves the efficiency of the PV system significantly. The percentage of power saved in this case can be calculated as follows:

$$\%P_{saved} = \frac{P_{w\_mpp} - P_{w\_mpp}}{P_{w\_mpp}}$$

$$\%P_{saved} = \frac{100-3.3}{100} \times 100\%$$

The power saved = 96.7%

Case II:

Table 5-6 lists the conditions for the second simulation. Note that the temperature is constant but the irradiance is changing. The aim is to examine if the tracking process kept up with the change in the light density received by the array.

Table 5-6: Case II simulation data

I_{rr}	Time	T	R	P_{PV} (Expected)
1000 W/m^2	0-1 sec	25°C	30 Ω	100.7 kW
600 W/m^2	1-2 sec			58.52 kW
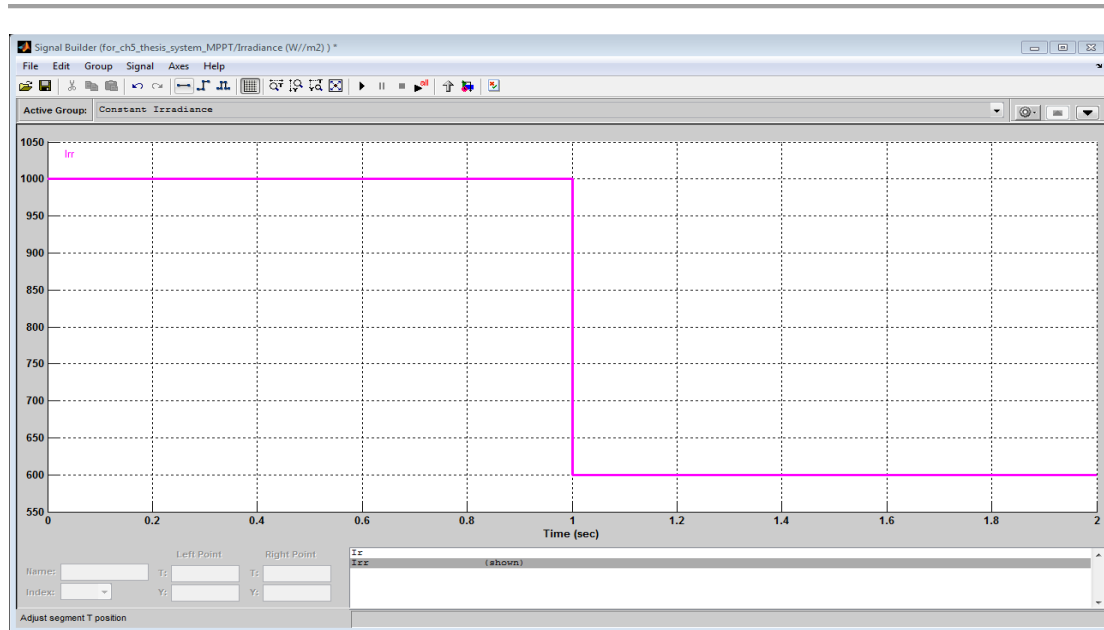
Figure 5.18: Irradiance source window in Matlab/Simulink

The irradiance level in this case changes with time from 1000 to 600 W/m^2, representing a shadow above the array or moving clouds. Fortunately, Matlab/Simulink includes a tool that allows the user to draw the desired set for irradiance. Figure 5.18 shows how this tool looks with the irradiance data implemented from Table 5-6.
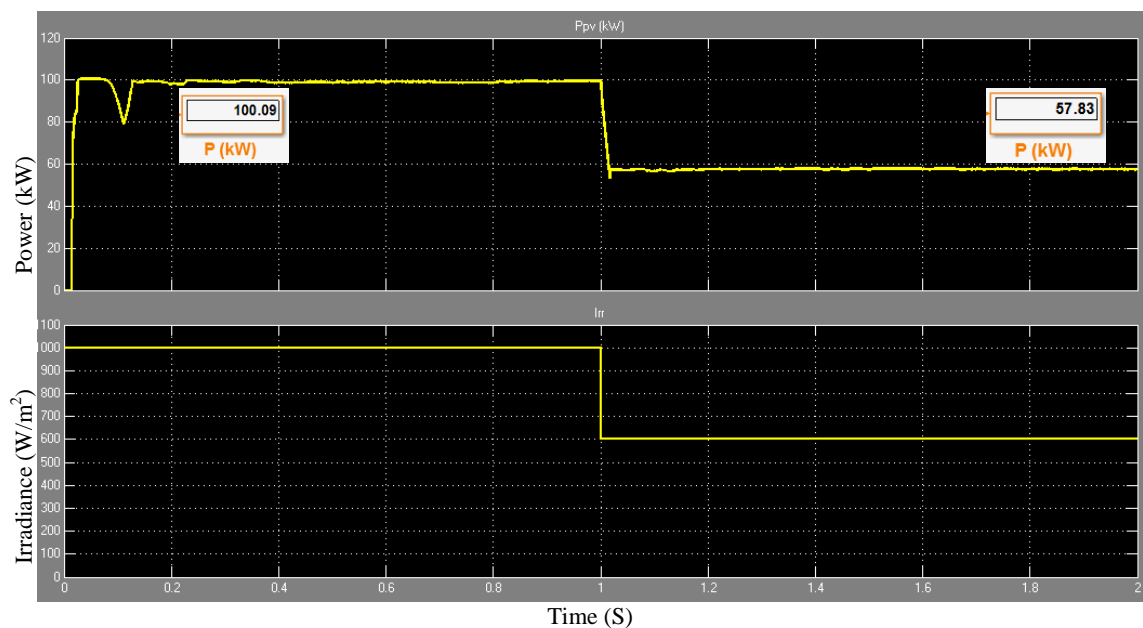
Figure 5.19: PV power and the irradiance signal

The simulation result is shown in Figure 5.19. The lower figure presents the irradiance signal injected to the PV, while the top figure shows the PV output power. Both curves are combined to see the tracking behaviour when the irradiance declines by 40%. Consequently, the power drops by almost the same amount, which proves the linear relationship explained earlier in this chapter. However, the power curve shows that the PV delivered 57.83 kW, which is nearly the maximum power this array could generate at the set irradiance. Table 5-7 compares the measured and expected values and calculates the efficiency of the MPPT.

Table 5-7: The MPPT efficiency

Irr	P_{PV} (Expected)	P_{PV} (Measured)	Efficiency
1000 W/m^2	100.7 kW	100.09 kW	99.4%
600 W/m^2	58.52 kW	57.83 kW	98.82%

In conclusion, this simulation validates the functionality of the MPPT unit. Eventually, the MPPT shows great performance in tracking the MPP under different lighting conditions. Nevertheless, the PV continues to deliver its maximum power regardless of the load volume. This tracking process is carried out with a very high efficiency of more than 99%.

Case III:

Table 5-8 lists the conditions for the third simulation. Note that both the temperature and the irradiance are constant. The aim is to determine whether the array maintains delivery of maximum power even with the change in the load. The load started with a value of 20 Ω; after 1 sec, another 20 Ω load was connected in parallel through a breaker, making a new 10 Ω load in total.

Table 5-8: Case III simulation data

I_{rr}	T	R	Time	P_{PV} (Expected)
1000 W/m^2	25°C	20 Ω	0-1 sec	100.7 kW
		10 Ω	1-2 sec	
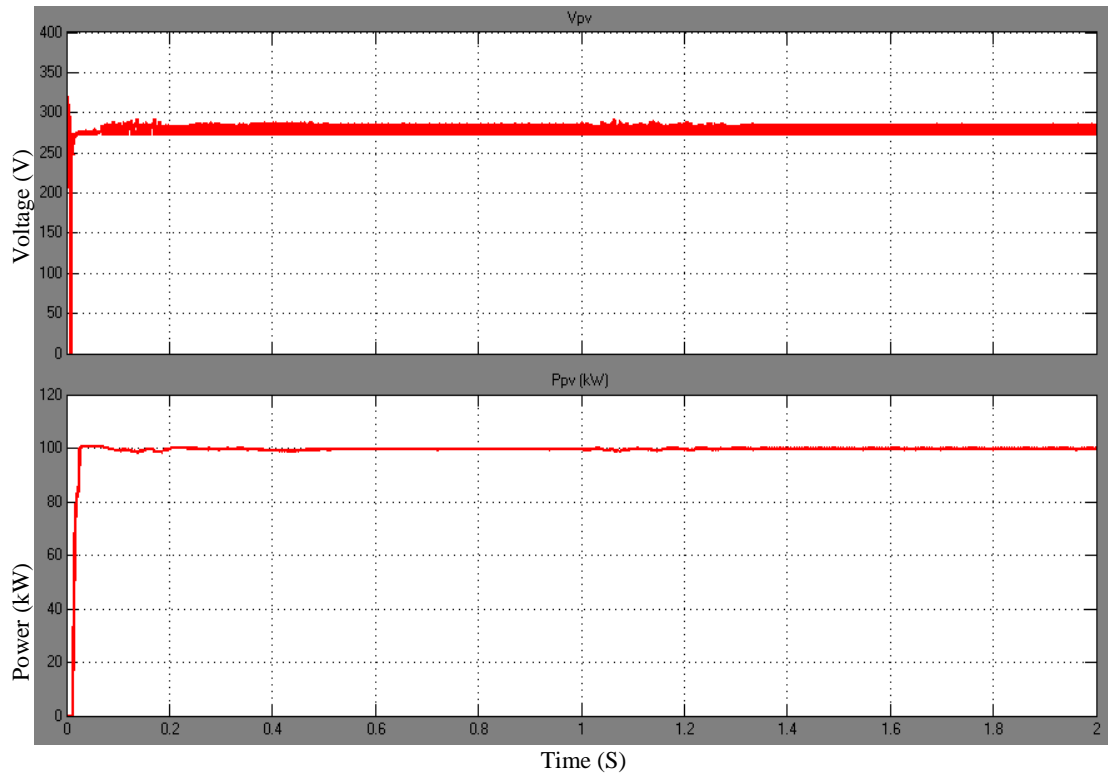
Figure 5.20: The PV voltage and power for case III

The PV power, as Figure 5.20 shows, is delivered at a maximum output regardless of the change in load after 1 sec. Consequently, the operating voltage remains at the same level even when the new load is connected. This behaviour verifies that the tracker extracts the maximum power from the array regardless of the load volume.
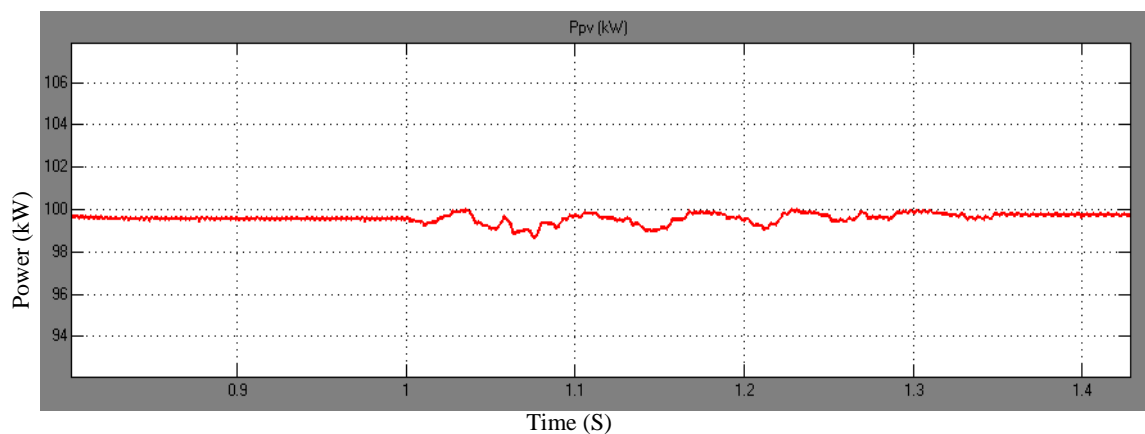
Figure 5.21: Case III PV power after connection of the new load

One detail that should be mentioned is that a power disturbance occurs at the time of the connection of the new load, lasting a very short period of time before recovery of the PV and restoration of maximal power output. Figure 5.21 shows the interruption in the power flow after the first second before it reverts to its initial level at 1.35 sec.

In conclusion, the MPPT functions well by tracking the MPP regardless of the load size. This test has been carried out using a circuit breaker to cause the sudden change in the load. A short and expected disturbance occurred when the extra load was added, followed by reversion to normal power flow.

Case IV:

Table 5-9 lists the conditions for the fourth simulation. Note that, the temperature remains constant but the irradiance does not. The aim is to examine if the array keeps supplying power at a maximum output, even with changes in the load. In Case IV, the load started with a value of 20 Ω; after 2 sec, another 20 Ω load was connected in parallel through a breaker, making a new 10 Ω load in total.

Table 5-9: Case IV simulation data

Scenario	Time	I_{rr}	T	R	P_{PV} (Expected)
1	0-1 sec	1000 W/m^2		20 Ω	100.7 kW
2	1-1.5 sec	600 W/m^2	25°C	20 Ω	58.52 kW
3	1.5-2 sec	600 W/m^2		10 Ω	58.52 kW
4	2-3 sec	1000 W/m^2		10 Ω	100.7 kW
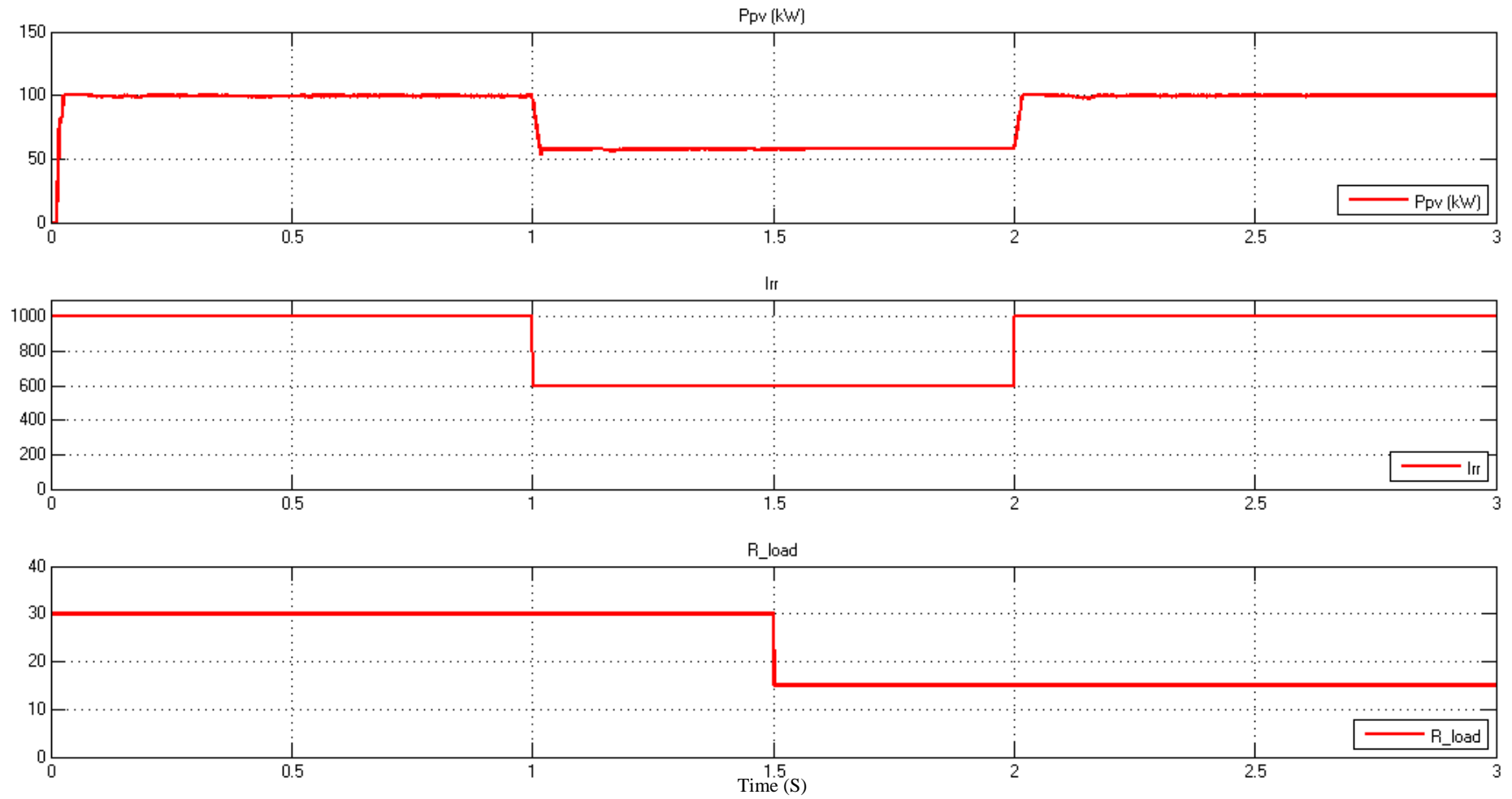
Figure 5.22: The PV output voltage and power for case IV

The PV energy output in this case operates according to the four scenarios presented in Table 5-9. The first scenario is at 1000 W/m^2 irradiance and 20 Ω load for 1 sec. In the second, the irradiance level drops to 600 W/m^2 but the load stays the same for another 0.5 sec. Then, the load decreases to 15 Ω while the irradiance stays constant. In the last scenario, the irradiance bounces back to 1000 W/m^2 with the new load. The quick change in the sunlight amount could represent a moving cloud that impacts PV productivity.

Figure 5.22 shows the Simulink's scope window. The three graphs within the window show, from top to bottom, the output power, irradiance and load, respectively. The middle and lower graphs represent the four scenarios with respect to time. On the other hand, the top graph is the PV power, which starts from zero at the beginning of the simulation. Then, the power increases gradually until the maximum power is reached at around 100 kW. The power then continues to supply the same amount until the first second. Soon the power declines due to the moving clouds above the array, dipping below the maximum power output at the new irradiance level for a very short time. Quickly thereafter, the PV was able to deliver at the maximum power level, which is around 58 kW in this case.

Later, a new load was added but the power delivery stayed unaffected by this incident apart from a small unnoticeable disturbance (which usually happens with any sudden connection to the circuit). Lastly, the PV power increased again when the sky becomes clear and the irradiance reaches the maximum level. The power was delivered at 100 kW despite modification of the load.

In conclusion, case IV was complicated to implement with the four scenarios. The circuit shows high performance under the different conditions, supporting the choice of the incremental conductance method. Additionally, this method proves its ability to extract the maximum available power within the PV array through different scenarios.

5.2.3.3 MPPT Efficiency

In this work, the MPPT showed its ability to track the MPP even when the atmospheric conditions were changed. However, the efficiency of this algorithm after connecting the whole system can be calculated from the equation:

$$MPPT_{Efficiency} = \frac{P_{measured}}{P_{expected}} \times 100 \qquad\qquad 5.3$$

The first test is carried under STC:

$P_{Expected}$	$P_{Measured}$	$MPPT_{Efficiency}$
100.7 kW	100.06 kW	99.9 %

The MPPT shows a very high efficiency under STC with 99.9%, which proves the high quality of the chosen MPPT algorithm in this system. However, this percentage might fall with changes in the testing conditions. Therefore, other tests are carried at different irradiance levels.

At 250 W/m^2:

$P_{Expected}$	$P_{Measured}$	$MPPT_{Efficiency}$
23.1 kW	22.5 kW	97.4 %

At 400 W/m^2:

$P_{Expected}$	$P_{Measured}$	$MPPT_{Efficiency}$
37.9 kW	37.6 kW	98.7 %

Calculating the MPPT efficiency at different irradiance conditions demonstrated the high performance of the chosen algorithm. The MPPT is able to track the maximum operating point accurately, even with a bad irradiance level.

5.2.3.4 MPPT under Changing Weather

The last test is run to monitor the tracking speed under rapid changing weather. The irradiance module for this scenario is shown in Figure 5.24. The signal is drawn to vary from 1000 W/m^2 to 250 W/m^2 in two steps. Then, it recovers to 800 W/m^2 for 2 sec and declines again to 400 W/m^2. Finally, the irradiance returns to its initial value until the end.

This rapid change should challenge the MPPT algorithm and it does so. However, the reaction of the MPPT is quick; by looking at Figure 5.24 and Figure 5.25 (top) it can be seen how fast the MPPT responds to the irradiance change. The bottom plot in Figure 5.25 is the output power measured around the load. The effect of the irradiance into the output power is clear and the amount of power loss varies from time to time, especially around the area where the irradiance changes.

The tracking time is measured for all 5 irradiance intervals. The tracking time is always less than 25 ms, proving the high performance of the selected MPPT method.
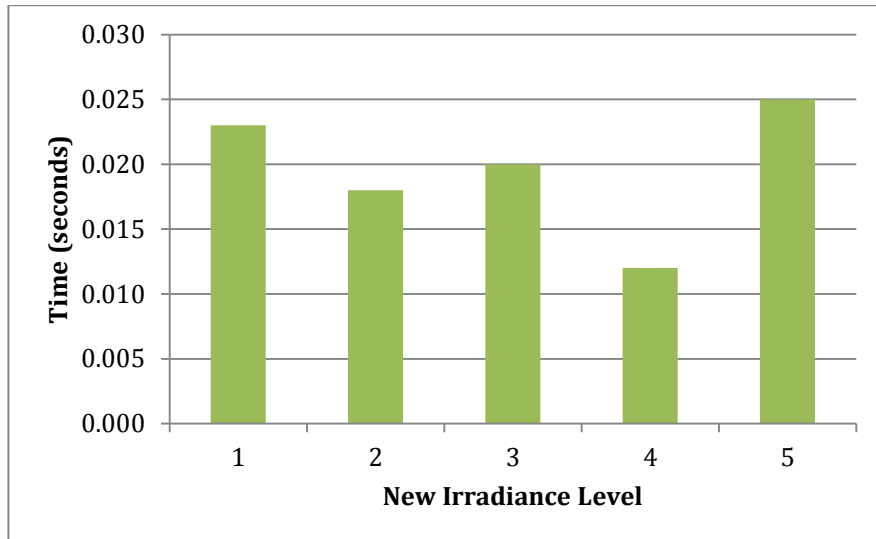
Figure 5.23: Tracking time vs change in irradiance

5.2.4 Reshaping Converter

The output of the MPPT converter is injected into the reshaping or the rectified sinusoidal pulse-width modulation (RSPWM) converter, which is the other contribution of this thesis. This converter, explained in Chapter 4, aims to reshape the DC voltage from a straight line to a rectified sine wave. This functionality happens due to the change in the control topology of the converter. Since converters usually are controlled by a PWM signal, this converter is controlled by a rectified SPWM signal. The converter and the control source are built based on the design criteria in Chapter 4.
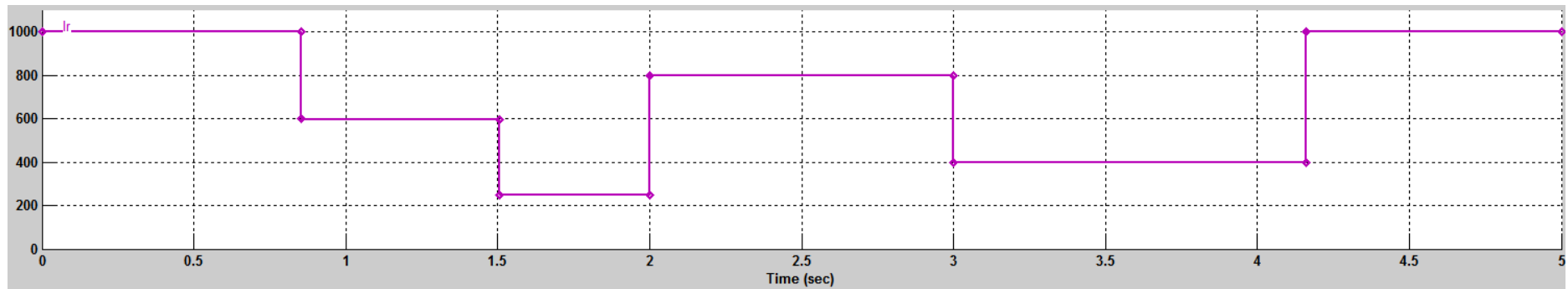
Figure 5.24: Irradiance source vs time
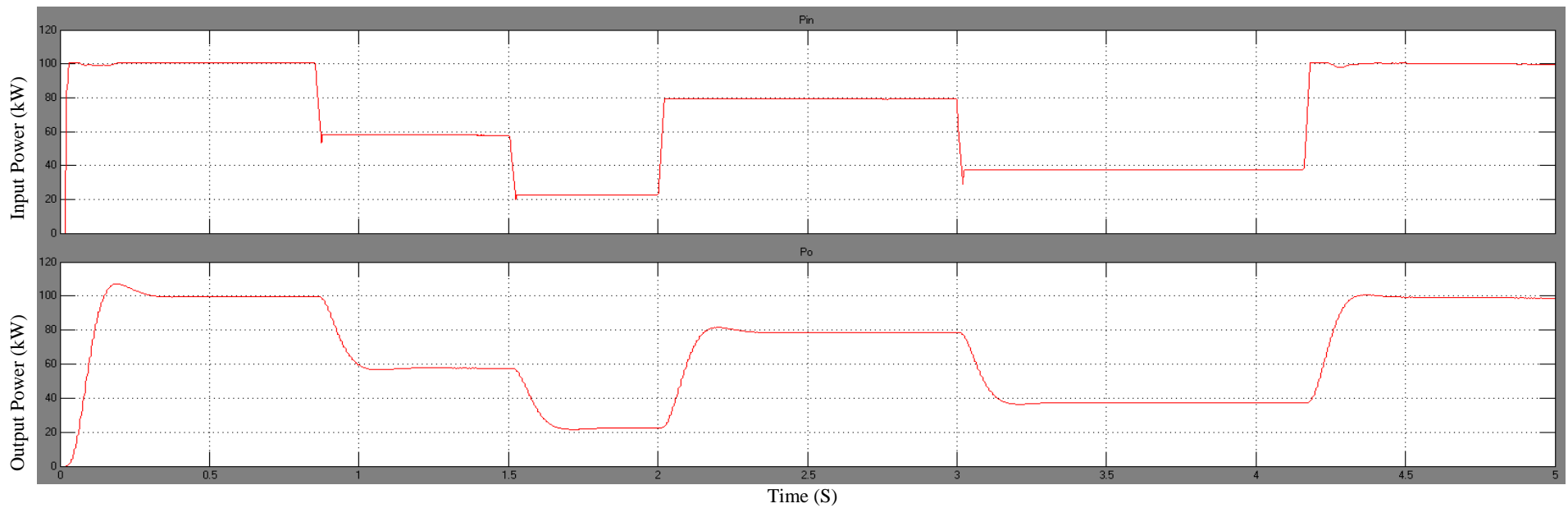
Figure 5.25: Input power (top) and output power (bottom) in kW vs time

The control signal can be built in many ways in Matlab/Simulink by using the available tools from the programme library. Figure 5.26 shows the combination of the RSPWM generator that has been implemented in this simulation. The input and output signals of this generator are plotted in Figure 5.27.
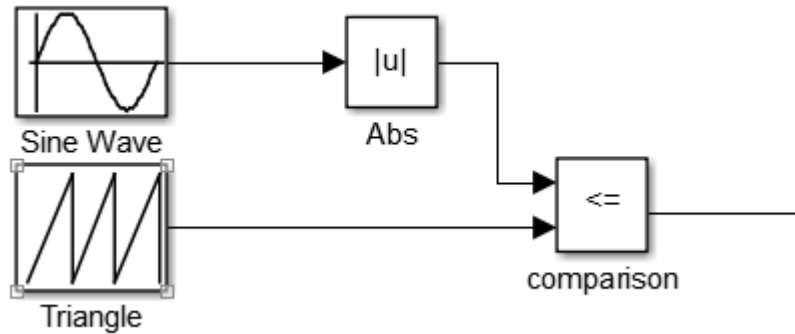
Figure 5.26: RSPWM generator
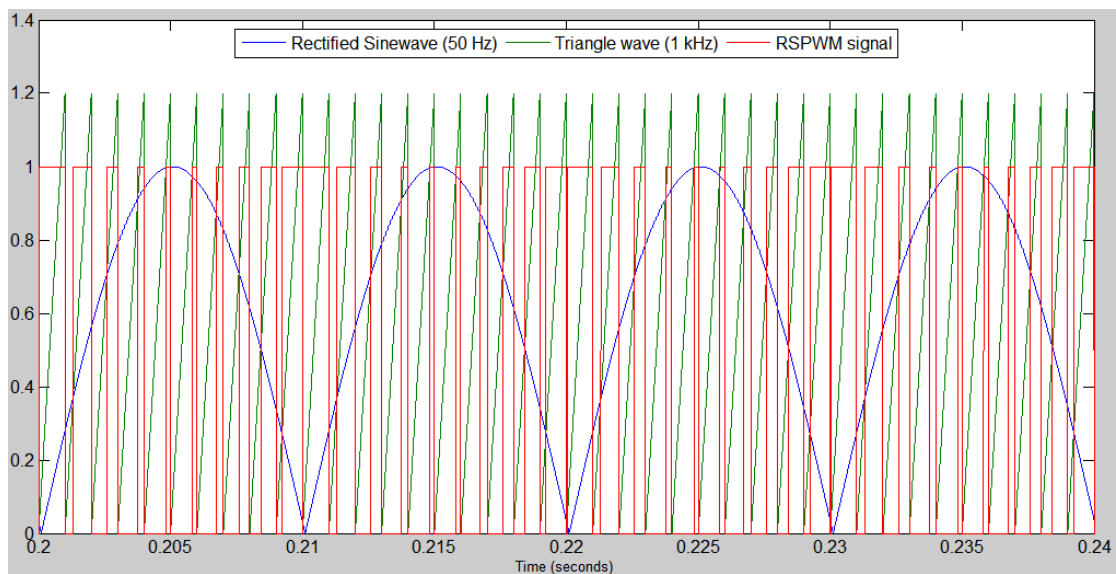
Figure 5.27: The RSPWM controller signal

The output voltage of the RSPWM converter looks like a rectified sine wave that contains some harmonics, as Figure 5.28 shows. However, this converter is designed to minimise these harmonics by wisely choosing the volume of the converter's components. The design is illustrated in detail in Chapter 4.
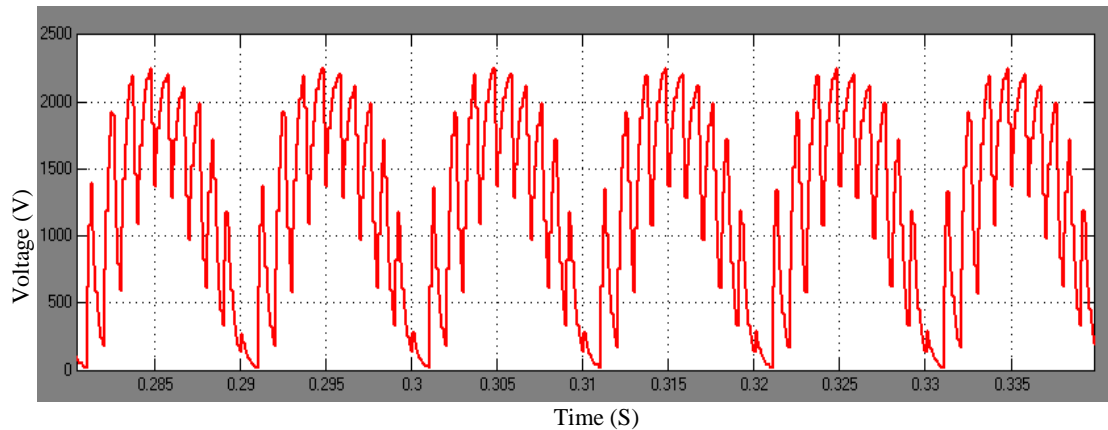
Figure 5.28: Reshaping the converter output voltage

The boost converter steps-up the voltage and regenerates it as a result of the control pulses fed into the switch. The frequency of these pulses is 1 kHz for the carrier wave (the triangular waves), and 50 Hz for the desired wave (rectified sine wave).

In Figure 5.29, the top window represents the input voltage to the converter, the middle window shows the output voltage of the converter and the bottom window shows the desired rectified sine wave. This input is injected into the H-bridge inverter and into the load. On the other hand, in order to get rid of the harmonics that distorted the voltage wave, a filter must be added to the circuit.

With respect to the purpose of this approach (newly proposed by this thesis), the aim of adding the converter is to minimise the switching losses in the DC-AC inverting area. Surely, adding an extra switching component, the reshaping converter, to the interface results in more switching losses, but it is important to remember that this addition is to replace multi-level inverter topology with a single H-bridge inverter. This new inverting topology benefits from the utilisation of the reshaping converter, significantly minimising the switching losses in the inverter.
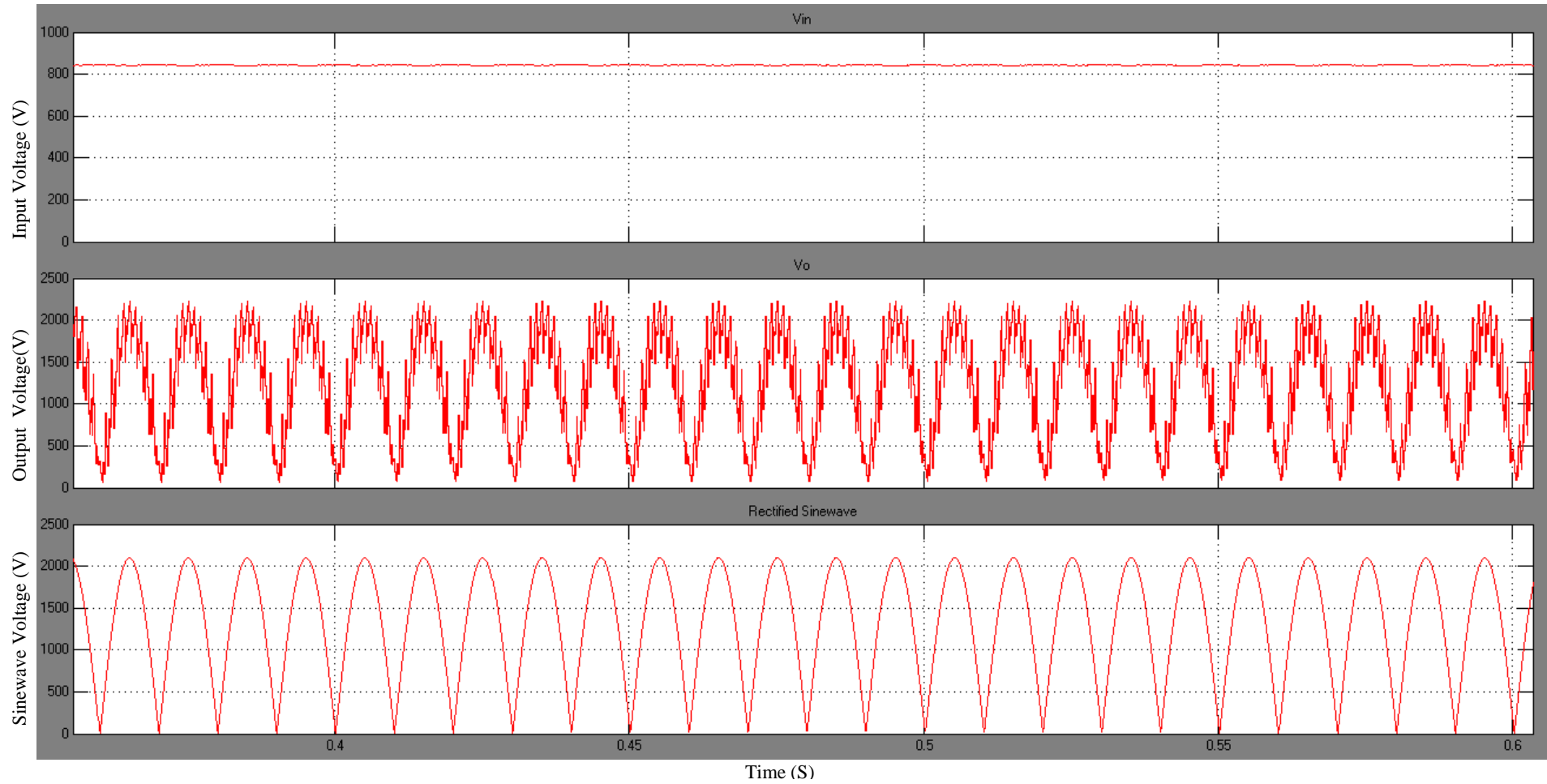
Figure 5.29: Reshaping converter V_{in}, V_0 and the desired pure rectified sine wave

5.2.5   H-Bridge Inverter

The other component of the proposed configuration is the H-bridge inverter. Usually, an inverter is used to convert the DC voltage to AC, and that may be done by implementing a multi-level inverter in order to get the output likewise a sinusoidal wave form. Furthermore, this topology requires the employment of many switches that operate at high frequency. This operation results in a significant amount of switching power loss. On the other hand, the inverter topology applied in this configuration is very simple. The H-bridge inverter consists of 4 switches, shown in Figure 5.30. The control source sends two Boolean signals every 0.02 seconds. Each signal is responsible for turning on two switches—either switches 1 and 2 or switches 3 and 4. When switches 1 and 2 are on, the positive half cycle passes to the load. Otherwise, the negative half wave passes through switches 3 and 4 when they are on. More details about the functionality of the H-bridge inverter are presented in Chapter 4.
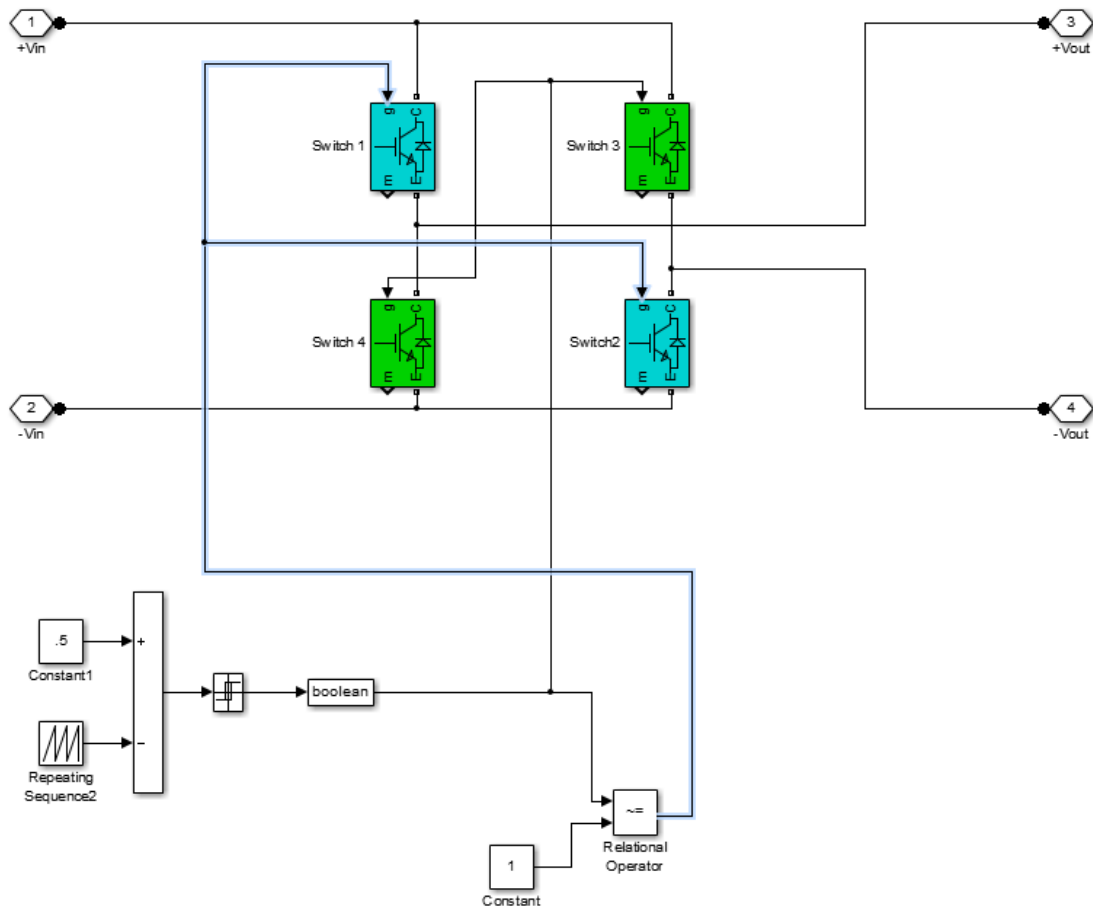
Figure 5.30: The H-bridge inverter and the control source

The inverter receives the voltage signal from the converter in a rectified sine wave form. Then, by using only four switches, which operates in line frequency 50 Hz, the inverter flip-flops the received signal and delivers a full sine wave to the load. Implementing this technique reduces power loss by a significant amount due to the switching at high frequency. Besides that, the control of this inverter is much simpler than the one used for the multi-level inverter.

Figure 5.31 shows three windows of a Matlab/Simulink Scope icon. The top window shows the input voltage; as can be seen, it takes a positive sine wave shape. Moreover, the middle window shows the inverter output voltage, which has the form of a sine wave. Lastly, the bottom window shows the two different control pulses, which are responsible for producing the output form from the received input form. The control of switch 1 and 2 is shown by the red pulses; the pink pulses are for switches 3 and 4.

5.2.6   Total Harmonic Distortion (THD)

The topology used in this configuration to convert the DC voltage to AC is by reshaping the DC voltage to a rectified sine wave with a subsequent flip-flop at half cycle to get the full sine wave. However, the outcome from the reshaping converter is not a pure sine wave. In Chapter 4, the optimisation of the converter design to purify the output as much as possible was described. The minimum THD reached is 15.3% while the IEEE THD standard highlighted the minimum acceptable THD at 5% for applications operating between 1 kV to 69 kV (the case this thesis is interested in).

Matlab/Simulink has a tool called 'FFT analysis' (found in the Powergui block) that calculates the THD of any chosen signal in the system. FFT is a shortcut for Fast Fourier Transform, which transforms the signal from the time domain to the frequency domain to calculate the THD. Within the FFT window, shown in Figure 5.32, the user can choose the wanted signal from the available signal in the right top corner and select the desired display style from the right bottom corner. Additionally, the user is allowed to change the axis values and implement any required edits so the graph is displayed perfectly. Figure 5.33 shows a different display for the same signal after making some modifications, such as changing the Y-axis values. Finally, the THD in the output of the proposed configuration is 15.38%, as Figure 5.32 shows.
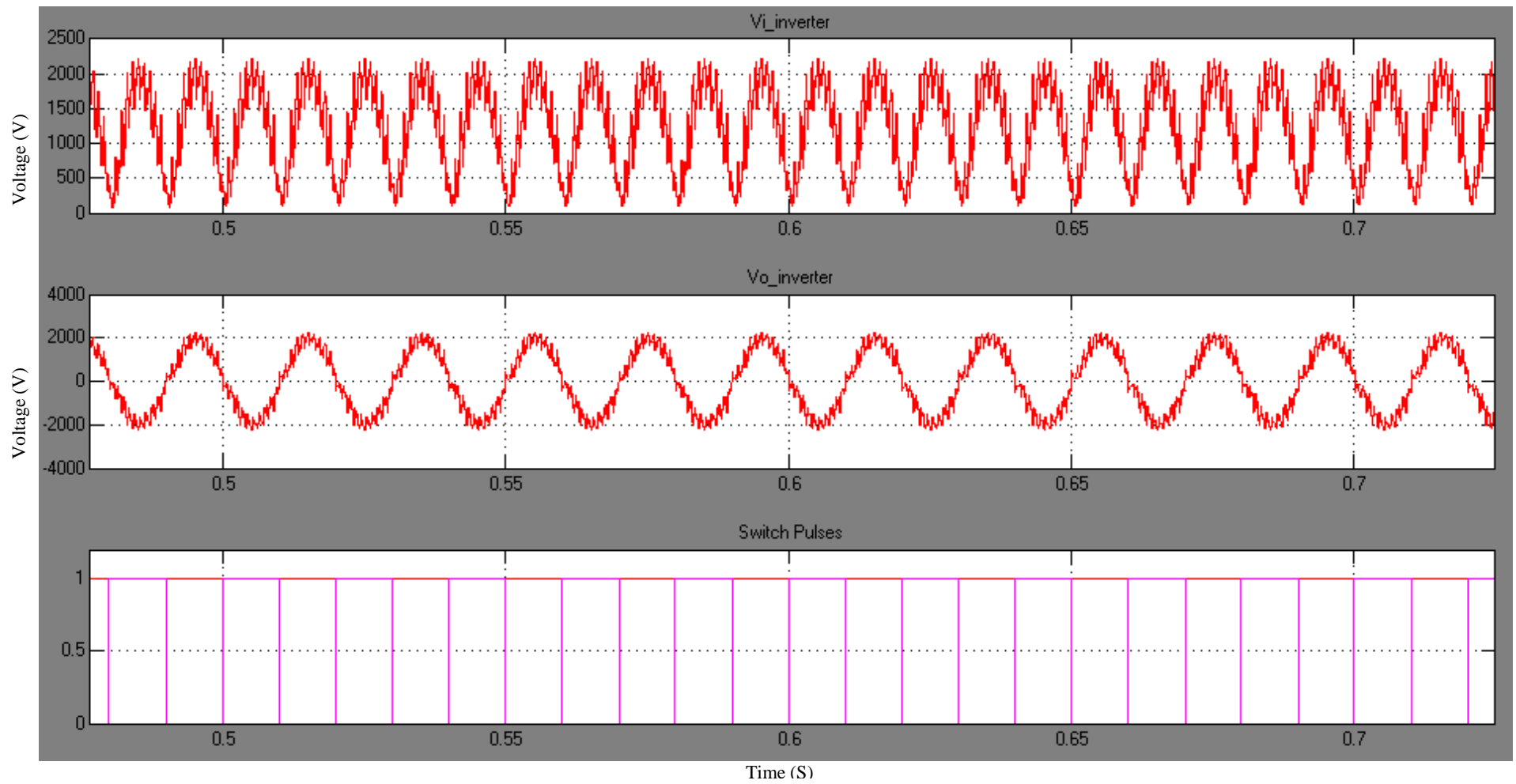
Figure 5.31: Inverter input voltage, inverter output voltage, inverter control pulses
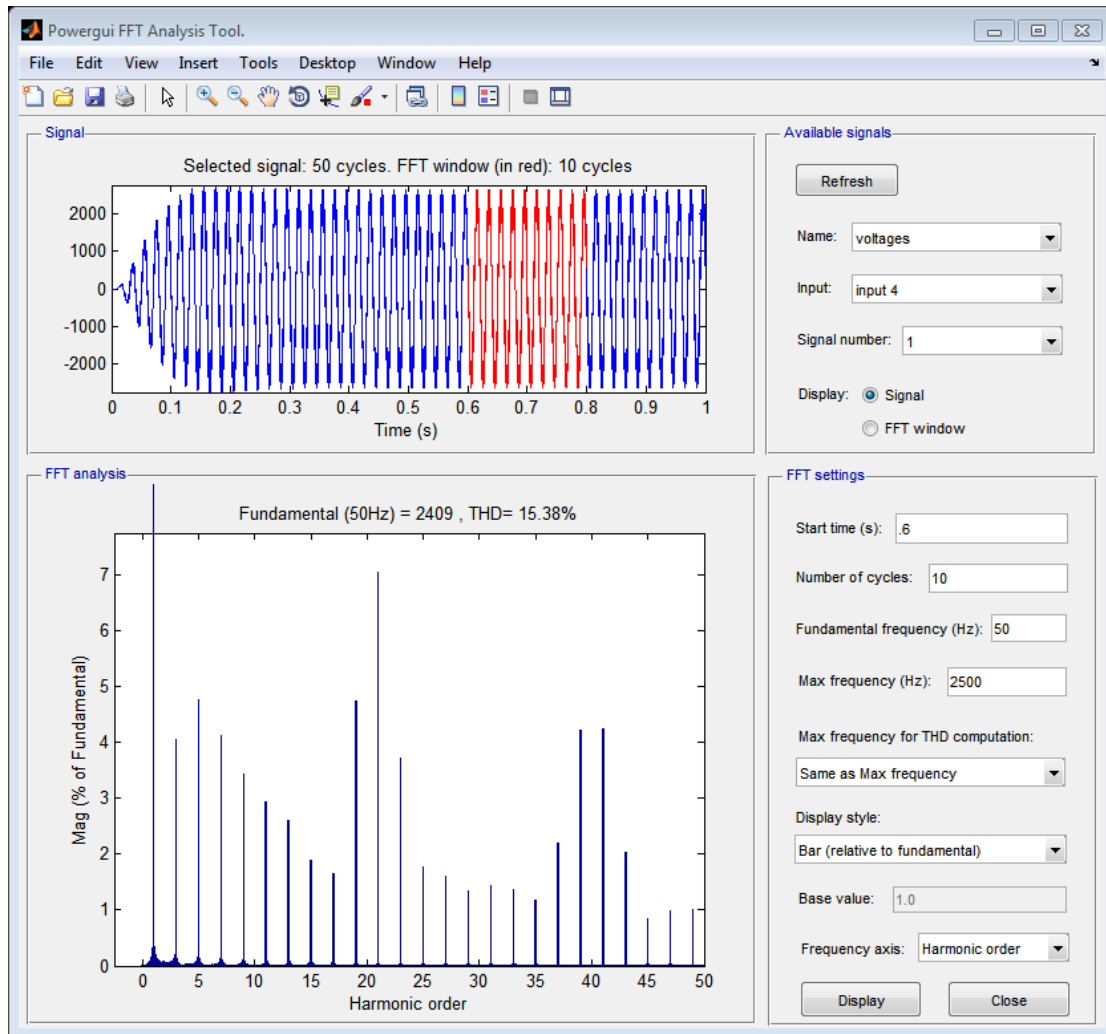
Figure 5.32: THD window in Matlab/Simulink
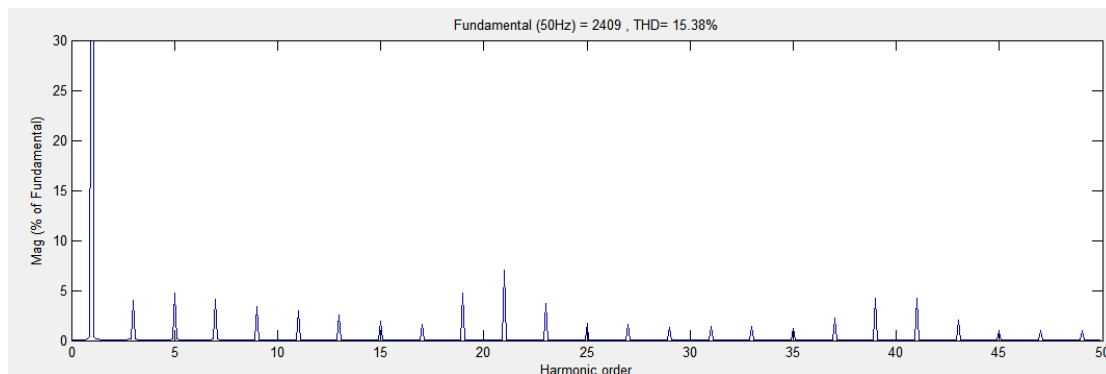
Figure 5.33: Another display of the THD graph

5.2.7   Output Filter

With any load, the ideal case is to receive a pure sinusoidal waveform voltage; this pure wave would have a zero THD. However, the output voltage of the proposed system contains more than 15% THD and this amount of distortion must be filtered out before it reaches the load. Because of this, a filter is added into the end of the system directly after the inverter. The design of this filter was explained in Chapter 4; the influence of the filter on the circuit is elaborated on here.

The filter used in this circuit is a low-pass L-C filter (shown in Figure 5.35) and is located at the inverter output end. It should only allow the fundamental component only to pass through to the load. Any higher order harmonics are targeted by this filter, which operates as a sink for them all. The aim of this filter is to eliminate all of the harmonic components shown in Figure 5.34. The figure shows a total THD of 15.38% along with many individual harmonics with values higher than 3%, the maximum acceptable value for individual harmonic components as per the IEEE.
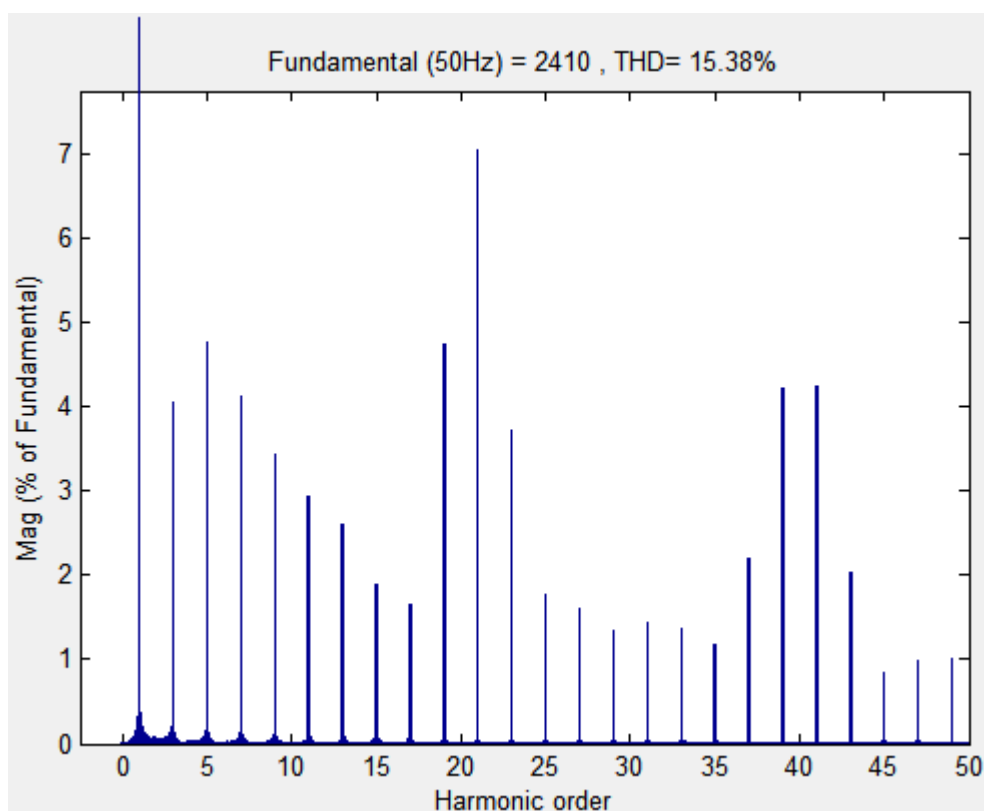
Figure 5.34: The fundamental and harmonics components of Vo before filtering
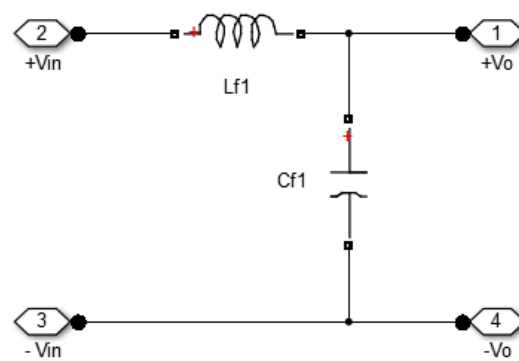
Figure 5.35: LC low pass filter
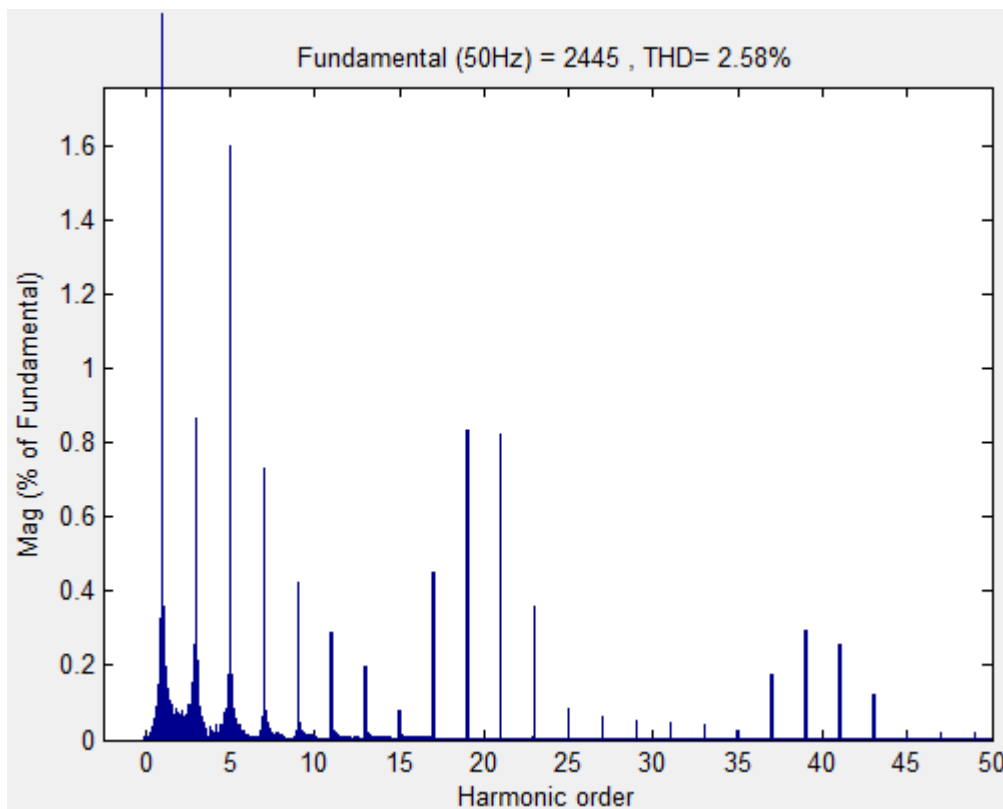
Figure 5.36: The harmonics components of V_0 after filtering

By adding the L-C filter, the THD is reduced from 15.38% to 2.58%. The new THD is within the favourite range and as Figure 5.36 shows, all individual harmonics are below 3%. Figure 5.37 shows the output voltage before filtering (top window), which contains the harmonic components; and after filtering (bottom window), which shows the pure sinusoidal waveform.

To conclude, the filter is used to clean up the harmonics that would otherwise reach the load. By adding this component, the configuration guarantees the delivery of pure sine wave voltage to the load.
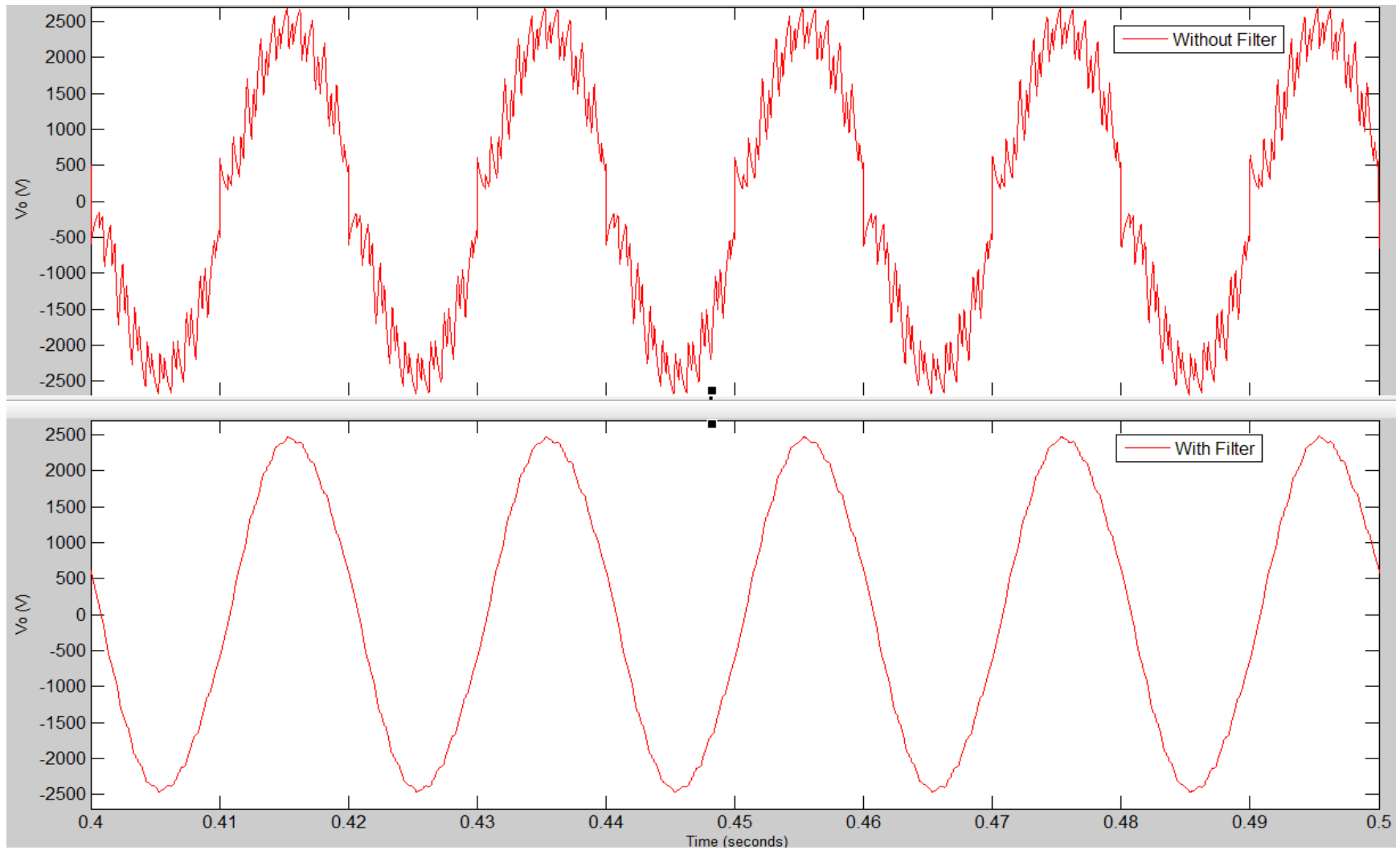
Figure 5.37: The inverter output voltage before and after filtering

5.3   The Proposed Configuration Efficiency

Now, after all the components of the modelled system in Figure 5.1 are explained, the whole system is examined in this section.

The goal of this thesis is to design a new PV inverter system configuration with high efficiency. This goal can be reached by optimising the design of every single component of the configuration and by reducing the number of switches, especially those that operate at high frequency. The system efficiency can be calculated by:

$$\eta = \frac{P_o}{P_i} \times 100 \qquad\qquad 5.4$$

where:

P_i: is the PV output power

P_o: is the load power

Both values are taken from the measurement tools in Matlab/Simulink.

First, the system efficiency is calculated at STC with resistive load R:

P_i	P_o	η
100.6 kW	99.5 kW	98.91 %

The efficiency of the proposed configuration is 98.91 %, which is significantly high. However, the power loss within the system can be calculated by:

$$P_{loss} = P_i - P_o \qquad\qquad 5.5$$

$$P_{loss} = \sum P_s + \sum P_D + P_x \qquad\qquad 5.6$$

where:

P_s: Represents the power losses at a switch.

P_D: Represents the power losses at a diode.

P_x: Represents the power losses at other elements.

P_s and P_D can be measured using Matlab/Simulink tools and the value of P_x can be calculated if these values are known.

The power losses at each switch P_s include the conductivity and switching power losses. These can be measured by activating the measurement port in the

switch dialog box. Nevertheless, the power losses in a switch are frequency dependent, with high frequency leading to higher losses. For this reason, the proposed PV configuration aimed to minimise the number of switches as well as minimise to the extent possible the use of high-frequency switching. Table 5-10 shows power losses in each switch in the proposed configuration, the number of switches, and the operational frequency for them. As it is seen, the power losses at the MOSFET in the MPPT converter are the highest among the other switches because it runs at the highest frequency in the circuit (20 kHz).

Table 5-10: Power losses at each switch of the proposed PV configuration

Switch	Number	Frequency	P_s
MOSFET in MPPT Conv.	1	20 kHz	100 W
IGBT in Reshaping Conv.	1	1000 Hz	4.4 W
IGBTs + diodes in The Inverter	4	50 Hz	1.6×4 W
Total	6		111.04 W

The losses in a diode (P_D) are frequency dependent as well because they operate in relation to the switch in the same circuit. The diodes in the H-bridge inverter are inclusive with the switches so their losses are already obtained in Table 5-10. The other two diodes in this configuration are located inside the two boost converters. Table 5-11 shows the losses in each diode and the huge amount that is wasted in the MPPT converter's diode. That's because this converter operates at a high frequency (20 kHz).

Table 5-11: Diodes power losses

Diode	Number	Frequency	P_s
MPPT converter Diode	1	20 kHz	120 W
Reshaping Converter diode	1	1000 Hz	0.48 W
Total	2		120.48 W

Now, using the available data the power losses within the circuit can be clarified. First, implementing equation 5.5

$$P_{loss} = P_i - P_o = 100600 - 99500 = 1100 \ W$$

$$P_{loss} = \sum P_S + \sum P_D + P_x$$

$$\sum P_S = 111.04 \ W, \sum P_D = 120.48 \ W$$

$$P_x = 1100 - 111.04 - 120.48 = 868.48 \ W$$

To summarise these outputs, Figure 5.38 shows the power losses as a percentage of the total delivered power. Moreover, Figure 5.39 shows the sources of the power losses and their contributions to the total power losses.
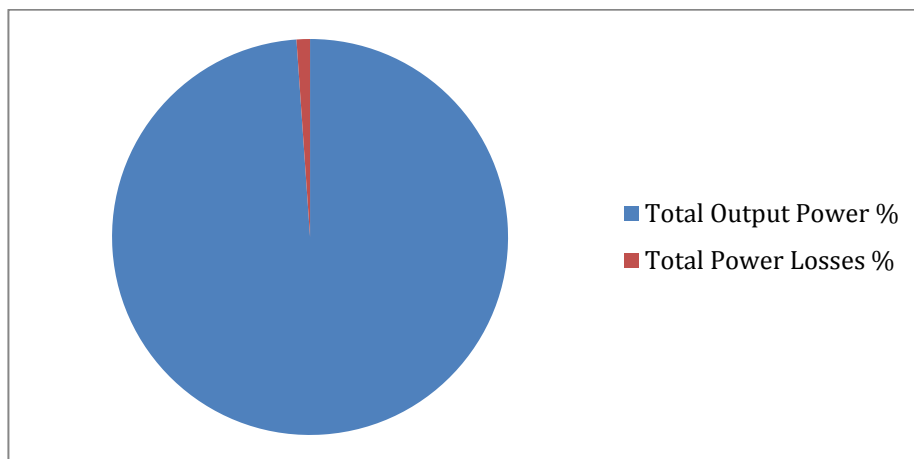
Figure 5.38: Total output power V$_s$ loss power in the circuit
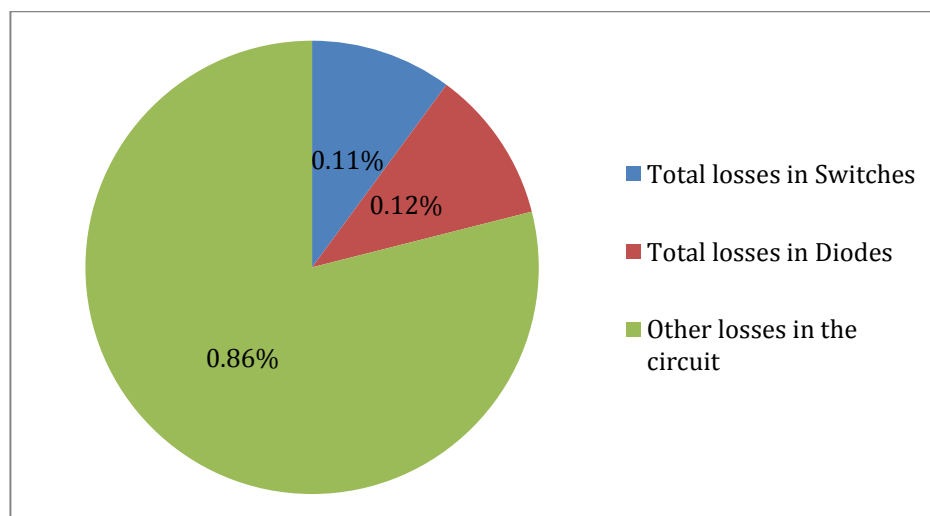
Figure 5.39: Sources of losses in the circuit

The proposed configuration proves its solid characteristics in transferring power and converting it from DC to AC. This configuration uses only one switch at high frequency (above 1 kH), which results in low power losses at the switches. Nevertheless, this switch causes the most power loss compared to the losses caused by the other switches. Furthermore, it should also be noted that this efficiency, which is measured at 98.91 %, is at a certain point of operation and that percentage could be up to 3 % lower. This is due to many reasons:

- The power losses at high frequency switches and diodes are variable with time
- The human error in reading the measurements
- The difficulty of obtaining an average value for some of the parameter losses
- The change in irradiance level
- The change in temperatures and the rise of the components' temperature

5.3.1.1 The Proposed Configuration under Changing Irradiation

The system efficiency is tested with a 30-ohm resistive load and supplied by an irradiance source. This source starts at 200 W/m^2, then, increases to 600 W/m^2 after one second and furthermore to 1000 W/m^2 for the last second. Figure 5.40 shows the whole scenario of the irradiance source.

The output power by the load and the generated power from the PV are combined in Figure 5.41. The figure shows the impact of changing irradiance on the system efficiency, revealing that the efficiency is irradiance dependent. The efficiency decreases very slightly as the irradiance increases. Overall, the configuration efficiency rate is high, recommending the implementation of this configuration.
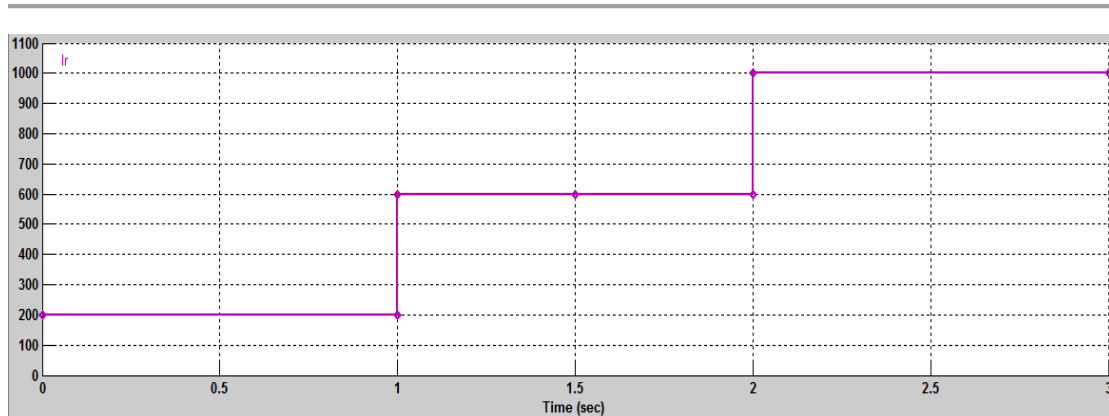
Figure 5.40: Irradiance source
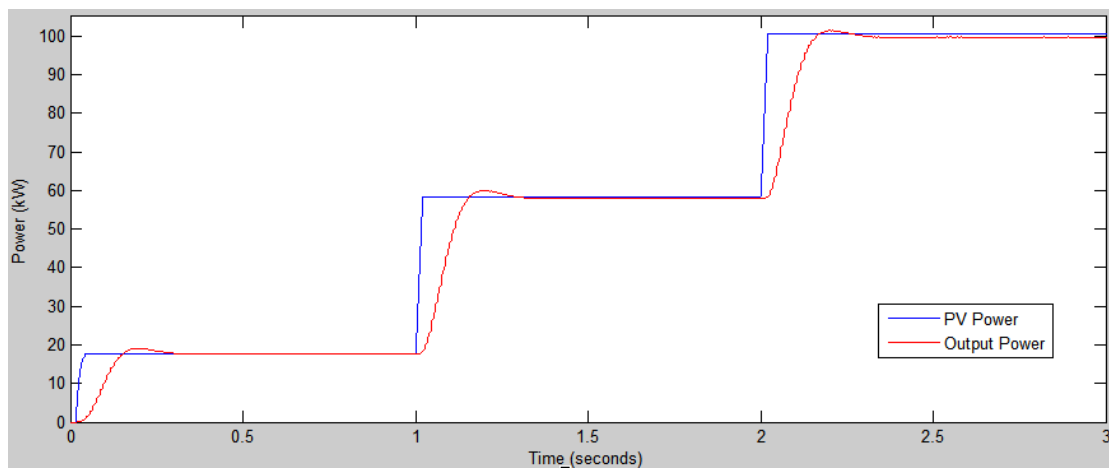
Figure 5.41: PV power and output power

5.4 Summary

This chapter discusses the PV configuration model in Matlab/Simulink. Firstly, a brief overview about the software is presented. Then, the configuration parameters are individually presented and simulated. The PV model in Matlab/Simulink is obtained with the supported of different P-V and I-V characteristics graphs. Furthermore, the MPPT unit is explained and tested in different scenarios, and the tracking speed and efficiency are presented. These results show that the chosen MPPT has very high efficiency and tracking speed even under rapidly changing weather conditions.

Likewise, the reshaping converter is tested and its results are presented. In addition, the H-bridge inverter circuit is presented and its functionality is explained

backed with the simulation results. These components formed the proposed PV configuration, which connects the PV array to the load.

Afterward, a THD analysis is performed using Matlab/Simulink tools. Moreover, the design of the proper filter is optimised to decrease the THD and individual harmonic components to the limit advised by the IEEE standard for harmonics in power systems. Finally, the proposed PV configuration efficiency is analysed and shows a high efficiency rate of 98.91%. The concluding remarks and future work follow in the last chapter.

Chapter 6

Conclusions and Future Work

Chapter 6. Conclusions and Future Work

6.1 Conclusions

The aim of this thesis is to design a high efficiency PV inverter system configuration. This configuration attempts to minimise the number of high frequency switches in the circuit in order to reduce the losses in those switches. Therefore, a boost converter and H-bridge inverter in the proposed configuration have replaced the multilevel inverter topologies. The following tasks have been achieved and represent contributions to the current body of knowledge in the field of PV systems:

1. A critical review of the current MPPT methods has been carried out and concluded by a critical comparison between them. Furthermore, a deep analysis of PV converter topologies has been conducted to assess which converter was most suited to the proposed configuration.

2. A decision matrix analysis has been carried out in order to select the MPPT that most improved the efficiency of the proposed configuration. The selection criteria were selected and weighted by the author; the incremental conductance method had the highest score and was chosen. The mechanism of the incremental conductance method is simple, and it provides a high tracking efficiency with good speed under changing weather conditions. A flowchart is used to display the details of the incremental conductance method and describe its advantages.

3. The topology of the reshaping converter (RSPWM converter) has been analysed and mathematically modelled. The optimum design for this converter (defined by delivery of the voltage with the minimum THD) has been achieved. This THD has been measured at 15.38 %, which still needs to be filtered to reduce it to less than or equal to 5 % (the IEEE standard for THD). In addition, the new control pulses for this converter have been obtained in detail. This controller operates at 1000-Hz frequency; therefore, an IGBT switch has been used in this converter.

4. A low-pass filter has been designed to remove the unwanted harmonics at the output end. The intent of this filter is to create pure sinusoidal AC voltage during delivery while ensuring the THD remains within the IEEE limits (less

than or equal to 5 % for systems operating between 1 kV and 69 kV, with 3 % for each individual harmonic).

5. The inverter topology and control have been presented. This inverter aims to flip-flop the incoming rectified sinewave voltage from the reshaping converter and obtain a full sine wave output. The four switches in this inverter operate at 50 Hz, reducing the amount of power significantly compared to the multi-level inverter. Then, a comparison between the efficiency of the implemented inverter and other multi-level inverter topologies is presented. It can be assumed that high-frequency switches consume more energy and reduce system efficiency.

6. Following the design of the proposed PV inverter configuration, an investigation has been conducted to find the most suitable software to simulate the system. Matlab/Simulink software provides an attractive environment and contains a rich power electronics library that allows the user to build any desired system. Additionally, this platform is open source, which gives the user the ability to build any function and connect it to the system. Moreover, the user can conduct different modes of operation and display the simulation outcomes in many ways. For these reasons, Matlab/Simulink software was chosen for the design and simulation of the proposed PV inverter system configuration.

7. The proposed system parameters have been designed in Matlab/Simulink. Then, different scenarios have been simulated to verify the functionality of each part of the system and the overall system performance. The results of simulating the different scenarios have been discussed, leading to the following achievements:

• The PV system has been modelled and simulated, validating the accuracy of the designed model compared to actual manufactured models under various weather conditions.

• The functionality of the MPPT has been examined in order to verify its importance to the efficiency of the PV system. The PV array was tested with and without the MPPT, with the outputs showing that at certain conditions the MPPT increases the efficiency of the PV by 96.7 %. Overall, the MPPT-measured efficiency in the simulation varied between 97.4 % and 99 % depending on the weather conditions. These results demonstrated the high efficiency of the MPPT algorithm.

- The MPPT performance under changing weather conditions has been simulated. The MPPT has shown high performance every time when adapting to sudden changes in the weather. The time taken by the MPPT to adjust operation so the PV system runs at maximum power after a sudden weather change is below 25 ms.

- Each of the individual components of the entire PV inverter configuration have been designed, including the PV array, the MPPT algorithm and its converter, the reshaping converter and its control source, the H-bridge inverter, the filter and the load.

- The overall system efficiency has been examined. The total power losses have been measured for each switch in the configuration. The switch and diode of the MPPT converter were set to have the highest losses among the other switches, as they operate at the highest frequency in the circuit (20 kHz). However, the proposed configuration efficiency is 98.81 %, which reflects the distinction of the proposed PV system.

6.2 Future Work

The work in this thesis has proposed a high efficiency PV inverter configuration. Areas of future work to be considered are as follows:

- A further study can be carried out in the control units of the switches to investigate the possibility of compromise the MPPT with the RSPWM. This should help to minimise the number of components in the circuit and improve efficiency. However, the complexity of the control should be considered.

- The proposed configuration was tested as a stand-alone connection. Therefore, the opportunity exists to investigate the configuration for a grid-connected system, as well as determine how the configuration performs with different types of loads, such as inductive and capacitive loads.

- More investigation is needed into a new MPPT approach that could offer a better performance than the existing algorithms.

- A complete cost analysis of the proposed system should be undertaken to compare it with the other existing configurations.

- Further research could also consider the optimum frequency of the reshaping converter and the impact of this frequency on the pureness of the rectified sine wave; such research could allow for more informed decisions when choosing between frequencies that product better output versus fewer energy losses.

References

Adams, W.G. and Day, R. (1876) 'The Action of Light on Selenium.', *Proceedings of the Royal Society of London,* 25(171-178), pp. 113-117.

Ahmad, J. (2010) 'A fractional open circuit voltage based maximum power point tracker for photovoltaic arrays', *Software Technology and Engineering (ICSTE), 2010 2nd International Conference on.* IEEE, V1-247-V1-250.

Ahmed, E.M. and Shoyama, M. (2010) 'Highly efficient variable-step-size maximum power point tracker for PV systems', *Electrical and Electronics Engineering (ISEEE), 2010 3rd International Symposium on.* IEEE, 112-117.

Al-Amoudi, A. and Zhang, L. (1998) 'Optimal control of a grid-connected PV system for maximum power point tracking and unity power factor', *Power Electronics and Variable Speed Drives, 1998. Seventh International Conference on (Conf. Publ. No. 456).* IET, 80-85.

Alqarni, M. and Darwish, M.K. (2012) 'Maximum power point tracking for photovoltaic system: modified perturb and observe algorithm', *Universities Power Engineering Conference (UPEC), 2012 47th International.* IEEE, 1-4.

Alqarni, M. and Darwish, M.K. (2014) 'A maximum power point tracking for a photovoltaic system based on optimum sinusoidal modulated control pulses', *Power Engineering Conference (UPEC), 2014 49th International Universities.* , 1-4.

Alsadi, S. and Alsayid, B. (2012) 'Maximum power point tracking simulation for photovoltaic systems using perturb and observe algorithm', *International Journal of Engineering and Innovative Technology (IJEIT),* 2(6), pp. 80-85.

Arias, J., Linera, F., Martin-Ramos, J., Pernia, A.M. and Cambronero, J. (2004) 'A modular PV regulator based on microcontroller with maximum power point tracking', *Industry Applications Conference, 2004. 39th IAS Annual Meeting. Conference Record of the 2004 IEEE.* IEEE, 1178-1184.

Barchowsky, A., Parvin, J.P., Reed, G.F., Korytowski, M.J. and Grainger, B.M. (2012) 'A comparative study of MPPT methods for distributed photovoltaic generation', *Innovative Smart Grid Technologies (ISGT), 2012 IEEE PES.* IEEE, 1-7.

Bhide, R. and Bhat, S. (1992) 'Modular power conditioning unit for photovoltaic applications', *Power Electronics Specialists Conference, 1992. PESC'92 Record., 23rd Annual IEEE.* IEEE, 708-713.

Blaabjerg, F., Chen, Z. and Kjaer, S.B. (2004) 'Power electronics as efficient interface in dispersed power generation systems', *Power Electronics, IEEE Transactions on,* 19(5), pp. 1184-1194.

Bodur, M. and Ermis, M. (1994) 'Maximum power point tracking for low power photovoltaic solar panels', *Electrotechnical Conference, 1994. Proceedings., 7th Mediterranean.* IEEE, 758-761.

Chapin, D., Fuller, C. and Pearson, G. (1954) 'A new silicon p-n junction photocell for converting solar radiation into electrical power', *Journal of Applied Physics,* 25(5), pp. 676-677.

Chiang, S., Chang, K. and Yen, C. (1998) 'Residential photovoltaic energy storage system', *Industrial Electronics, IEEE Transactions on,* 45(3), pp. 385-394.

Chomsuwan, K., Prisuwanna, P. and Monyakul, V. (2002) 'Photovoltaic grid-connected inverter using two-switch buck-boost converter', *Photovoltaic Specialists Conference, 2002. Conference Record of the Twenty-Ninth IEEE.* IEEE, 1527-1530.

El Chaar, L., Lamont, L. and Elzein, N. (2010) 'PV Technology-Industry update', *Power and Energy Society General Meeting, 2010 IEEE.* IEEE, 1-6.

Enrique, J., Duran, E., Sidrach-de-Cardona, M. and Andujar, J. (2007) 'Theoretical assessment of the maximum power point tracking efficiency of photovoltaic facilities with different converter topologies', *Solar Energy,* 81(1), pp. 31-38.

Enslin, J.H. and Snyman, D.B. (1992a) 'Simplified feed-forward control of the maximum power point in PV installations', *Industrial Electronics, Control, Instrumentation, and Automation, 1992. Power Electronics and Motion Control., Proceedings of the 1992 International Conference on.* IEEE, 548-553.

Enslin, J.H. and Snyman, D. (1992b) 'Simplified feed-forward control of the maximum power point in PV installations', *Industrial Electronics, Control, Instrumentation, and Automation, 1992. Power Electronics and Motion Control., Proceedings of the 1992 International Conference on.* IEEE, 548-553.

Esram, T. and Chapman, P.L. (2007) 'Comparison of photovoltaic array maximum power point tracking techniques', *IEEE Transactions on Energy Conversion EC,* 22(2), pp. 439.

Faranda, R., Leva, S. and Maugeri, V. (2008) 'MPPT techniques for PV systems: energetic and cost comparison', *Power and Energy Society General Meeting-Conversion and Delivery of Electrical Energy in the 21st Century, 2008 IEEE.* IEEE, 1-6.

Farivar, G., Asaei, B. and Rezaei, M.A. (2010) 'A novel analytical solution for the PV-arrays maximum power point tracking problem', *Power and Energy (PECon), 2010 IEEE International Conference on.* IEEE, 917-922.

Femia, N., Petrone, G., Spagnuolo, G. and Vitelli, M. (2005) 'Optimization of perturb and observe maximum power point tracking method', *Power Electronics, IEEE Transactions on,* 20(4), pp. 963-973.

Glasner, I. and Appelbaum, J. (1996) 'Advantage of boost vs. buck topology for maximum power point tracker in photovoltaic systems', *Electrical and Electronics Engineers in Israel, 1996., Nineteenth Convention of.* IEEE, 355-358.

Green, M. (1990) 'Photovoltaics: Coming of age', *Photovoltaic Specialists Conference, 1990., Conference Record of the Twenty First IEEE.* IEEE, 1-8.

Hart, D.W. (2011) *Power electronics.* Tata McGraw-Hill Education.

Hart, G., Branz, H. and Cox Iii, C. (1984a) 'Experimental tests of open-loop maximum-power-point tracking techniques for photovoltaic arrays', *Solar Cells,* 13(2), pp. 185-195.

Hart, G., Branz, H. and Cox Iii, C. (1984b) 'Experimental tests of open-loop maximum-power-point tracking techniques for photovoltaic arrays', *Solar Cells,* 13(2), pp. 185-195.

Hauke, B. (2009) 'Basic calculation of a boost converter's power stage', *Texas Instruments: Application Report [online], .*

Hiyama, T., Kouzuma, S. and Imakubo, T. (1995) 'Identification of optimal operating point of PV modules using neural network for real time maximum power tracking control', *Energy conversion, IEEE transactions on,* 10(2), pp. 360-367.

Hou, C., Wu, J., Zhang, M., Yang, J. and Li, J. (2004) 'Application of adaptive algorithm of solar cell battery charger', *Electric Utility Deregulation, Restructuring and Power Technologies, 2004.(DRPT 2004). Proceedings of the 2004 IEEE International Conference on.* IEEE, 810-813.

Hua, C. and Lin, J. (2001) 'Fully digital control of distributed photovoltaic power systems', *Industrial Electronics, 2001. Proceedings. ISIE 2001. IEEE International Symposium on.* IEEE, 1-6.

Hussein, A., Hirasawa, K., Hu, J. and Murata, J. (2002) 'The dynamic performance of photovoltaic supplied dc motor fed from DC-DC converter and controlled by neural networks', *Neural Networks, 2002. IJCNN'02. Proceedings of the 2002 International Joint Conference on.* IEEE, 607-612.

Hussein, K., Muta, I., Hoshino, T. and Osakada, M. (1995) 'Maximum photovoltaic power tracking: an algorithm for rapidly changing atmospheric conditions', *IEE Proceedings-Generation, Transmission and Distribution,* 142(1), pp. 59-64.

IEEE-519 (2014) *IEEE Recommended Practice and Requirements for Harmonic Control in Electric Power Systems.*

Irisawa, K., Saito, T., Takano, L. and Sawada, Y. (2000) 'Maximum power point tracking control of photovoltaic generation system under non-uniform insolation by means of monitoring cells', *Photovoltaic Specialists Conference, 2000. Conference Record of the Twenty-Eighth IEEE.* IEEE, 1707-1710.

Johns, M., Le, H. and Seeman, M. (2009) 'Grid-Connected Solar Electronics', *University of California at Berkeley, Department of Electrical Engineering and Computer Sciences, EE-290N-3–Contemporary Energy Issues, EE-290N-3–Contemporary Energy Issues, .*

Jung, Y., So, J., Yu, G. and Choi, J. (2005) 'Improved perturbation and observation method (IP&O) of MPPT control for photovoltaic power systems', *Photovoltaic Specialists Conference, 2005. Conference Record of the Thirty-first IEEE.* IEEE, 1788-1791.

Khaehintung, N., Pramotung, K., Tuvirat, B. and Sirisuk, P. (2004) 'RISC-microcontroller built-in fuzzy logic controller of maximum power point tracking for solar-powered light-flasher applications', *Industrial Electronics Society, 2004. IECON 2004. 30th Annual Conference of IEEE.* IEEE, 2673-2678.

Khalifa, A.S. and El-Saadany, E.F. (2011) 'Control of three phase grid-connected photovoltaic arrays with open loop maximum power point tracking', *Power and Energy Society General Meeting, 2011 IEEE.* IEEE, 1-8.

Kim, T., Kang, D., Lee, Y. and Hyun, D. (2001) 'The analysis of conduction and switching losses in multi-level inverter system', *Power Electronics Specialists Conference, 2001. PESC. 2001 IEEE 32nd Annual.* IEEE, 1363-1368.

Kitano, T., Matsui, M. and Xu, D. (2001) 'Power sensor-less MPPT control scheme utilizing power balance at DC link-system design to ensure stability and response', *Industrial Electronics Society, 2001. IECON'01. The 27th Annual Conference of the IEEE.* IEEE, 1309-1314.

Kjær, S.B. (2005) *Design and control of an inverter for photovoltaic applications* Aalborg University.

Knight, J., Shirsavar, S.A. and Holderbaum, W. (2006) 'An improved reliability Cuk based solar inverter with sliding mode control', *Power Electronics, IEEE Transactions on,* 21(4), pp. 1107-1115.

Kobayashi, K., Takano, I. and Sawada, Y. (2006) 'A study of a two stage maximum power point tracking control of a photovoltaic system under partially shaded insolation conditions', *Solar Energy Materials and Solar Cells,* 90(18), pp. 2975-2988.

Kobayashi, K., Matsuo, H. and Sekine, Y. (2004) 'A novel optimum operating point tracker of the solar cell power supply system', *Power Electronics Specialists Conference, 2004. PESC 04. 2004 IEEE 35th Annual.* IEEE, 2147-2151.

Kouro, S., Leon, J.I., Vinnikov, D. and Franquelo, L.G. (2015) 'Grid-Connected Photovoltaic Systems: An Overview of Recent Research and Emerging PV Converter Technology', *Industrial Electronics Magazine, IEEE,* 9(1), pp. 47-61.

Kumari, J.S. and Babu, C.S. (2011) 'Comparison of maximum power point tracking algorithms for photovoltaic system', *International Journal of Advances in Engineering & Technology,* 1(5), pp. 133-148.

Kuo, Y., Liang, T. and Chen, J. (2001) 'Novel maximum-power-point-tracking controller for photovoltaic energy conversion system', *Industrial Electronics, IEEE Transactions on,* 48(3), pp. 594-601.

Masoum, M.A., Dehbonei, H. and Fuchs, E.F. (2002) 'Theoretical and experimental analyses of photovoltaic systems with voltageand current-based maximum power-point tracking', *Energy conversion, IEEE transactions on,* 17(4), pp. 514-522.

Middlebrook, R. and Cuk, S. (1970) 'A general unified approach to modelling switching-converter power stages', *Power Electronics Specialists Conference, 1970 IEEE.* IEEE, 18-34.

Midya, P., Krein, P.T., Turnbull, R.J., Reppa, R. and Kimball, J. (1996) 'Dynamic maximum power point tracker for photovoltaic applications', *Power Electronics Specialists Conference, 1996. PESC'96 Record., 27th Annual IEEE.* IEEE, 1710-1716.

Mocci, F. and Tosi, M. (1989) 'Comparison of power converter technologies in photovoltaic applications', *Electrotechnical Conference, 1989. Proceedings.'Integrating Research, Industry and Education in Energy and Communication Engineering', MELECON'89., Mediterranean.* IEEE, 11-15.

Murtaza, A.F., Sher, H., Chiaberge, M., Boero, D., De Giuseppe, M. and Addoweesh, K. (2012) 'A novel hybrid MPPT technique for solar PV applications using perturb & observe and fractional open circuit voltage techniques', .

Narendiran, S. (2013) 'Grid tie inverter and MPPT-A review', *Circuits, Power and Computing Technologies (ICCPCT), 2013 International Conference on.* IEEE, 564-567.

Ngan, M.S. and Tan, C.W. (2011) 'A study of maximum power point tracking algorithms for stand-alone photovoltaic systems', *Applied Power Electronics Colloquium (IAPEC), 2011 IEEE.* IEEE, 22-27.

Noguchi, T., Togashi, S. and Nakamoto, R. (2000) 'Short-current pulse based adaptive maximum-power-point tracking for photovoltaic power generation system', *Industrial Electronics, 2000. ISIE 2000. Proceedings of the 2000 IEEE International Symposium on.* IEEE, 157-162.

Nowak, S. (2015) *Trends in photovoltaic applications survey report of selected IEA countries between 1992 and 2014.* Switzerland: IEA.

Patcharaprakiti, N., Premrudeepreechacharn, S. and Sriuthaisiriwong, Y. (2005) 'Maximum power point tracking using adaptive fuzzy logic control for grid-connected photovoltaic system', *Renewable Energy,* 30(11), pp. 1771-1788.

Reisi, A.R., Moradi, M.H. and Jamasb, S. (2013) 'Classification and comparison of maximum power point tracking techniques for photovoltaic system: a review', *Renewable and Sustainable Energy Reviews,* 19, pp. 433-443.

Rogers, E. (1999a) 'Understanding boost power stages in switchmode power supplies', *Texas Instrument Application Reports, .*

Rogers, E. (1999b) 'Understanding Buck-Boost Power Stages in Switch Mode Power Supplies', .

Salas, V., Olias, E., Barrado, A. and Lazaro, A. (2006) 'Review of the maximum power point tracking algorithms for stand-alone photovoltaic systems', *Solar Energy Materials and Solar Cells,* 90(11), pp. 1555-1578.

Sawin, J.L., Sverrisson, F., Chawla, K., Lins, C., Adib, R., Hullin, M., Leitner, S., Mazzaccaro, S., Murdock, H. and Williamson, L.E. (2014) 'Renewables 2014. Global status report 2014', .

Sawin, J. (2012) 'Renewables 2012–Global Status Report, Renewables Energy Police Network of the 21st Century (REN21)', *Zuletzt eingesehen am,* 22, pp. 2012.

Schoeman, J. and Van Wyk, J. (1982) 'A simplified maximal power controller for terrestrial photovoltaic panel arrays', *PESC'82; 13th Annual Power Electronics Specialists Conference.* , 361-367.

Simoes, M.G., Franceschetti, N. and Friedhofer, M. (1998) 'A fuzzy logic based photovoltaic peak power tracking control', *Industrial Electronics, 1998. Proceedings. ISIE'98. IEEE International Symposium on.* IEEE, 300-305.

Simonsen, S.O. (2009) 'Development of a Grid Connected PV System for Laboratory Use', .

Skretas, S.B. and Papadopoulos, D.P. (2009) 'Efficient design and simulation of an expandable hybrid (wind–photovoltaic) power system with MPPT and inverter input voltage regulation features in compliance with electric grid requirements', *Electric Power Systems Research,* 79(9), pp. 1271-1285.

Sugimoto, H. and Dong, H. (1997) 'A new scheme for maximum photovoltaic power tracking control', *Power Conversion Conference-Nagaoka 1997., Proceedings of the.* IEEE, 691-696.

Sun, X., Wu, W., Li, X. and Zhao, Q. (2002) 'A research on photovoltaic energy controlling system with maximum power point tracking', *Power Conversion Conference, 2002. PCC-Osaka 2002. Proceedings of the.* IEEE, 822-826.

Sundareswaran, K., Vigneshkumar, V., Sankar, P., Simon, S.P., Srinivasa Rao Nayak, P. and Palani, S. (2016) 'Development of an Improved P&O Algorithm Assisted Through a Colony of Foraging Ants for MPPT in PV System', *Industrial Informatics, IEEE Transactions on,* 12(1), pp. 187-200.

Tsai, H., Tu, C. and Su, Y. (2008) 'Development of generalized photovoltaic model using MATLAB/SIMULINK', *Proceedings of the world congress on engineering and computer science.* Citeseer, 1-6.

United States of America: Department of Defense (1991) *Military Handbook: Reliability Prediction of Electronic Equipment: MIL-HDBK-217F: 2 December 1991.* Department of defense.

Veerachary, M., Senjyu, T. and Uezato, K. (2003) 'Neural-network-based maximum-power-point tracking of coupled-inductor interleaved-boost-converter-supplied PV system using fuzzy controller', *Industrial Electronics, IEEE Transactions on,* 50(4), pp. 749-758.

Villalva, M.G., Gazoli, J.R. and Ruppert Filho, E. (2009) 'Analysis and simulation of the P&O MPPT algorithm using a linearized PV array model', *Industrial Electronics, .*

Won, C., Kim, D., Kim, S., Kim, W. and Kim, H. (1994) 'A new maximum power point tracker of photovoltaic arrays using fuzzy controller', *Power Electronics Specialists Conference, PESC'94 Record., 25th Annual IEEE.* IEEE, 396-403.

Wu, W., Pongratananukul, N., Qiu, W., Rustom, K., Kasparis, T. and Batarseh, I. (2003) 'DSP-based multiple peak power tracking for expandable power system', *Eighteenth Annu. IEEE Appl. Power Electron. Conf. Expo. ,* 525-530.

Wu, Y., Shen, C. and Wu, C. (2009) 'Research and improvement of maximum power point tracking for photovoltaic systems', *Power Electronics and Drive Systems, 2009. PEDS 2009. International Conference on.* IEEE, 1308-1312.

Xiao, W. and Dunford, W.G. (2004) 'A modified adaptive hill climbing MPPT method for photovoltaic power systems', *Power Electronics Specialists Conference, 2004. PESC 04. 2004 IEEE 35th Annual.* Ieee, 1957-1963.

Yuvarajan, S. and Xu, S. (2003a) 'Photo-voltaic power converter with a simple maximum-power-point-tracker', *Circuits and Systems, 2003. ISCAS'03. Proceedings of the 2003 International Symposium on.* IEEE, III-399-III-402 vol. 3.

Yuvarajan, S. and Xu, S. (2003b) 'Photo-voltaic power converter with a simple maximum-power-point-tracker', *Circuits and Systems, 2003. ISCAS'03. Proceedings of the 2003 International Symposium on.* IEEE, III-399-III-402 vol. 3.

Zhao, Z., Xu, M., Chen, Q., Lai, J. and Cho, Y. (2012) 'Derivation, analysis, and implementation of a boost–buck converter-based high-efficiency PV inverter', *Power Electronics, IEEE Transactions on,* 27(3), pp. 1304-1313.

Zhou, Q., Xun, C., Dan, Q. and Liu, S. (2015) 'Grid-connected PV inverter reliability considerations: A review', *Electronic Packaging Technology (ICEPT), 2015 16th International Conference on.* IEEE, 266-274.

Appendix A
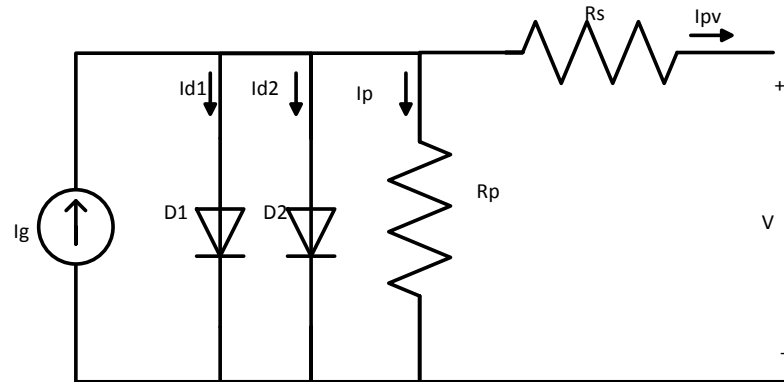
PV cell, double diodes model

Figure A-1: PV model with two parallel diodes

The relationship between the PV cell output current and terminal voltage is governed by

$$I_{pv} = I_g - I_{d1} - I_{d2} - \frac{V + I_{pv}R_s}{R_P}$$

$$I_{d1} = I_{01} \left(e^{\frac{q\left(V + I_{pv}R_s\right)}{akT}} - 1 \right)$$

$$I_{d2} = I_{02} \left(e^{\frac{q\left(V + I_{pv}R_s\right)}{akT}} - 1 \right)$$

where,

I_{pv}: is the cell output current

I_g: is the current from the DC current source (the photogenerated current)

I_{01} & I_{02}: is diode saturation current for diode 1 and 2 respectively

q: is the electron charge $(1.60217646 \times 10^{-19} C)$

k: is Boltzmann constant $(1.3806503 \times 10^{-23}$ J/K)

T: is the diode temperature in Kelvin

a: is the diode ideality constant

V: is the output PV voltage

R_s: is the resistance in series

R_p: is the resistance in parallel

Appendix B

Sunpower 305 PV panel data sheet

SUNPOWER

BENEFITS

Highest Efficiency
Panel efficiency of 18.7% is higher than any commercially available competitor panel

More Power
SunPower 305 delivers 50% more power per unit area than conventional solar panels and 100% more than thin film solar panels

Reduces Installation Cost
More power per panel means fewer panels per install. This saves both time and money

Reliable and Robust Design
Proven materials, tempered front glass, and a sturdy anodized frame allow panel to operate reliably in multiple mounting configurations

SPR-305-WHT

305 SOLAR PANEL
EXCEPTIONAL EFFICIENCY AND PERFORMANCE

The SunPower 305 Solar Panel provides today's highest efficiency and performance. Utilizing 96 next generation SunPower all-back contact solar cells, the SunPower 305 delivers an unprecedented total panel conversion efficiency of 18.7%. The 305 panel's reduced voltage-temperature coefficient and exceptional low-light performance attributes provide outstanding energy delivery per peak power watt.

SunPower's High Efficiency Advantage - Up to Twice the Power

Comparable systems covering 1000 m² / 10,750 ft²			
	Thin Film	Conventional	SunPower
Watts / Panel	65	165	305
Efficiency	9.0%	12.0%	18.7%
kWs	90	120	187

SUNPOWER

305 SOLAR PANEL

EXCEPTIONAL EFFICIENCY AND PERFORMANCE

Electrical Data

Measured at Standard Test Conditions (STC): Irradiance of 1000/m², air mass 1.5 g, and cell temperature 25° C

Peak Power (+/-5%)	Pmax	305 W
Rated Voltage	Vmp	54.7 V
Rated Current	Imp	5.58 A
Open Circuit Voltage	Voc	64.2 V
Short Circuit Current	Isc	5.96 A
Maximum System Voltage	IEC, UL	1000 V, 600 V
Temperature Coefficients		
	Power	–0.38% / °C
	Voltage (Voc)	–176.6 mV/°C
	Current (Isc)	3.5 mA/°C
Series Fuse Rating		15 A
Peak Power per Unit Area		187 W/m², 17.4 W/ft²
CEC PTC Rating		282.1 W

Mechanical Data

Solar Cells	96 SunPower all-back contact monocrystalline
Front Glass	4.0 mm (5/32 in) tempered
Junction Box	IP-65 rated with 3 bypass diodes
Output Cables	900 mm length cables / Multi-Contact connectors
Frame	Clear anodized aluminum alloy type 6063
Weight	24 kg, 53 lbs

IV Curve
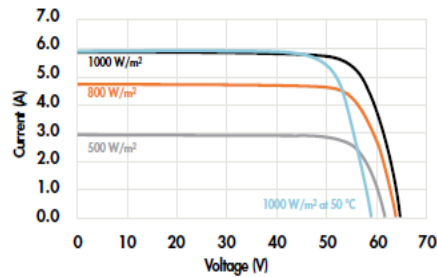
Current/voltage characteristics with dependence on irradiance and module temperature.

Tested Operating Conditions

Temperature	–40° C to +85° C (–40° F to +185° F)
Max load	50 psf (2400 Pascals) front and back
Impact Resistance	Hail – 25mm (1 in) at 23 m/s (52 mph)

Warranty and Certifications

Warranty	25 year limited power warranty
	10 year limited product warranty
Certifications	IEC 61215 , Safety tested IEC 61730;
	UL listed (UL 1703), Class C Fire Rating

Dimensions
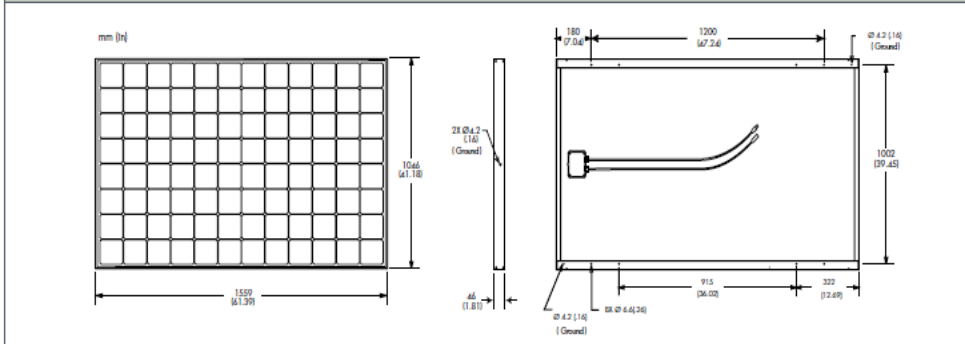
CAUTION: READ SAFETY AND INSTALLATION INSTRUCTIONS BEFORE USING THE PRODUCT. Go to www.sunpowercorp.com/panels for details

About SunPower

SunPower designs, manufactures and delivers high-performance solar electric technology worldwide. Our high-efficiency solar cells generate up to 50 percent more power than conventional solar cells. Our high-performance solar panels, roof tiles and trackers deliver significantly more energy than competing systems.

Document #001-42209 Rev*A

♻ Printed on recycled paper